



Department of Energy
Office of Civilian Radioactive Waste Management
Yucca Mountain Site Characterization Office
P.O. Box 364629
North Las Vegas, NV 89036-8629

QA: N/A

JUL 29 2002

OVERNIGHT MAIL

Janet R. Schlueter, Chief
High-Level Waste Branch
Division of Waste Management
Office of Nuclear Materials Safety
and Safeguards
U.S. Nuclear Regulatory Commission
Two White Flint North
Rockville, MD 20852

TRANSMITTAL OF INFORMATION ADDRESSING KEY TECHNICAL ISSUE (KTI) AGREEMENT ITEMS UNSATURATED AND SATURATED FLOW UNDER ISOTHERMAL CONDITIONS (USFIC) 5.13 AND TOTAL SYSTEM PERFORMANCE ASSESSMENT AND INTEGRATION (TSPAI) 2.02, COMMENTS 3 AND 12

This letter transmits a hard copy and a CD of a two-part report entitled *Thermochronological Evolution of Calcite Formation at the Potential Yucca Mountain Repository Site, Nevada: Part 1, Secondary Mineral Paragenesis and Geochemistry* (enclosure 1); and *Thermochronological Evolution of Calcite Formation at the Potential Yucca Mountain Repository Site, Nevada: Part 2, Fluid Inclusion Analyses and U-Pb Dating* (enclosure 2); which provides the basis for closure of KTI Agreement USFIC 5.13. The agreement USFIC 5.13 reads as follows:

USFIC 5.13 - "Provide the evaluation of the ongoing fluid inclusion studies (for example, UNLV, State of Nevada, and USGS).

DOE's consideration of the fluid inclusion studies will be documented in an update to the Saturated Zone Flow and Transport PMR expected to be available in FY 2002, subject to availability of the studies."

Agreement Item TSPAI 2.02, comments 3 and 12, concern the technical basis for the screening arguments for *Features, Events and Processes* (FEP) 2.2.10.03.00 and FEP 2.2.10.13.00. These comments are linked to Agreement Item USFIC 5.13.

The U.S. Department of Energy (DOE) has evaluated the enclosed report, agrees with its conclusions, and notes that it is consistent with results of prior DOE analyses. Although USFIC 5.13 was written in anticipation that the information to be provided would be documented in the *Saturated Zone Flow and Transport Process Model Report*, the information has been included in this letter. This different method of documentation is consistent with the discussion at the April 15-16, 2002, U.S. Nuclear Regulatory Commission (NRC)/DOE Technical Exchange and Management Meeting on KTIs.

AMISE-7
LUM-11
SPAD
Sherman

On July 24, 1998, the Nuclear Waste Technical Review Board (the Board) provided the Acting Director, Office of Civilian Radioactive Waste Management, with its evaluation of and conclusions about a set of material provided to it by the state of Nevada Attorney General's office. The set of material was presented as new evidence regarding the possible future upwelling of water into the proposed nuclear waste repository at Yucca Mountain.

The Board concluded that the material it reviewed did not significantly affect the conclusions of the 1992 National Academy of Sciences (NAS) report on similar issues, *Groundwater at Yucca Mountain: How High Can it Rise*. The NAS considered such a scenario to be not credible. The DOE agreed with that conclusion then and now. The Board also suggested that DOE consider conducting some additional analyses to determine the ages of fluid inclusions in mineral deposits at Yucca Mountain.

As the Board suggested, DOE funded a joint research program coordinated by Jean S. Cline, University of Nevada, Las Vegas (UNLV), in which scientists from the state of Nevada, the U.S. Geological Survey (USGS), and UNLV conducted analyses of the fluid inclusions found in mineral deposits. Participants met on a regular basis between March 1999 and March 2001 to establish a common methodology for sample collection and handling, and share the results of their investigations. The NRC staff was present at quarterly meetings and other forums where the work was presented.

The original DOE position was confirmed again by USGS scientists. For example, Paces et al., state in the abstract of the 2001 USGS report *Ages and Origins of Calcite and Opal in the Exploratory Studies Facility Tunnel, Yucca Mountain, Nevada* (USGS Water-Resources Investigations Report 01-4049), "The physical and isotopic data from calcite and opal indicate they formed from solutions of meteoric origin percolating through a limited network of connected fracture pathways in the unsaturated zone rather than by inundation from ascending groundwater originating in the saturated zone." This report was based, in part, on some of the USGS results from the joint program. More USGS results from the joint research program are presented in *Physical and Stable-Isotope Evidence for Formation of Secondary Calcite and Silica in the Unsaturated Zone, Yucca Mountain, Nevada* by Whelan et al., in *Applied Geochemistry*, Volume 17, pp. 735-750.

The purpose of the Cline study was to independently examine the secondary mineral deposits, especially the fluid inclusions within these secondary minerals, and interpret the observations regarding the origin of the fluid inclusions and secondary mineralization. The two-part report that resulted from the Cline study (enclosures 1 and 2) provides independent confirmation of work on secondary minerals by DOE scientists. Nicholas S. F. Wilson, Dr. Cline, and Yuri Amelin, state in the abstract for Part 2 of the report, "Results from this study are consistent with a model of descending meteoric water that infiltrated the cooling tuff sequence, became heated, and precipitated secondary minerals within the vadose zone . . ." Further, "This study demonstrates that the hypothesis of geologically recent upwelling hydrothermal fluids is untenable and should not disqualify the Yucca Mountain as a potential nuclear waste storage site."

JUL 29 2002

The DOE recently received a copy of a report prepared for the Attorney General of the state of Nevada, *Suitability of the Yucca Mountain Site to Accommodate a Permanent Repository for the High-Level Radioactive Waste and Spent Nuclear Fuel: An Independent Assessment*. This report appears to relate, in part, to the joint fluid inclusion program, but the DOE has not had time to thoroughly review it. However, the position on the upwelling issue by scientists representing the state of Nevada seems unchanged. In a pre-publication excerpt from the *Scientific Status of the Lingering 'Upwelling Water' Controversy in Light of the Joint UNLV/USGS/State of Nevada Research Project* by Jerzy S. Szymanski and Yuri V. Dublyansky, May 2001, p. 19, "The proposed conceptual model implies that the vadose zone is occasionally subjected to an upward flux of heat and gas-charged fluid, in addition to being subjected to a small flux of infiltrating rainwater."

The data collected by both DOE and UNLV researchers confirm that the conceptual model of descending percolation is correct. The DOE further concludes that the "upwelling waters" or "seismic pumping" hypotheses for the origin of secondary mineralization at the Yucca Mountain site have been adequately addressed and may be discounted, and DOE's screening of FEPs is appropriate.

The *Features, Events, and Processes in SZ Flow and Transport Analysis Model Report* (ANL-EBS-MD-000002) will be updated to incorporate the results of the enclosed report, as agreed in TSPA I 2.02, comments 3 and 12. Note, that because the results of the fluid inclusion studies corroborated the earlier results, the FEPs screening relative to upwelling will be unchanged.

This letter makes no new regulatory commitments. Please direct any questions concerning this letter and its enclosures to Timothy C. Gunter at (702) 794-1343 or Drew H. Coleman at (702) 794-5537.



Joseph D. Ziegler
Acting Assistant Manager
Office of Licensing and Regulatory Compliance

OL&RC:TCG-1551

Enclosures:

1. As stated
2. As stated
3. CD copy of Enclosures 1 and 2

cc w/encl 3:

J. W. Andersen, NRC, Rockville, MD
D. D. Chamberlain, NRC, Arlington, TX
R. M. Latta, NRC, Las Vegas, NV
S. H. Hanauer, DOE/HQ (RW-2), Las Vegas, NV
B. J. Garrick, ACNW, Rockville, MD
Richard Major, ACNW, Rockville, MD
Budhi Sagar, CNWRA, San Antonio, TX
W. C. Patrick, CNWRA, San Antonio, TX
J. R. Egan, Egan & Associates, McLean, VA
J. H. Kessler, EPRI, Palo Alto, CA

JUL 29 2002

cc w/encl 3: (continued)

Steve Kraft, NEI, Washington, DC
W. D. Barnard, NWTRB, Arlington, VA
R. R. Loux, State of Nevada, Carson City, NV
Margorie Paslov-Thomas, State of Nevada, Carson City, NV
Alan Kalt, Churchill County, Fallon, NV
Irene Navis, Clark County, Las Vegas, NV
George McCorkell, Esmeralda County,
Goldfield, NV
Leonard Fiorenzi, Eureka County, Eureka, NV
Andrew Remus, Inyo County, Independence, CA
Michael King, Inyo County, Edmonds, WA
Mickey Yarbrow, Lander County, Battle Mountain, NV
Lola Stark, Lincoln County, Caliente, NV
L. W. Bradshaw, Nye County, Pahrump, NV
David Chavez, Nye County, Tonopah, NV
Josie Larson, White Pine County, Ely, NV
Arlo Funk, Mineral County, Hawthorne, NV
R. I. Holden, National Congress of American
Indians, Washington, DC
Allen Ambler, Nevada Indian Environmental Coalition,
Fallon, NV
CMS Coordinator, BSC, Las Vegas, NV
OL&RC Library

cc w/o encls:

L. L. Campbell, NRC, Rockville, MD
C. W. Reamer, NRC, Rockville, MD
N. K. Stablein, NRC, Rockville, MD
S. L. Wastler, NRC, Rockville, MD
Margaret Chu, DOE/HQ (RW-1), FORS
S. E. Gomberg, DOE/HQ (RW-2), FORS
R. A. Milner, DOE/HQ (RW-2), FORS
A. B. Brownstein, DOE/HQ (RW-52), FORS
N. H. Slater-Thompson, DOE/HQ (RW-52), FORS
R. B. Murthy, DOE/OQA (RW-3), Las Vegas, NV
Richard Goffi, BAH, Washington, DC
N. H. Williams, BSC, Las Vegas, NV
S. J. Cereghino, BSC, Las Vegas, NV
Donald Beckman, BSC, Las Vegas, NV
K. M. Cline, MTS, Las Vegas, NV
R. B. Bradbury, MTS, Las Vegas, NV
R. P. Gamble, MTS, Las Vegas, NV
R. C. Murray, MTS, Las Vegas, NV
R. D. Rogers, MTS, Las Vegas, NV
E. P. Opelski, NQS, Las Vegas, NV
W. J. Boyle, DOE/YMSCO, Las Vegas, NV

JUL 29 2002

Janet R. Schlueter

-5-

cc w/o encls: (continued)

J. R. Dyer, DOE/YMSCO, Las Vegas, NV
T. C. Gunter, DOE/YMSCO, Las Vegas, NV
C. L. Hanlon, DOE/YMSCO, Las Vegas, NV
E. T. Smistad, DOE/YMSCO, Las Vegas, NV
G. W. Hellstrom, DOE/YMSCO, Las Vegas, NV
D. G. Horton, DOE/YMSCO, Las Vegas, NV
S. P. Mellington, DOE/YMSCO, Las Vegas, NV
C. M. Newbury, DOE/YMSCO, Las Vegas, NV
G. L. Smith, DOE/YMSCO, Las Vegas, NV
M. C. Tynan, DOE/YMSCO, Las Vegas, NV
J. D. Ziegler, DOE/YMSCO, Las Vegas, NV
R. E. Spence, DOE/YMSCO, Las Vegas, NV
J. T. Sullivan, DOE/YMSCO, Las Vegas, NV
C. A. Kouts, DOE/YMSCO (RW-2), FORS
R. N. Wells, DOE/YMSCO (RW-60), Las Vegas, NV
Records Processing Center = "10"
(ENCLS = READILY AVAILABLE)

Document No.: TR-02-005.1

Document Title: Thermochronological Evolution of Calcite Formation at the Proposed Yucca Mountain Repository Site, Nevada: Part 1, Secondary Mineral Paragenesis and Geochemistry

Document Revision: 0

Originators: Nicholas S. F. Wilson and Jean S. Cline; Department of Geoscience, University of Nevada Las Vegas, 4505 Maryland Parkway, Box 454010, Las Vegas, Nevada, USA 89154-4010

PI (Jean S. Cline) signature: Jean S. Cline

Date: 5/20/02

QA Manager (Amy Smiecinski) signature: Amy J. Smiecinski

Date: 5/20/02

Technical Reviewer: Robert Bodnar, Virginia Tech, Blacksburg, Virginia

Technical Reviewer signature: Robert J. Bodnar

Date: 05/16/2002

Table of Contents

Table of Contents	2
Table of Abbreviations	3
Abstract	4
1. INTRODUCTION	6
2. GEOLOGIC SETTING	6
3. PREVIOUS RESEARCH	8
3.1. Petrographic and Paragenetic studies.....	8
3.2. Cathodoluminescence	8
3.3. Calcite Composition.....	8
3.4. Stable Isotopes	9
4. METHODOLOGY	9
4.1. Sample Collection.....	9
4.2. Thin Section Preparation and Petrography	10
4.3. Electron Microprobe	10
4.4. Cathodoluminescence	10
4.5. LA-ICP-MS.....	10
4.6. C and O isotopes	11
5. MINERALOGY AND PETROLOGY	11
5.1. Mineral Occurrences and Spatial Variations	11
5.2. Petrography	12
6. CHEMICAL COMPOSITION	15
6.1. Microprobe Analyses	15
6.2. Cathodoluminescence	16
6.3. LA-ICP-MS Analyses.....	17
6.4. C and O Isotope Analyses.....	17
7. PARAGENESIS	18
7.1. Paragenesis of Lithophysal Cavities	18
7.2. Paragenesis of Fractures and Breccias	19
8. DISCUSSION	20
8.1. Mineral correlation.....	20
8.2. C and O isotope Data	21
8.3. Significance of Mg-enriched Growth-zoned Sparry Calcite	21
8.4. Variability of Secondary Minerals.....	22
8.5. Formation of Secondary Minerals in the Vadose Zone	23
9. CONCLUSIONS.....	24
REFERENCES.....	26
FIGURE AND TABLE CAPTIONS	29
FIGURES	32

Table of Abbreviations

BZ	barren zone
CAZ	calcite alteration zone
CL	cathodoluminescence
DOE	Department of Energy
DPTS	doubly polished thick sections
ECRB	Enhanced Characterization of the Repository Block Cross Drift
EPMA	electron probe microanalyses
ESF	Exploratory Studies Facility
IFZ	intensely fractured zone
LA-ICP-MS	ablation inductively coupled plasma mass spectrometry
LC	lithophysal cavities
LCZ	lithophysal cavity zone
MGSC	magnesium-enriched growth-zoned sparry calcite
NPR	north portal and ramp
PMC	patchy Mg-enriched calcite
PTn	Paintbrush Tuff nonwelded
SPR	south portal and ramp
SZ	saturated zone
UCCSN	University and Community College System of Southern Nevada
USGS	United States Geological Survey
UZ	unsaturated zone
WDS	wavelength dispersive spectrometry

Abstract

In the near future a decision will be made as to whether or not Yucca Mountain, 90 miles northwest of Las Vegas, Nevada is a suitable site for a permanent, underground, high level nuclear waste repository. A major factor in determining the suitability of Yucca Mountain as a repository is the potential for the site to be flooded by water during the regulatory lifetime. The current study was undertaken to examine the past fluid history at the site, to gain a better understanding of the possibility of flooding in the near geologic future. To estimate the past fluid flux into the repository horizon, research has focused on secondary minerals that precipitated in open space in lithophysal cavities, fractures, and breccias in the host Miocene tuffs. U.S. Geological Survey researchers concluded that secondary minerals formed from descending surficial meteoric fluids in a vadose environment. State of Nevada scientists observed 2-phase fluid inclusions with homogenization temperatures of 35 to 85 °C in secondary minerals and concluded that these minerals formed in the phreatic environment from upwelling hydrothermal fluids. They further concluded that upwelling hydrothermal fluids repeatedly invaded the site, have invaded the site in the recent geologic past, and could do so again making Yucca Mountain an unsafe site for high level nuclear waste storage. These studies did not constrain the timing of incursion of the fluids with elevated temperatures or the extent of this fluid flux across the site.

This report provides the geologic context for subsequent fluid inclusion and geochronological studies (Wilson et al., 2002) that identified the temperature and extent of the fluid incursion and placed absolute temporal constraints on the fluid history at Yucca Mountain. Here we describe a detailed paragenetic study that determined the depositional history of secondary minerals at Yucca Mountain.

One hundred and fifty-five samples of secondary minerals were collected from lithophysal cavities, fractures, and breccias at Yucca Mountain. Extensive petrography, paragenetic studies, and microprobe mapping indicate that early secondary minerals were heterogeneously distributed across the site and consist of variable amounts of calcite, opal, chalcedony, fluorite, and quartz. Early calcite contained variable trace amounts of Mg (up to 1.3 wt. %). Intermediate minerals consist of mainly calcite, often in bladed habits, with minor opal, and chalcedony and quartz. These minerals contain no diagnostic trace element variations. The latest secondary minerals deposited across the site consist of sparry calcite and minor intergrown opal. This sparry calcite exhibits fine (~ 50 µm) Mg-enriched and depleted growth zones and is chemically distinct from all other calcite. Mg-enriched growth-zoned sparry calcite (MGSC) contains up to ~ 1.0 wt. % Mg and has been identified in > 65 % of the samples collected from across the site. MGSC and associated opal are always the paragenetically youngest minerals; where MGSC is not present, young secondary minerals did not precipitate.

Calcite exhibits ranges for $\delta^{13}\text{C}$ from -8.5 ‰ to 9.5 ‰, and for $\delta^{18}\text{O}$ from 5.2 ‰ to 22.1 ‰. Samples exhibit generally consistent trends of decreasing C and increasing O isotopic compositions from paragenetically older to younger calcite. C and O isotope signatures for MGSC are between 16 ‰ and 20 ‰ for $\delta^{18}\text{O}$ and -3 ‰ and -8.5 ‰ for $\delta^{13}\text{C}$. However, signatures for the various stages are not unique and are not diagnostic in correlating secondary mineral stages across the site.

Early calcite is generally more luminescent than later calcite, but luminescence was not sufficiently consistent to aid in constraining the paragenetic sequence. LA-ICP-MS analyses indicate that higher levels of U, Th, and Sr are locally present in MGSC compared to paragenetically early calcite, however, this variation is not present in all samples.

An important observation is that 90% of primary and secondary open space in the tuffs at Yucca Mountain contains no secondary mineral record. Where secondary minerals are present, the older secondary mineral record is heterogeneous across the site. However, MGSC, which forms the youngest part of the secondary mineral record, is present in a majority of samples and exhibits a more homogeneous distribution across the site.

Secondary mineral abundances and textures indicate that secondary minerals precipitated in a vadose environment. The observed features are not consistent with secondary mineral precipitation in a phreatic environment saturated with aqueous fluids. Growth zoning in the outermost MGSC is consistent with formation from discontinuous influx of small fluid volumes with variable Mg content from surficial fluids that percolated downwards. Fluctuations in the Mg content in MGSC may be related to climate changes that occurred in the last few million years.

1. INTRODUCTION

Yucca Mountain, Nevada is currently the only site being studied by the U.S. Department of Energy (DOE) as a potential high-level nuclear waste repository (U.S. Department of Energy, 1988). The Yucca Mountain site is unique among repository sites owing to its location, underground, above a deep water table (Winograd, 1981). A major goal of this study was to ascertain whether the deep water table is a stable feature with a lengthy geologic history, or whether fluctuations in water table elevation occurred in the recent geologic past. Such fluctuations would indicate an increased potential for fluctuations during the regulatory lifetime of the repository and would adversely affect the integrity of the site.

To assist in assessing the long-term stability of the site, research has focused on examining secondary minerals that precipitated in primary and secondary pore spaces in the host tuffs. Since secondary minerals formed from fluids that invaded the repository rocks, the secondary minerals have been examined to determine whether they formed in a vadose or phreatic environment, and from downward percolating meteoric fluids or from upwelling hydrothermal fluids.

Previous research on the origin of secondary minerals from lithophysal cavities (LC), breccias, and fractures has led to much controversy. Scientists from the U.S. Geological Survey (USGS) concur that calcite precipitated from downward percolating cold meteoric fluids in a vadose environment (e.g. Paces et al., 1996; 1997; Whelan et al., in press). However, Dublyansky (1998) and Dublyansky et al. (1998; 2001), representing the State of Nevada, reported the presence of two-phase, aqueous fluid inclusions in calcite. They interpreted these fluid inclusions to have trapped upwelling hydrothermal fluids in a system analogous to epithermal mineral deposits, with mineral precipitation occurring in a phreatic environment.

This study focused on determining the origin and timing of precipitation of secondary minerals at Yucca Mountain. In this paper we report results of integrated studies on the petrography of the secondary minerals, electron probe microanalyses (EPMA), cathodoluminescence (CL), laser ablation inductively coupled plasma mass spectrometry (LA-ICP-MS), and C and O stable isotopes to construct a paragenetic sequence for secondary minerals. These paragenetic relationships provided the geologic context for fluid inclusion and geochronological analyses that constrained the absolute temperature and timing of formation of the secondary minerals (Wilson et al., 2002).

2. GEOLOGIC SETTING

Yucca Mountain is located 90 miles northwest of Las Vegas at the western edge of the Nevada Test Site. The mountain is within the Miocene southwest Nevada volcanic field (Christiansen et al, 1977) and the south-central part of the Basin and Range province. Yucca Mountain was initially chosen for study as a waste repository site because of its arid climate with less than 25 cm of rain per year (U.S. DOE, 1988), and the presence of a deep unsaturated zone (UZ) with a water table 400 – 600 m below the present day surface (Winograd, 1981).

Yucca Mountain is a north trending fault block ridge composed of a 1 – 3 km thick sequence of felsic welded and non-welded volcanic tuffs of the Paintbrush Group (Sawyer et al. 1994), and is bounded on either side by alluvial basins (Fig. 1). The Paintbrush Group is

comprised of the Topopah Spring, Pah Canyon, Yucca Mountain, and Tiva Canyon Tuffs, which dip gently to the east at less than 10 °.

The Topopah Spring Tuff, dated at 12.8 Ma, directly overlies bedded rhyolite tuffs of the Calico Hills Formation (Sawyer et al., 1994) and is about 380 m thick in the vicinity of Yucca Mountain (Stuckless and Dudley, in press). In turn the thin Pah Canyon and Yucca Mountain Tuffs overlie the Topopah Spring Tuff and together comprise the nonwelded Paintbrush Tuff (PTn) (Fig. 1). The Pah Canyon Tuff varies from welded to moderately welded and has a maximum thickness of 78 m in the north part of Yucca Mountain (Stuckless and Dudley, in press). The Yucca Mountain Tuff is non-welded throughout much of the Yucca Mountain area and reaches 45 m in thickness. The PTn is an important hydrogeological unit as flow changes from fracture flow in the overlying Tiva Canyon Tuff, to matrix flow in the PTn (Stuckless and Dudley, in press). The Pah Canyon and Yucca Mountain Tuffs are overlain by the Tiva Canyon Tuff, dated at 12.7 Ma (Sawyer et al. 1994) and composed of lower crystal-poor and upper crystal-rich members. The Tiva Canyon Tuff reaches a thickness of 175 m. After deposition of the Paintbrush Group, Basin and Range extension generated normal faults that cut the sequence (e.g. Stewart, 1988) (Fig. 1). Basaltic volcanism generated cinder cones during the late Tertiary and formed the recent Lathrop Wells Cone at around 77 Ka (Heizler et al., 1999). Detailed descriptions of the geology at Yucca Mountain are given by Sawyer et al. (1994), Buesch et al. (1996), and Stuckless and Dudley (in press).

The Exploratory Studies Facility (ESF) was excavated through the Tiva Canyon Tuff, PTn, and Topopah Spring Tuff to allow characterization of the volcanic stratigraphy (Figs. 1 and 2). To further examine the Topopah Spring Tuff, which is the potential repository horizon, and the Solitario Canyon fault zone a second tunnel, the Enhanced Characterization of the Repository Block Cross Drift (ECRB), was constructed (Mongano et al., 1999). The ECRB was excavated entirely within the Topopah Spring Tuff and trends northeast to southwest about 15 m above the potential repository site.

The potential repository horizon is about 300 m below the surface and approximately 200 – 400 m above the water table. At Yucca Mountain the UZ extends from the surface to depths of 500 – 700 m where the water table is encountered and the saturated zone (SZ) begins (Fig. 1). The barren zone (BZ) straddles the UZ and SZ and contains minor calcite relative to other regions. The top of the barren zone is approximately 100 - 300 m above the water table and it extends to approximately 400 m below the water table (Vaniman and Chipera, 1996). Underlying the BZ and at depths greater than 1 km is the calcite alteration zone (CAZ), characterized by tuffs and lavas that are altered to carbonate-bearing assemblages that have chemically distinct Mn-rich calcite (Denniston et al., 1997). The shallower part of this zone contains analcime and calcite, whereas albite and calcite dominate at greater depths (Bish and Chipera, 1989). The upper boundary of the CAZ appears to be the upper boundary of an 11 Ma fossil hydrothermal zone beneath Yucca Mountain (Bish, 1989). The majority of CAZ calcite forms pseudomorphs after feldspar phenocrysts within the rock matrix (Caporusico et al., 1982) and the calcite-albite-quartz-barite alteration assemblage indicates formation at about 250 °C (Vaniman, 1994).

Secondary minerals within the UZ are restricted to the footwalls and bases of LC, fractures, and breccias (Whelan et al., 1996). LC are roughly bedding parallel and formed as gases exsolved during deposition and cooling of the tuffs. Exsolving high temperature fluids altered the margins of LC and cooling fractures, producing distinctive bleached halos and vapor-phase veinlets consisting of tridymite, cristobalite, alkali feldspar, hematite and other accessory minerals subparallel to bedding (Carlos, 1994; Levy et al., 1996). Lithophysal cavities are

commonly connected by fine fractures, some of which are altered by vapor-phase mineralization. Fracture types include early cooling joints and later tectonic joints which have similar near vertical orientations, and joints that formed in response to erosional unloading (Stuckless and Dudley, in press). Breccias have variable features, some of which are associated with fault zones across the site.

3. PREVIOUS RESEARCH

3.1. Petrographic and Paragenetic studies

Previous petrographic studies documented the presence of a variety of calcite morphologies (Whelan et al., 1994; Dublyansky, 1998; Whelan and Moscati, 1998). A generalized paragenetic sequence presented by Whelan et al. (in press), which evolved over several years (e.g. Whelan et al. 1994; 1998; 2000; Paces et al., 2001), indicates initial high-temperature deposition of vapor-phase tridymite and hematite along cooling joints, fractures, and at the bases of LC. Early deposition of calcite, fluorite, and chalcedony-quartz was followed by intermediate and late deposition of calcite with minor opal. Whelan et al. (in press) documented the presence of distinctive bladed calcite with scepter overgrowths of clear 'late stage' calcite. The authors suggested that this general paragenetic sequence could be correlated across the site based on similar trends in $\delta^{13}\text{C}$ and $\delta^{18}\text{O}$ values (Whelan et al., 1998), comparable $^{230}\text{Th}/\text{U}$ and U-Pb ages of opal from fracture and LC occurrences (Paces et al., 2001), and the similarity in parageneses of secondary minerals in shallowly dipping fractures and adjacent LC (Paces et al., 2001).

Dublyansky et al. (2001) discussed secondary minerals but did not provide detailed petrographic descriptions or paragenetic relationships. Limited petrographic observations are, however, consistent with the paragenesis presented by Whelan et al. (in press).

3.2. Cathodoluminescence

Previous cathodoluminescence studies of Yucca Mountain calcite are limited; Denniston et al. (1997) studied calcite from the UZ and CAZ and Whelan et al. (1994; 2000; 2001) studied UZ calcite. Denniston et al. (1997) observed 1 – 20 μm alternating luminescing and nonluminescing bands in UZ calcite. Suture-form discontinuities between domains of fine bands indicated a hiatus between events of calcite precipitation. Whelan et al. (1994) examined drill core samples and observed that some UZ calcite displayed orange luminescent growth zoning. Preliminary observations by Whelan et al. (in press) indicated that some of the early-stage calcite and most of the late-stage calcite display fine growth zoning defined by orange luminescence and white UV fluorescence. They further observed that intermediate-stage calcite contained only widely separated luminescent growth zones in a non-luminescent background.

3.3. Calcite Composition

The chemical composition of calcite in the UZ and SZ was investigated in drill core samples by Vaniman (1993; 1994) using electron microprobe and instrumental neutron activation analyses. Prominent negative Ce and Eu anomalies and low concentrations of transition metals (Fe, Mn, Mg, and Sc) were observed only in UZ calcite. These variations distinguished UZ calcite from

SZ calcite. Investigation of trace elements in the calcite from drill core samples by electron microprobe, ICP-MS, and secondary ion mass spectrometry (Denniston et al., 1997) showed that UZ calcite had small variations in REEs and that Mn, Fe, and Sr abundances varied considerably within most calcite samples. Samples from the UZ were depleted in Mn, were similar to samples from the soil zone, and were clearly different from Mn-enriched CAZ samples (Denniston et al., 1997). Denniston et al. (1997) observed that CAZ calcites contained flat Ce patterns and minimum negative Eu allowing them to be differentiated from UZ calcites.

3.4. Stable Isotopes

Previous C and O isotopic studies of micro-sampled calcite from secondary minerals crusts (Whelan and Moscoti, 1998; Whelan et al., in press) showed that $\delta^{13}\text{C}$ decreased from about 10 ‰ in early calcite to -8 ‰ in late-stage calcite, as $\delta^{18}\text{O}$ increased from about 13 ‰ in early calcite to 20 ‰ in late-stage calcite. In spite of this general trend, the ranges of values determined for early, intermediate, and late calcite are not unique, and isotopic signatures cannot be used to determine the age of the calcite (Whelan et al., in press). Nevertheless, their data suggest general trends: calcite older than 4 Ma has $\delta^{13}\text{C}$ values greater than -4 ‰ and calcite younger than 1 Ma has $\delta^{13}\text{C}$ values less than -4.5 ‰ (Paces et al., 1997; Whelan et al., in press). Early calcite that had $\delta^{18}\text{O}$ compositions of less than 10 ‰ was interpreted to have formed from fluids with temperatures of 50 – 80 °C (Paces et al., 1997; Whelan et al., in press). $\delta^{18}\text{O}$ signatures of later calcite were interpreted to be compatible with deposition of secondary minerals from local meteoric or ground waters (Paces et al., 1997). $\delta^{13}\text{C}$ compositions were interpreted to indicate surficial sources for carbon dissolved in the downward-percolating solutions (Paces et al., 1997). This interpretation is supported by the similarity between the C and O isotopic signatures obtained from overlying pedogenic carbonates and the calcite from secondary mineral crusts (Whelan et al., in press).

Dublyansky et al. (2001) presented limited C and O isotope data for mineral crusts from vertical fractures in the Tiva Canyon Tuff from near the north portal of the ESF. $\delta^{18}\text{O}$ varied between 18.5 – 20.0 ‰ (conversion to $\delta^{18}\text{O}_{\text{VSMOW}}$ after Coplen et al., 1983) and in most samples compositions were consistent across the calcite crusts. $\delta^{13}\text{C}$ compositions for calcite were typically negative (Dublyansky et al., 2001). These ranges in $\delta^{18}\text{O}$ and $\delta^{13}\text{C}$ are narrower than ranges obtained by the USGS, and contrast with isotopic data from samples across the site (Whelan et al., in press). A comparison of the two data sets suggests that results by Dublyansky et al. (2001) from a limited part of the ESF probably only reflect part of the paragenetic sequence of the mineral crusts.

4. METHODOLOGY

4.1. Sample Collection

One hundred and fifty-five samples of secondary minerals and adjacent wall rock were collected from LC, fracture, and breccia occurrences from the ESF, ECRB, and exploration alcoves at Yucca Mountain. Sample locations are shown in Figure 2. The sample suite is representative of secondary mineral occurrences at Yucca Mountain. Samples collected in the tunnels were wrapped in aluminum foil, placed in cloth bags, and transported in a cooler to minimize

temperature variations. Because previous fluid inclusion studies indicated that homogenization temperatures could be as low as 35 °C, samples were kept between 0 – 35 °C in accordance with quality assurance (QA) procedures. Within this restricted temperature range fluid inclusions in the samples are unlikely to be modified owing to freezing or overheating.

4.2. Thin Section Preparation and Petrography

Owing to their fragile nature, samples selected for polished sections were impregnated with room temperature curing epoxy under vacuum. Samples were cut using a Buehler Isomet[®] slow speed saw with a Buehler[®] diamond wafering blade. Doubly polished thick sections (DPTS) were ground to a thickness of approximately 200 µm using a Hilquist[®] diamond cup wheel. Water was used for all cutting, grinding, and polishing steps to keep the sections cool. Final polishing by hand produced sections approximately 100 µm thick. A total of 5 sections were made from each billet. Two sections were used in this study; one of the sections was used for microprobe investigations and the other section was used for all other analyses. Of the remaining three sections, one was prepared for the State of Nevada and two were prepared for the USGS to provide equivalent sample material, produced under sample QA procedures, for independent studies.

Images of the sections were created using an Olympus slide scanner and/or Visioneer 7600 flatbed scanner to record the sections and assist with the petrographic studies. Petrographic investigations were made using Olympus BX-60 and Nikon OPTIPHOT-POL microscopes. Photomicrographs were captured using a Polaroid DMC IE digital camera.

4.3. Electron Microprobe

Quantitative analyses and qualitative X-ray maps were produced using a JEOL JXA-8900R Electron Probe Microanalyzer at UNLV. Natural standards (dolomite, calcite, strontianite, siderite, and rhodonite) were used for calibration and as reference materials. Quantitative point analyses were performed using an accelerating voltage of 10 kV, 7 nA probe current, and a 10 µm beam diameter with a 10 second counting time. Qualitative X-ray maps were collected with a single pass, dwell time of 20 ms, accelerating voltage of 15 kV, and a 20 nA probe current.

4.4. Cathodoluminescence

Cathodoluminescence studies were conducted using an automated 8200 Mk4 Cambridge Image Technologies Limited (CITL) cold cathodoluminescence stage, with an accelerating potential of 15 – 20 kV, beam current of 400 – 600 µA, and chamber vacuum of about 20 mbar. The stage was attached to a Nikon OPTIPHOT-POL microscope with a Nikon FX35-DX camera and an automatic AFX-DX controller. Photomicrographs were obtained using 1600 ASA/ISO color film.

4.5. LA-ICP-MS

Laser ablation inductively coupled plasma mass spectrometry (LA-ICP-MS) was performed on a Micromass[®] Platform ICP-HEX-MS quadrupole mass spectrometer with ICP ion source and hexapole collision cell, for removal of interfering polyatomic ion species, integrated with an in-

situ Merchantek[®] UV laser ablation microprobe. National Institute of Standards and Technology (NIST) glass standard reference materials were used as standards and in calibration of the ICP-MS (sample reference materials 610 (500 ppm), 612 (50 ppm), 614 (1 ppm), and 616 (0.02 ppm). Signals were collected for the instrument blank without firing the laser, and then collected on material ablated from 3 NIST glass standards for 200 milliseconds. Signal collection was repeated for 1 minute for each standard and all signals were integrated. Unknown samples were analyzed and concentrations were calculated from equations of lines generated by blanks and standards and corrected for matrix and drift correction and interfering polyatomic ion species.

4.6. C and O isotopes

Samples for C and O isotope analyses were drilled from DPTS using a Merchantek Micromill. Milled samples were typically 100 – 150 μg and were collected with a scalpel blade and placed in labeled polyethylene microcentrifuge tubes. Drill paths were digitized onto digital images of the samples.

Powdered calcite samples were roasted under vacuum for one hour at 380 °C to remove volatile components and stored in a desiccator. Desiccated sample powders were loaded into individual borosilicate or quartz reaction vessels used in an automated Finnigan[®] Kiel III Carbonate Device. Samples were reacted with 2 drops of anhydrous H_3PO_4 at 74 °C. Resultant water and CO_2 were cryogenically separated and pure CO_2 was transferred to a micro-volume for introduction to a Finnigan[®] MAT 252 isotope ratio mass spectrometer for analysis. Isotopic measurements were performed at the University of Iowa and were calibrated against laboratory reference gas (LASIS). All carbonate CO_2 isotopic analyses were corrected for ^{17}O contribution and acid fractionation effects. Results are expressed as ‰ deviation; $\delta^{13}\text{C}$ values were reported relative to V-PBD, and $\delta^{18}\text{O}$ values are reported relative to VSMOW. Analytical precision is greater than ± 0.1 ‰ for both carbon and oxygen isotope ratios and was monitored through daily analysis of duplicate sample aliquots and powdered carbonate standards (NBS-18, 19, 20 and other in-house carbonate standards).

5. MINERALOGY AND PETROLOGY

5.1. Mineral Occurrences and Spatial Variations

An important observation at Yucca Mountain is that most fractures, breccias, and LC do not contain secondary minerals. In sites where secondary minerals are present, these minerals fill only a fraction of the available open space and form thin (2 - 3 mm) crusts. At outcrop scale, mineral phases and abundances vary significantly at each sample site and across the site.

During sampling it was noted that the secondary mineral habits and abundances correlate, to some degree, with host lithology and sample location. Secondary minerals in the Tiva Canyon Tuff and upper nonlithophysal unit of the Topopah Spring Tuff in the north portal and ramp (NPR; Fig. 2) are generally present in fractures and breccias. Where present, the secondary minerals usually fill the available open space and are dominated by chalcedony, quartz, and opal rather than calcite. Some samples also contain significant fluorite. Lithophysal cavities are the predominant site for secondary minerals in the lithophysal cavity zone (LCZ; Fig. 2) which occurs in the upper lithophysal unit and lower nonlithophysal unit of the Topopah Spring Tuff.

This locality exhibits some of the thickest crusts, which are dominantly calcite with lesser opal, chalcedony, and quartz. Samples collected in the intensely fractured zone (IFZ; Fig. 2) are from the lower nonlithophysal unit of the Topopah Spring Tuff and contain only calcite with minor fluorite along thin fractures. In the south portal and ramp (SPR; Fig. 2) samples were collected from units between the lower nonlithophysal unit of the Topopah Spring Tuff and the Tiva Canyon Tuff. These samples are from fracture, LC, and breccia occurrences and contain calcite, chalcedony, quartz, minor opal and fluorite. ECRB cross drift (ECRB; Fig. 2) samples were collected from LC in the upper lithophysal to lower nonlithophysal units of the Topopah Spring Tuff, and consist primarily of calcite with minor opal, chalcedony, and quartz. A few fracture and breccia samples contain calcite. Samples collected from alcoves 6 and 7 are dominantly fracture and breccia samples, probably owing to proximity to the Ghost Dance Fault. These samples primarily contain calcite.

In thin section differences between samples from LC, breccias and fractures are apparent (Fig. 3). Crusts from LC can reach 4.5 cm in thickness and exhibit some of the most complex mineral stratigraphies observed (Fig. 3a). In many cases, however, LC samples are comprised of a single calcite habit (Fig. 3b; bladed calcite), or exhibit thin layers of calcite (Fig. 3c) that average 0.5 cm in thickness. In general, thicker crusts exhibit multiple layers (e.g. Fig. 3a; 3 layers) with distinctly different textures that are related to different generations of mineral precipitation. Fractures can contain thin calcite crusts (Fig. 3d) or thicker complex crusts (e.g. Figs. 3e and f). Steeply dipping fractures from the Topopah Spring Tuff commonly contain thin layers of calcite. Fractures from the NPR and SPR contain complex crusts and with significantly more silica mineralization than other sample locations. The silica phases typically occur adjacent to the wall rock and were overgrown by later calcite (Fig. 3e). Breccia samples (Figs. 3g to i) may contain abundant open space. In Figure 3g, two mineral crusts exhibit finer grained, thin layers of calcite at the base, that were overgrown, in turn, by coarser, slender bladed calcite and clear sparry calcite. Such samples are paragenetically equivalent to many LC samples. Other breccia samples are composed of fine to coarse pieces of tuff cemented by calcite. In most cases these breccias are only partially cemented by thin rims of calcite that line pore spaces, suggestive of meniscus textures, and abundant open space is present between adjacent tuff pieces (Figs. 3h and i). Smaller pores were typically filled, whereas larger pores are only partially filled. As Figure 3 illustrates, abundant porosity is associated with all occurrences of secondary minerals at both micro and macro scales.

5.2. Petrography

During the paragenetic study, the occurrences and habits of the older and intermediate calcite were observed to be variable. For example, some samples are composed of primarily bladed calcite that precipitated directly on the wall rock (e.g. sample ESF 28+81; Fig. 3b), whereas in other samples primarily blocky calcite is present (e.g. sample ECRB 10+10). In contrast to the variability of older phases, younger secondary minerals were observed to be relatively continuous across the repository site. In particular, a chemically distinct sparry calcite, that contains fine Mg-enriched growth zones (termed Mg-enriched growth-zoned sparry calcite (MGSC); see section 6.1) forms the outermost mineral layer in most of the samples. The continuous nature of this MGSC indicates that the younger history of calcite deposition at Yucca Mountain was consistently recorded across the site.

A comparison of all samples, patterns of mineral deposition, and textural relationships shows that the various calcite habits reflect the timing of mineral deposition. This comparison further demonstrated that no single location or sample recorded the entire history of secondary mineralization, indicating that processes responsible for secondary mineral deposition did not occur uniformly throughout the repository horizon. As a result, a relatively large number of samples must be examined in order to identify all depositional events and periods of non-deposition, and to determine the relative timing of deposition of the various mineral events.

5.2.1. Calcite

Calcite is the most abundant mineral within LC, fractures and breccias, occurs throughout the mineral paragenesis, and makes up more than 95% of all secondary minerals within the site.

Basal calcite in LC, which is somewhat variable, is commonly overgrown by bladed calcite, and subsequently by MGSC, the outermost layer of calcite in most mineral crusts. Basal calcite forms irregular, interlocking, subhedral crystals adjacent to the wall rock (Fig. 4a). This early calcite commonly overgrows tuff fragments and is typically finer-grained and darker than most younger calcite. Basal calcite also occurs as blocky calcite containing numerous tuff fragments and fluid inclusions. This calcite exhibits cleavage (Fig. 4b) and, at some localities, has no distinctive characteristics.

Bladed calcite occurs as small bladed and longer bladed crystals that comprise the majority of LC crusts. The abundance of bladed calcite may be, in part, a function of available open space. These crystals are also present in fracture and breccia samples, overgrowing earlier basal calcite in all occurrences.

A single, chemically distinctive calcite layer, MGSC (see section 6.1) consistently forms the outermost and youngest mineral layer across the site. MGSC forms both clear calcite and dark patchy calcite (Figs. 4c and d) delineating growth zones. The dark growth zones can contain rare, liquid-only fluid inclusions and are locally highlighted by intergrowths of opal (Fig. 4e). The dark color observed in some samples probably results from microporosity along the growth zones. In samples in which MGSC is not present, textural relationships indicate that MGSC did not precipitate, and the sample site did not record the complete history of secondary mineral precipitation. For example, bladed calcite overgrown by MGSC is evident in Figures 4c and 4f; in Figure 3b, however, bladed calcite forms the outermost mineral layer. MGSC is not present and, therefore, did not precipitate at this site.

In fracture and breccia occurrences, the earliest calcite adjacent to the wall rock is usually finely layered calcite (Fig. 4g) which contains tuff fragments and, at some localities, small cubic fluorite inclusions. In some samples from the IFZ, fluorite was the first secondary mineral to precipitate on the wall rock and was overgrown by multiple later generations of calcite (Fig. 4h). Layered calcite is present in fractures and breccias in the Topopah Spring Tuff, but has not been observed in samples from the Tiva Canyon Tuff. Layered calcite is overgrown by calcite exhibiting a number of different habits including fine dark, bladed calcite, clear calcite, and MGSC. As observed in LC, the outermost calcite in many fracture occurrences is MGSC (Figs. 4d and i).

All of these observations indicate a similar paragenesis for LC and fracture and breccia occurrences, although certain mineral layers tend to be thicker or thinner, or present or absent at various sample localities. Paragenetic relationships are particularly consistent in the ECRB

where samples from LC, fractures, and breccias have identical parageneses and all samples exhibit bladed calcite overgrown by MGSC.

5.2.2. Opal

Opal is colorless to dark brown (nearly opaque) in plane polarized light (Figs. 4c - e) and occurs as thin layers and isolated hemispheres. Under short-wave UV light and CL, outer clear opal and some brown opal fluoresce and luminesce bright green, respectively, highlighting the growth layering in the samples.

Brown opal commonly occurs in the older basal portions of secondary mineral crusts (Figs. 4d, i and j) and clear opal occurs in the younger central and outer parts of the crusts (Figs. 4c and e), however, young brown opal and old clear opal have been observed (Wilson et al., 2002). Brown opal is typically associated with early chalcedony and quartz and rarely with fluorite, and forms distinct layers and irregular masses. This opal is common in fractures in the NPR and SPR where it is usually associated with chalcedony (Fig. 4d). The presence of inclusions of anhedral calcite in opal at the base of mineral crusts, and irregular boundaries between opal and calcite suggest some dissolution of calcite and replacement by opal. In most fracture occurrences brown opal is overgrown by MGSC (Fig. 4d).

Most clear opal is intergrown with MGSC in the outer part of the crusts. This opal occurs as both continuous and discontinuous layers and as isolated hemispheres and clusters of hemispheres (Figs. 4c and e). Within MGSC, multiple distinct opal layers can be present (Figs. 4c and e). Calcite is optically continuous across these opal layers which can vary in thickness. The contact between opal and underlying calcite is usually planar but in some samples, dissolution of the underlying calcite and replacement by opal is indicated. The presence of opal layers and hemispheres aligning growth zones in the calcite, and the presence of adjacent opal and calcite that exhibit serrated contacts in the growth direction (Fig. 4e) suggest that, at some localities, opal and calcite are coeval. However, in other samples opal layers cut across growth zones in MGSC (Fig. 4c).

5.2.3. Chalcedony

Chalcedony occurs as layered or massive radial growths of crystallites (Figs. 4f, i, and j). Chalcedony commonly exhibits bright green fluorescence under short wave UV light, but the fluorescence is often masked by the stronger fluorescence of associated brown opal.

Chalcedony is commonly spatially associated with quartz and, at most localities, euhedral quartz crystals precipitated on outermost chalcedony (Fig. 4j). In fact, chalcedony commonly appears to form 'roots' at the base of euhedral quartz crystals. A number of observations indicate that chalcedony replaced earlier calcite. These include irregular boundaries between chalcedony and underlying calcite (Figs. 4f and i; Fig. 5b), the presence of inclusions of anhedral calcite in chalcedony (white arrows in Fig. 4i), and pseudomorphs of calcite cleavage in the chalcedony (black arrows in Fig. 4i).

In LC samples, chalcedony forms layers associated with brown opal (Fig. 4j). Chalcedony commonly occurs as thick layers in the NPR and SPR (Figs. 4d and i), and is most common in the NPR. In fractures, chalcedony is intergrown with opal, and multiple generations of chalcedony and opal are commonly present (Fig. 4j). Chalcedony is not associated with MGSC in the outermost part of mineral crusts. This relationship is significant in that it constrains

chalcedony to be paragenetically early to intermediate in age, consistent with dates obtained using U-Pb methods (Wilson et al., 2002).

5.2.4. Quartz

Quartz occurs primarily as small, euhedral crystals adjacent to the wall rock and associated with chalcedony and brown opal in the basal parts of crusts in all sample occurrences (Figs. 4i – k). ‘Roots’ of chalcedony commonly form the base of euhedral quartz crystals, but clusters of quartz crystals can occur without associated chalcedony. At some localities, particularly in the NPR, quartz adjacent to the wall rock contains inclusions of fluorite (Fig. 4k). At some sample locations quartz has not been overgrown by later minerals, and drusy quartz forms the outermost mineral layer. However, in most samples quartz is overgrown by later minerals and ultimately by MGSC, indicating quartz is early to intermediate in age.

5.2.5. Fluorite

Fluorite occurs as cubic and irregularly shaped inclusions (Fig. 4k), nodular growths (Fig. 4k), continuous and discontinuous layers (Fig. 4h), hemispherical masses, and as massive cements around tuff pieces within fractures, breccias, and LC. Under plane polarized light fluorite is usually clear, but fluorite can be purple and exhibit growth zoning. Fluorite typically exhibits massive and nodular forms that precipitated around vapor-phase minerals, wall rocks, and at the base of the secondary crusts. In LC samples, small cubic inclusions of fluorite occur within calcite at the base of the crusts adjacent to the wall rocks. Fluorite has not been observed in MGSC. The presence of fluorite both at the base of secondary minerals and within early calcite, and the lack of fluorite in MGSC suggests that more than one episode of fluorite precipitation occurred, but that all episodes were early to early – intermediate in age.

6. CHEMICAL COMPOSITION

6.1. Microprobe Analyses

Electron microprobe studies included quantitative wavelength dispersive spectrometry (WDS) point analyses using extended count times over the entire spectra of elements, and using shorter count times over a specific range of elements (Sr, Mn, Fe, Mg, K, Ca, Al, U, Si, and F). Early results showed that the majority of the calcite (80 – 90 %) does not contain significant and consistently detectable trace or minor elements using EPMA. However, Mg was detected in the majority of samples in early calcite and late MGSC. Quantitative analyses determined that Sr, Fe, and Mn were present at low levels. Typically calcite (e.g. basal, bladed, and MGSC) contained concentrations of these elements at levels below detection limits to around 0.4 – 0.7 wt. % for Sr, 0.3 – 0.7 wt. % for Mn, and 0.4 – 0.9 wt. % for Fe. The presence or absence of these elements does not coincide with calcite habit and concentrations are comparable in all calcite types. Strontium and Mg show fairly even distributions, whereas Mn and Fe are more variable. X-ray mapping did not show any consistent growth-related variation in Sr, Mn, or Fe; however, in a few samples, Mg and Sr were negatively correlated. In contrast, Mg is clearly related to specific calcite habit and paragenetic stage. Quantitative analyses of opal, chalcedony,

quartz, and fluorite did not show any consistent variations in trace or minor elemental compositions.

Electron microprobe X-ray mapping of the majority of samples revealed the presence of chemically distinct Mg-enriched calcite that could be correlated across the site. Magnesium-enriched calcite exhibits two morphologies: irregular Mg-enriched patches in early calcite and complex oscillatory growth zoning in late sparry calcite (Fig. 5). Mg-enrichment in calcite that does not display growth zoning is termed patchy Mg-enriched calcite (PMC). PMC usually occurs adjacent to vapor-phase minerals, commonly tridymite, fluorite, and around the wall rock at the base of the secondary crusts (Figs. 5a and b). In some samples PMC occurs in outermost calcite, but this is because in these samples only older calcite is present, which has not been overgrown by younger secondary minerals. Patchy Mg-enrichment varies in thickness over short distances and is discontinuous. Unlike Mg-enriched growth zoning, PMC cannot be clearly related to crystal habit; however, PMC is not observed in bladed or outer sparry calcite and it is restricted to paragenetically early calcite. PMC contains up to 1.3 wt. % MgO, however, concentrations vary across patches (Figs. 5a and b).

Calcite that contains Mg-enrichment that displays growth zoning is referred to as magnesium-enriched growth-zoned sparry calcite, or MGSC. More than 120 samples were X-ray mapped, typically for Mg, Fe, Sr, and Mn, and the outermost layer in more than 65 % of these samples is MGSC. Mg-enriched growth zoning always occurs in outer sparry calcite and more than 75 % of the collected samples contain MGSC. These samples include 65 % of the samples that were X-ray mapped and an additional 10 % of the samples that contain readily identifiable MGSC (i.e. visible growth zones, sparry habit, and associated clear opal).

MGSC (Figs. 5b and c; Fig. 6) contains numerous oscillatory growth zones that are typically ~50 to 100 μm thick, but which thicken locally. Individual MGSC growth zones are planar and asymmetrically around crystal axes, and overgrow earlier minerals that do not contain Mg (Figs. 5b and c; Fig. 6). Within MGSC the Mg composition varies from below the detection limit to around 1 wt. % Mg; however, this range can vary along individual growth zones.

The thickness of the MGSC layer ranges from hundreds of micrometers to centimeters at various sample sites. Where present in the NPR and SPR, MGSC commonly occurs as thin to thick (≥ 0.5 cm) layers. In the LCZ and ECRB, MGSC is present in the majority of samples. The layer is commonly less than 0.5 cm at these localities; however, the thickness of the MGSC overgrowths can vary considerably between adjacent sample localities. MGSC occurs as thin overgrowths (typically less than 500 μm) in the southern part of the IFZ, but MGSC is rare in other parts of the IFZ.

The consistent presence of this mineral layer and its occurrence as the youngest secondary mineral reflects a single site-wide precipitation event. The variability in the detailed growth zoning and thickness of this layer in different samples limits development of a 'cement stratigraphy' that can be correlated from sample site to sample site. Nevertheless, MGSC forms a single micro-stratigraphic unit that reflects a geologically recent fluid flow event across the site.

6.2. Cathodoluminescence

Cathodoluminescence is observed in the calcite crusts, but has not been as diagnostic as chemistry in correlating secondary minerals across the site because it is more variable. Cathodoluminescence investigations focused on calcite, opal, and fluorite because quartz, chalcedony and vapor-phase minerals did not luminesce.

Most calcite is not luminescent. Calcite that does luminescence exhibits fine ($\sim 50 \mu\text{m}$), planar to curved, irregular, and oscillatory (Fig. 4l) orange growth zones within some crystals, with more massive luminescence zones, where fine growth zones are not observed, along grain boundaries and within some crystals. Similar colors and intensities are generally observed. Luminescence highlights discontinuous growth zoning revealing precipitation breaks in optically continuous calcite.

All samples from the IFZ exhibit the most strongly luminescent and complex growth zoning (Fig. 4l). Luminescence in layered calcite adjacent to the wall rock is common in these samples and this calcite is typically overgrown by calcite exhibiting oscillatory luminescent growth zoning. Thin, concentric luminescent growth zones highlight partially filled pore spaces and indicate a pore filling texture.

Generally, early calcite that rims vapor-phase minerals in LC is luminescent. Bladed calcite can contain luminescent growth zoning and is luminescent along grain boundaries. Typically MGSC is not luminescent, but in some samples fine luminescent growth zoning is present. This luminescence coincides with growth zones visible under transmitted light and those observed in MGSC, but does not occur in many samples. Typically, samples from the ECRB exhibit more luminescence throughout the crust than similar samples from the ESF.

Outer clear opal generally exhibits bright green luminescent growth zoning with some layers luminescing much more strongly than the majority of the opal. Fluorite exhibits green luminescent growth zones and, locally, this luminescence reveals discontinuities related to fluorite dissolution and re-precipitation.

6.3. LA-ICP-MS Analyses

LA-ICP-MS analyses of MGSC, luminescent, non-luminescent, and basal calcite did not identify any significant elemental variations at levels below detection levels of the EPMA. Analyses showed that there is some enrichment in MGSC of U, Th, and Sr compared to calcite from the inner parts of the samples. However, this variation was not consistent. Orange luminescence commonly reflects the presence of Mn^{2+} as an activator (Machel et al., 1991), but variations in Mn^{2+} were not confirmed using LA-ICP-MS analyses and both non-luminescent and luminescent calcite contained similar amounts of Mn.

6.4. C and O Isotope Analyses

Eighty micro-samples of calcite from different stages were collected from across the repository site, and were analyzed for C and O isotopic compositions. The results are given in Table 1 and shown in Figure 7. Samples exhibit ranges for $\delta^{13}\text{C}$ from -8.5 to 9.5 ‰, and for $\delta^{18}\text{O}$ from 5.2 to 22.1 ‰. Samples exhibit generally consistent trends in C and O isotopes from paragenetically early calcite to the younger and outermost parts of the crusts. Most older calcite has lower $\delta^{18}\text{O}$ compositions, which increase in the younger minerals (Table 1; Fig. 7). Alternatively, $\delta^{13}\text{C}$ compositions decrease from positive values in older calcite at the base of crusts to negative values around -6.0 to -8.0 ‰ in the youngest calcite. All $\delta^{18}\text{O}$ and $\delta^{13}\text{C}$ data have a negative correlation of $r = -0.72$.

MGSC has relatively consistent signatures of $16 - 20$ ‰ for $\delta^{18}\text{O}$ and -3.0 to -8.5 ‰ for $\delta^{13}\text{C}$. However, these signatures are not diagnostic because samples of bladed, intermediate, and outermost non-descript calcite can have similar isotopic compositions (Fig. 7). Bladed calcite

exhibits a very large range in $\delta^{13}\text{C}$ of about 18 ‰ and the higher end of this range overlaps with signatures determined for MGSC. Intermediate calcite from the central parts of crusts also has a wide range of carbon isotope compositions, generally similar to bladed calcite and this range of signatures also overlaps with isotopic signatures determined for MGSC. Outermost calcite that is not Mg-enriched, and which has no distinguishing characteristics, has similar isotopic compositions to MGSC, but exhibits a somewhat shifted range in $\delta^{13}\text{C}$. The net result is that several morphologically distinct types of intermediate and outer calcite have similar isotopic compositions, even though paragenetic relationships show conclusively that the absolute ages of these calcites are different.

Filled symbols on Figure 7 identify isotopic signatures of calcite samples that are spatially associated with two-phase fluid inclusions (Wilson et al., 2002) and the symbols correspond to the habit and/or relative paragenetic position of the calcite. Most two-phase fluid inclusions occur in basal, bladed and intermediate calcites that have positive $\delta^{13}\text{C}$ compositions (Fig. 7). A few basal and intermediate calcites associated with two-phase fluid inclusions have $\delta^{13}\text{C}$ compositions as low as -3 ‰. These samples also have low $\delta^{18}\text{O}$ compositions that are less than values determined for MGSC. It is significant that samples of bladed calcite that contain two-phase inclusions have carbon isotopic signatures that are distinctly different from bladed calcite that contains only 1-phase inclusions (Fig. 7; Wilson et al., 2002). This is suggestive that bladed calcite precipitated over a prolonged period of time from a fluid that varied in temperature and isotopic composition.

7. PARAGENESIS

By integrating the petrographic observations with EPMA, cathodoluminescence, LA-ICP-MS, and C and O isotopes it is possible to better constrain the paragenetic sequence for secondary minerals in each sample, and to link these parageneses across the site. Although there is significant mineralogical variability, particularly in the older parts of the crusts, a paragenetic framework that displays consistent textural relationships for secondary minerals in all samples can be constructed. Vertical slices through Figure 8 at various points across the diagram represent individual parageneses observed at various sample sites. Collectively, these parageneses illustrate the history of secondary mineral precipitation across the site, highlight significant mineral relationships, and illustrate the variation between individual sample sites with respect to early stages of secondary minerals and the consistency of latest MGSC.

7.1. Paragenesis of Lithophysal Cavities

After the tuff was deposited, vapor-phase minerals (tridymite, drusy quartz, platy hematite, \pm fluorite?) formed adjacent to the wall rock and were overgrown by early fluorite. Fluorite occurs as nodular growths around the wall rock and can also form massive cement around tuff pieces. Tuff, vapor-phase minerals, and fluorite were overgrown by calcite that exhibits a variety of habits. For example, some samples contain basal blocky calcite with distinctive cleavage (Fig. 8c) and which cements tuff pieces, overgrown by small bladed calcite (Fig. 8c), irregular calcite grains (Fig. 8b), clear calcite, and dark inclusion-rich (i.e. tuff, mineral and lesser fluid inclusions) calcite (Fig. 8c). Basal calcite is usually finer-grained than calcite in outer parts of the crusts (Figs. 8b and c). These early calcites locally contain cubic fluorite crystals or, rarely, clear

opal hemispheres (Fig. 8b). Some basal calcite contains patchy Mg-enrichment around fluorite and tridymite, but outboard of this basal calcite, significant trace elements, other than in MGSC, are not detected (see Fig. 5b). Basal calcite is commonly luminescent and exhibits oscillatory growth zones at the base of crusts and along some grain boundaries. C and O isotopic signatures for basal calcite typically have positive $\delta^{13}\text{C}$ and $\delta^{18}\text{O}$ below about 17 ‰ (Fig. 7).

Some LC samples, primarily those from the ESF, contain a quartz-chalcedony-brown opal layer. This layer may consist of fine chalcedony overgrown by euhedral quartz crystals (Fig. 8d) or, alternatively, a relatively thick layer of intergrown chalcedony and brown opal overgrown by quartz crystals (Fig. 8e). Dissolution and replacement of earlier calcite by quartz-chalcedony-brown opal (Fig. 8e) are indicated by highly irregular boundaries between the silica minerals and the underlying calcite, and the presence of isolated, but optically continuous anhedral calcite inclusions in the chalcedony-quartz (Fig. 8e). In some samples chalcedony-quartz-brown opal contains fluorite. Chalcedony-quartz-brown opal generally occurs in a single layer in LC, whereas multiple layers are common in fracture occurrences (see Fig. 4d). The silica layer overgrows earlier calcite as well as earlier vapor-phase minerals. Virtually all two-phase fluid inclusions observed during this study were present in basal calcite below, and paragenetically older than, the silica layer (Wilson et al., 2002).

Bladed calcite precipitated on early calcite or silica and is present in virtually all LC samples in the ESF and ECRB (Fig. 8f). Where bladed calcite occurs, silica is typically minor and bladed calcite comprises the majority of these crusts (Fig. 8o). Where calcite blades form overgrowths on earlier calcite, the overgrowths are usually optically continuous. Early, inner cores of bladed calcite crystals rarely contain two-phase fluid inclusions, whereas the middle and outer parts of the blades contain only rare, liquid-only inclusions (Wilson et al., 2002) and have different C and O isotopic compositions (Fig. 7). Petrography and C and O isotopic trends indicate that bladed calcite that contains two-phase fluid inclusions is older than bladed calcite that contains liquid-only inclusions. Virtually all bladed calcite is free of consistent trace element variations detectable by EPMA; however, this calcite does locally luminesce along growth zones and crystal boundaries.

Where present, MGSC and locally intergrown opal overgrow and exhibit consistent relative age relationships with all other secondary minerals (Figs. 8g – k, and n). Overgrowths of MGSC result in a regular outer surface (e.g. Fig. 3a) as compared to the irregular bladed surfaces (Fig. 3b) of intermediate calcite. MGSC forms layers of variable thickness. Small, discontinuous, “golf-tee” shaped overgrowths can form on the tips of bladed calcite (Fig. 8h; see Whelan et al., 1996) or MGSC can comprise entire secondary mineral crusts (Fig. 8k). MGSC contains only liquid-only fluid inclusions indicating formation at low temperatures (Wilson et al., 2002). Opal layers can be numerous and locally continuous or discontinuous (Figs. 8i and j). Most importantly, MGSC provides a chemically distinct fingerprint that is paragenetically consistent, and which can be traced across Yucca Mountain allowing the histories of secondary minerals across the site to be linked.

7.2. Paragenesis of Fractures and Breccias

Fracture occurrences predominate in the NPR, SPR and the IFZ and the following paragenesis is compiled from samples within these three areas. The wall rock surface in most fracture and breccia samples consists of broken tuff that lacks vapor-phase minerals. These surfaces suggest that fracture/breccia development occurred after vapor-phase alteration of the host tuffs and, in

turn, indicate that secondary minerals in fractures and breccias began to precipitate later than secondary minerals in LC.

Layered calcite in fractures and breccias consists of multiple planar calcite layers defined by small tuff inclusions. Layered calcite, basal calcite, and fluorite precipitated around wall rock in the IFZ (Figs. 4g and h) and chalcedony-quartz-brown opal-fluorite was deposited in the NPR and SPR (Fig. 4; Fig. 8l). Chalcedony-quartz-brown opal is probably not present in the IFZ because silica deposition pre-dated the fracturing event. If this interpretation is correct, IFZ fluorite is younger than fluorite associated with chalcedony-quartz-brown opal in the NPR and SPR. Geochronology, fluid inclusion petrography, and microthermometry (Wilson et al., 2002) support these interpretations.

Chalcedony-quartz-brown opal-fluorite in fracture occurrences commonly forms multiple layers. These layers are different from the single layers of silica minerals in LC samples that contain less fluorite. In these fracture samples, sparse two-phase fluid inclusions have been observed in both quartz and fluorite growing around the host tuffs (Wilson et al., 2002).

Clearer calcite typically precipitated on the early, basal minerals described above (Fig. 8m). Calcite that precipitated on layered basal calcite in the IFZ is usually clear and exhibits strong orange luminescence. In these samples, this clear calcite comprises the majority of the crusts and later overgrowths are not generally present. Large bladed calcite crystals are uncommon in fracture occurrences; however, small blades are present in many samples where open space permitted crystal growth.

As in LC, the youngest calcite present in fractures and breccias is MGSC; however, it is more difficult to recognize than in LC (Fig. 4c). The growth zoning within MGSC is generally simpler in fracture and breccia samples and MGSC overgrowths are usually thin and discontinuous (Fig. 8i). However, in some fracture and breccia localities in the NPR and SPR, MGSC growth zoning is well developed and the layer is locally thick, complex, and continuous (Figs. 6 and 8n). MGSC in fractures and breccias contains concentrations of Mg (~1 wt. %) similar to those in LC, and is petrographically and geochemically equivalent to MGSC identified in LC. In some fracture samples that contained abundant open space, MGSC overgrowths occur on the outer surface, and also line inner pore spaces (e.g. sample ESF 78+05.2). Textures indicate that the MGSC is a late-stage overgrowth in these pores and is temporally related to the outer overgrowths.

8. DISCUSSION

8.1. Mineral correlation

MGSC is the single, chemically distinctive mineral layer that can be correlated across the site. Textural relationships and chemical data show that MGSC or intergrown associated opal precipitated last in the paragenetic sequence. Intergrown opal has been dated using U-Pb techniques and results indicate that MGSC began precipitating between 2.9 – 1.9 Ma and has continued to precipitate to within the past few thousands of years (Wilson et al., 2002).

Bladed calcite, which is present in a large number of samples, probably reflects precipitation over an extended period of time, or during discrete intervals over time. This calcite does not have a distinctive chemical composition or luminescence. C and O isotopic signatures of bladed calcite (Fig. 7) exhibit a broad range, consistent with precipitation over extended time.

Furthermore, fluid inclusion petrography has shown that early bladed calcite contains rare two-phase fluid inclusions, and only liquid-only fluid inclusions are present in later bladed calcite (Wilson et al., 2002).

Chalcedony-quartz-brown opal is present in LC and in some fracture and breccia samples. U-Pb dating indicates that the chalcedony precipitated between 4 – 9 Ma (Wilson et al., 2002), consistent with the “early to intermediate” paragenetic position determined for this layer by petrography. These ages indicate that all chalcedony in the silica layer did not form at the same time and the silica layer does not represent a time line that can be correlated across the site.

8.2. C and O isotope Data

A comparison of the isotopic data shown in Figure 7 with data from Whelan et al. (in press) shows that similar ranges of C and O isotopic signatures and trends of increasing $\delta^{18}\text{O}$ and decreasing $\delta^{13}\text{C}$ with respect to decreasing age were determined by both studies. These results show that careful micro sampling of calcite in growth zones within a well-constrained paragenetic sequence does not produce unique isotopic signatures for calcite of different ages and habits. The lack of unique signatures for secondary mineral layers is most clearly demonstrated by MGSC, which has isotopic compositions that overlap with compositions determined for paragenetically older calcite.

Current results parallel results reported by Whelan et al. (in press) and indicate that calcite precipitated from meteoric fluids as interpreted by Whelan et al. (in press). The interpretation that some early calcite formed from $\sim 50 - 80$ °C fluids (Paces et al., 1997) is consistent with the microthermometry data of Wilson et al. (2002). Finally, a meteoric fluid source is further indicated by low δD compositions of inclusion fluids from intermediate calcite and MGSC (Wilson et al., 2002).

8.3. Significance of Mg-enriched Growth-zoned Sparry Calcite

The presence of PMC and MGSC indicate that Mg was available and was incorporated into the calcite structure during two periods of calcite deposition. It is generally accepted that the Mg concentrations in calcite are positively correlated with elevated temperatures and elevated Mg/Ca ratios of the source fluid (e.g. Scoffin, 1987). Wilson et al. (2002) showed that some early calcite contains primary fluid inclusions indicating calcite deposition at temperatures of 35 – 85 °C; such elevated temperatures could explain the incorporation of Mg into early calcite around tridymite. However, the majority of calcite that precipitated at elevated temperatures does not exhibit Mg-enriched growth zoning. Furthermore, MGSC contains rare liquid-only fluid inclusions indicating formation from low temperature fluids (Wilson et al., 2002). Therefore, it is unlikely that temperature controlled the Mg composition of the calcite. Instead, Mg-enrichment is likely controlled by the Mg/Ca ratio of the fluid, and early fluids that precipitated PMC and late fluids that precipitated MGSC probably contained higher Mg/Ca than fluids from which most of the calcite precipitated.

The irreversible change in the deposition of calcite with growth zones of alternating Mg-enriched and Mg-free calcite during the last few million years reflects a permanent change in the fluids that accessed Yucca Mountain. The fine oscillatory growth zoning shows that the Mg/Ca ratio in the fluid fluctuated repeatedly and in a fairly regular, cyclical manner. However the source of the Mg and reason for this change in deposition of calcite type are less clear.

The consistent presence and oscillatory nature of the growth zones suggest that they may be recording fluctuations related to changes in climate from around 2.9 Ma to the present day (Wilson et al., 2002). This time period corresponds with a major change in Northern Hemisphere glaciation which occurred around 2.67 Ma (Prueher and Rea, 1998). An abrupt change in deep-sea sediment character related to a change from a non-glacial to a glacial environment occurred across the North Pacific at this time. This change occurred too rapidly to be a direct response to tectonic or orbital forcing (Prueher and Rea, 1998) and terrestrial changes that corresponded with deep sea-related changes would be expected. The gradual uplift of the Sierra Nevada, west of Yucca Mountain, caused a change in the water chemistry during the last 3 m.y. (Smith et al., 1983). This change in chemistry led to deposition of considerable dolomite and Mg-enriched clays in playas and lakes in the Amargosa desert during the Pliocene (3.2 - 2.1 Ma) (Hay et al., 1986). These minerals may have contributed Mg to fluids that percolated into Yucca Mountain during climate-related cycles, forming MGSC. This process may have been accelerated by the earlier Pliocene nonglacial environment, when the climate was substantially wetter and springs in the Amargosa Desert were more widespread and had greater discharge (Hay et al., 1986). Alternatively, it is possible that the increase in Mg could be related to atmospheric dusts related to erosion of Paleozoic dolomites in the southwest (*J. Stuckless, personal communication, 2000*).

The fine and complex growth zones are not continuous across a thin section suggesting that the larger calcite crystals formed by the constructive deposition of numerous small overgrowths. These discontinuities are small-scale versions of discontinuous MGSC present in numerous samples and illustrated in Figure 8. These discontinuities are not consistent with saturation of the site by aqueous fluids.

8.4. Variability of Secondary Minerals

The distribution of secondary minerals within the site indicates that processes responsible for their formation were dominantly controlled by the amount of fluid that infiltrated the volcanic rocks, the porosity and permeability of the depositional sites, and the temperature and trace element chemistry of the fluids. All of these variables probably changed through time. In general most of the host rocks, except where they are highly welded, are relatively porous and permeable (Whelan et al., in press). However, local porosity and permeability would change as secondary minerals precipitated and closed some fluid pathways. This could result in early mineral precipitation in some localities and later mineral precipitation in other sites. Some variations in the mineral record can be explained by varying fluid compositions and temperatures through time (Wilson et al., 2002). The presence of abundant silica minerals in the NPR and the absence of these minerals in the IFZ are probably related to the presence of early fluids with elevated temperatures and saturated in silica in the NPR, prior to formation of fractures in the IFZ.

An important variable controlling the distribution and abundance of secondary minerals at Yucca Mountain is probably the amount of aqueous fluid that infiltrated the site. Approximately 90 % of the open space at Yucca Mountain contains no secondary minerals or any record of fluid influx. Calculations of the abundance of secondary minerals along 30-m sections at 100 m intervals over the entire ESF showed that < 6 % of fractures greater than 1 m long contain mineral coatings (Whelan et al., in press). Mapping of LC over five 30 m sections indicated that between 1 - 42 % contained secondary minerals and the majority of cavities lacked any secondary mineral record (Whelan et al., in press). Secondary minerals that may have begun to precipitate more than 12 million years ago following deposition of the tuff rarely form

crusts more than a couple centimeters in thickness and, where present, are typically millimeters to less than a centimeter thick. This mineral record contrasts strongly with the sequence of calcite that precipitated at Devils Hole, Nevada under saturated conditions (Winograd et al., 1992). Devils Hole calcite precipitated at an average rate of 0.7 mm/1000 years (Ludwig et al., 1992) producing a thick layer of vein calcite more than 0.3 m thick in 500,000 years (Winograd et al., 1992). The sparse and thin secondary mineral record at Yucca Mountain argues strongly that aqueous fluids did not access most open space at Yucca Mountain or saturate the site in the past. The Yucca Mountain mineral record is, instead, consistent with formation in a vadose environment.

Input from a fluid with a consistent composition at constant temperature over time would produce a consistent secondary mineral record in depositional sites accessed by the fluids. Such a depositional record is exhibited by MGSC, which has been precipitating for the past 1.9–2.9 Ma (Wilson et al., 2002). Although the majority of open spaces do not contain this material, MGSC is distributed across Yucca Mountain, which suggests that there are preferred fluid pathways through the UZ.

8.5. Formation of Secondary Minerals in the Vadose Zone

The question of whether the secondary minerals formed in a vadose or phreatic environment cannot be directly answered, because no single texture observed in the rocks unequivocally identifies the environment of precipitation. This may simply be due to the limited fluid infiltration of the site. However, there are a number of observations that are not consistent with the formation of secondary minerals in the phreatic zone.

First, as discussed above, the majority of primary and secondary porosity contains no evidence of secondary minerals. If secondary minerals precipitated in a phreatic environment by upwelling hydrothermal fluids (Dublyansky, 1998; Dublyansky et al., 2001) or rising ground water (Szymanski, 1987, 1989), a more extensive record of secondary minerals would be expected in the available open space.

Second, some pores in LC, fractures, and breccias are rimmed by thin layers of calcite, suggestive of meniscus textures (e.g. Fig. 3; sample ESF 21+61.8) that indicate precipitation in a vadose environment (James and Choquette, 1990). Some pore fillings exhibit multiple luminescent growth zones under CL indicating multiple fluid events.

Third, the lack of isopachous textures at Yucca Mountain is not consistent with formation in the phreatic zone (James and Choquette, 1990). Our observations are in agreement with observations by USGS scientists (Whelan et al., 1996) that secondary minerals occur predominantly on the footwalls and bases of LC, fractures, and breccias, consistent with precipitation in the vadose zone.

Fourth, detailed growth zoning of MGSC indicates that repeated fluctuations in fluid composition are required to account for the Mg-enriched and depleted growth zoning. Such fluctuations are difficult to reconcile with a saturated environment. The discontinuous nature of the growth zones is consistent with addition of small amounts of fluid with fluctuating Mg concentrations.

Fifth, if upwelling hydrothermal fluids periodically invaded Yucca Mountain, the fluids would be cooled by contact with the colder rocks, and silica minerals, particularly quartz, would precipitate. Although silica minerals are relatively abundant in some samples in the NPR and

SPR, these minerals are part of the early to intermediate assemblages, and silica minerals are sparse in younger assemblages and in other parts of the site.

Sixth, no single location or sample records the entire history of secondary mineralization, suggesting that whatever process was responsible for deposition did not occur uniformly throughout the repository horizon. Such a record is difficult to reconcile with a phreatic environment, but is consistent with mineral precipitation in a vadose zone.

Finally, the presence of glass in the host tuffs suggest that these tuffs have not been below the static water level (Levy, 1991). These data strongly indicate that the volcanic rocks have not been in contact with fluids in a phreatic environment for any length of time during their history.

The above observations argue strongly for precipitation of secondary minerals within a vadose environment. The lack of any features that are typical of a phreatic environment make genetic models involving flooding of the repository by hydrothermal fluids or groundwater untenable. This study, alternatively, indicates that the most reasonable source of fluids responsible for secondary minerals is surficial waters that percolated into the mountain.

9. CONCLUSIONS

Detailed petrographic study of 155 samples collected from localities across the Yucca Mountain site allowed the construction of a paragenetic sequence based on extensive petrography integrated with trace element, isotopic, CL, and LA-ICP-MS analyses. The main conclusions from this study are summarized below.

1. Extensive petrography, paragenetic studies, and microprobe mapping indicate that early secondary minerals were heterogeneously distributed across the site. These early minerals consist of variable amounts of calcite, which is the most abundant mineral in the crusts, and lesser variable opal, chalcedony, fluorite, and quartz. Intermediate minerals consist of primarily calcite, often in distinctive bladed habits, with minor opal, chalcedony and quartz. These minerals contain no diagnostic trace element variations. The latest secondary minerals deposited across the site consist of sparry calcite and minor intergrown opal. This outermost calcite is chemically distinct, contains oscillatory Mg-enriched and depleted growth zones, is associated and intergrown with clear opal, and forms the youngest mineral layer that precipitated across the site. Petrographic studies indicated that secondary mineral crusts at most sample sites recorded an incomplete history of secondary mineral precipitation. Some samples contain only early, intermediate, or late minerals, and few samples exhibit a complete early to late sequence.
2. The youngest secondary minerals that precipitated were Mg-enriched growth zoned sparry calcite (MGSC) and intergrown opal. MGSC occurs in > 65 % of the samples and, with or without associated opal, is always the paragenetically youngest mineral. MGSC has a consistent texture and unique chemical signature, can be correlated across the site in LC, fracture, and breccia occurrences, and links the history of secondary mineral deposition at sample sites across Yucca Mountain. This allows construction of a mineral paragenesis that is representative of secondary minerals across the site and provides a basis for subsequent fluid inclusion and geochronology studies that constrain the time-temperature history of fluid flux through the site.

3. The textures and features of the secondary minerals in the unsaturated zone at Yucca Mountain are not consistent with saturation of the site by aqueous fluids and mineral formation in the phreatic environment, but are consistent with precipitation of secondary minerals in the vadose environment from surficial meteoric fluids. Outermost MGSC formed from the infiltration of small amounts of aqueous fluid. The oscillatory nature of the Mg growth zoning may be related to variations in climate during the last 3 Ma.

Acknowledgements. We would like to thank Joel Rotert, Drew Coleman, and Joe Whelan for their assistance during sample collection. Special thanks go to Mark Mercer (Petrographics, Montrose, CO) for making the spectacular polished sections, and to Bob Bodnar for his technical review of this report. Bob Bodnar, Yuri Dublyanski, Bob Goldstein, Ed Roedder, Joe Whelan and Ike Winograd are thanked for discussions on all aspects of this project. We thank the following for their technical assistance: Sarah Lundberg (UNLV, EPMA), Luis Gonzalez and Scott Carpenter (University of Iowa, stable isotopes), and Paul Lechler (Nevada Bureau of Mines, LA-ICP-MS). Funding for this study was awarded to JSC under DOE Cooperative Agreement DE-FC08-98NV-12081.

All data presented in this paper were collected under the UCCSN Quality Assurance program. Technical Data Management System data tracking number UN0203SPA004JC.001 correlates to data collected during this study. Access to electronic data was limited to task personnel and controlled with the use of passwords. Loss was prevented by use of backup files. Manual entry and file transfers were verified for accuracy. No electronic data were lost or corrupted.

REFERENCES

- Bish D. L. (1989) Evaluation of past and future alterations in tuff at Yucca Mountain, Nevada, based on the clay mineralogy of drill cores USW G-1, G-2, and G-3. Los Alamos National Laboratory Report LA-10667-MS.
- Bish D. L. and Chipera S. J. (1989) Revised mineralogic summary of Yucca Mountain, Nevada. Los Alamos Nat. Lab. Rept. LA-11497-MS.
- Buesch D. C., Spengler R. W., Moyer T. C. and Geslin J. K. (1996) Proposed stratigraphic nomenclature and macroscopic identification of lithostratigraphic units of the Paintbrush Group exposed at Yucca Mountain, Nevada. U. S. Geological Survey Open-File Report.
- Caporusico F., Vaniman D., Bish D., Broxton D., Arney B., Heiken G., Byers F., Gooley R. and Semarge E. (1982) Petrographic studies of drill cores USW G-2 and UE25b-1H, Yucca Mountain, Nevada. Los Alamos National Laboratory Report LA-10927-MS.
- Carlos B. A. (1994) Field guide to fracture-lining minerals at Yucca Mountain. Los Alamos National Lab. Rep. LA-12803-MS.
- Christiansen R. L., Lipman P. W., Carr W. J., Byers F. M Jr., Orkild P. P. and Sargent K. A. (1977) Timber Mountain-Oasis Valley caldera complex of southern Nevada. *GSA Bulletin* **88**, 943-959.
- Coplen T. B., Kendall C. and Hopple J. (1983) Comparison of stable isotope reference samples. *Nature* **302**, 236-238.
- Data Tracking Number UN0203SPA004JC.001. Thermochronological evolution of calcite formation at Yucca Mountain. Submittal date: 03/26/2002.
- Day W. C., Dickerson R. P., Potter C. J., Sweetkind D. S., San Juan, C. A., Drake R. M and Fridrich C. J. (1998) Bedrock geologic map of the Yucca Mountain area, Nye County, Nevada. *Geologic Investigations Series* - U. S. Geol. Survey. pp. 21, 1 sheet.
- Denniston R. F., Shearer C. K., Layne G. D. and Vaniman D. T. (1997) SIMS analyses of minor and trace element distributions in fracture calcite from Yucca Mountain, Nevada, USA. *Geochim. Cosmochim. Acta* **61**, 1803-1818.
- Dublyansky Y. (1998) Fluid inclusion studies of samples from the Exploratory Study Facility, Yucca Mountain, Nevada. Institute for Energy and Environmental Research Report, Washington.
- Dublyansky Y., Szymanski J., Chepizhko A., Lapin B. and Reutsky V. (1998) Geological history of Yucca Mountain (Nevada) and the problem of a high-level nuclear waste repository. In *Defense Nuclear Waste Disposal in Russia* (eds. M. Stenhouse and V. Kirko). NATO Series, Kluwer Academic Publishing, Netherlands, pp. 279-292.
- Dublyansky Y., Ford D. and Reutski V. (2001) Traces of epigenetic hydrothermal activity at Yucca Mountain, Nevada: preliminary data on the fluid inclusion and stable isotope evidence. *Chemical Geology* **173**, 125-149.
- Hay R. L., Pexton R. E., Teague T. T. and Kyser T. K. (1986) Spring-related carbonate rocks, Mg clays, and associated minerals in Pliocene deposits of the Amargosa Desert, Nevada and California. *GSA Bulletin* **97**, 1488-1503.
- Heizler M. T., Perry F. V., Crowe B. M., Peters L. and Appelt R. (1999) The age of the Lathrop Wells volcanic center: an $^{40}\text{Ar}/^{39}\text{Ar}$ dating investigation. *Jour. Geophys. Res.* **104**, 767-804.
- James, N.P. and Choquette, P.W. (1990) Limestones - the meteoric diagenetic environment. In *Diagenesis* (eds. I.A. McIlreath, and D.W. Morrow). Geoscience Canada Reprint Series

- 4, p. 35-73.
- Levy S. (1991) Mineralogic Alteration History and Paleohydrology at Yucca Mountain, Nevada, High Level Radioactive Waste Management, *Proc. Conf. High Level Rad. Waste Mgmt.*, 477-485.
- Levy S. S., Norman D. I. and Chipera S. J. (1996) Alteration history studies in the Exploratory Studies Facility, Yucca Mountain, Nevada, USA. *Proceedings of the Materials Research Society*, 412-790.
- Ludwig K. R., Simmons K. R., Szabo B. J., Winograd I. J., Landwehr J. M., Riggs A. C. and Hoffman R. J. (1992) Mass-spectrometric ^{230}Th - ^{234}U - ^{238}U dating of the Devils Hole calcite vein. *Science* **258**, 284-287.
- Machel H. G., Mason R. A., Mariano A. N. and Mucci A. (1991) Causes and emission of luminescence in calcite and dolomite. In *Luminescence Microscopy and Spectroscopy – Qualitative and quantitative applications* (eds. C. E. Barker and O. C. Kopp). Society for Sedimentary Geology, Short course 25, pp. 9-25.
- Mongano G. S., Singleton W. L., Moyer T. C., Beason S. C., Eatman G. L. W., Albin A. L. and Lung R.C. (1999) Geology of the ECRB Cross Drift - Exploratory Studies Facility, Yucca Mountain Project, Yucca Mountain, Nevada. U.S. Department Of Energy.
- Paces J. B., Neymark L. A., Marshall B. D., Whelan J. F. and Peterman Z. E. (1996) Ages and origins of subsurface secondary minerals in the exploratory studies facility (ESF). U.S. Geological Survey – Yucca Mountain Project Branch, Milestone report 3GQH450M.
- Paces J. B., Marshall. B. D., Whelan, J. F. and Neymark L. A. (1997) Progress Report on Unsaturated Zone Stable and Radiogenic Isotope Studies, U.S. Geological Survey Milestone report SPC23FM4.
- Paces J. B., Neymark, L. A., Marshall, B. D., Whelan J. F. and Peterman Z. E. (2001) Ages and origins of calcite and opal in the Exploratory Studies Facility Tunnel, Yucca Mountain, Nevada. U.S. Geological Survey, Water-Resources Investigations Report 01-4049.
- Pruher L. M. and Rea D. K. (1998) Rapid onset of glacial conditions in the subarctic North Pacific region at 2.67 Ma: Clues to causality. *Geology* **26**, 1027-1030.
- Sawyer D. A., Fleck R. J., Lanphere M. A., Warren R. G., Broxton D. E. and Hudson M. R. (1994) Episodic Caldera Volcanism in the Miocene Southwestern Nevada Volcanic Field: Revised Stratigraphic Framework, $^{40}\text{Ar}/^{39}\text{Ar}$ Geochronology, and Implications for Magmatism and Extension. *GSA Bulletin* **106**, 1304-1318.
- Scoffin T. P. (1987) *An introduction to carbonate sediments and rocks*, Blackie and Son Ltd., Glasgow.
- Smith G. L., Barczak V. J., Moulton G. and Liddicoat J. C. (1983) Core KM-3, a surface to bedrock record of late Cenozoic sedimentation in Searles Valley, California: U.S. Geological Survey Prof. Paper 1256.
- Stewart J. H. (1988) Tectonics of the Walker Lane Belt, Western Great Basin – Mesozoic and Cenozoic Deformation in a Zone of Shear. In *Metamorphism and crustal evolution of the western United States* (ed. W. G. Ernst), Vol. VII, Prentice-Hall Inc., New Jersey, pp. 684-713.
- Stuckless J. S. and Dudley W. W. (2001) The Geohydrologic Setting of Yucca Mountain, Nevada. *Applied Geochemistry*, in press.
- Szymanski J. S. (1987) Conceptual considerations of the Death Valley Groundwater System with Special Emphasis on the Adequacy of this System to Accommodate the High-Level

- Nuclear Waste Repository (Draft). DOE internal report, Yucca Mountain Project Office, Las Vegas Nevada.
- Szymanski J. S. (1989) Conceptual considerations of the Yucca Mountain Groundwater System with Special Emphasis on the Adequacy of this System to Accommodate the High-Level Nuclear Waste Repository. DOE internal report, Yucca Mountain Project Office, Las Vegas Nevada.
- U.S. Department of Energy (1988) Site characterization plan, Yucca Mountain site, Nevada research and development area, Nevada. U.S. Dept. Energy Report, DOE/RW-0199-8 Volumes.
- Vaniman D. T. (1993) Calcite deposits in fractures at Yucca Mountain, Nevada. *Proc. 4th Intl. Conf. High level Rad. Waste Mgmt.*, 1935-1939.
- Vaniman D. T. (1994) Calcite deposits in drill cores USW G-2 and USW GU-3/G-3 at Yucca Mountain, Nevada. Los Alamos National Lab. Rept. LA-12720-MS.
- Vaniman D. T. and Chipera S. J. (1996) Paleo-transport of lanthanides and strontium recorded in calcite compositions from tuffs at Yucca Mountain, Nevada. *Geochim. Cosmochim. Acta* **60**, 4417-4433.
- Whelan J. F. and Moscati R. J. (1998) 9 m.y. record of southern Nevada climate from Yucca Mountain secondary minerals. *Proc. Eighth Conf. High Level Rad. Waste Mgmt.*, 12-15.
- Whelan J. F., Vaniman D. T., Stuckless J. S. and Moscati R. J. (1994) Paleoclimatic and paleohydrologic records from secondary calcite: Yucca Mountain, NV. *Proc. Conf. High Level Rad. Waste Mgmt.*, 2738-2745.
- Whelan J. F., Moscati R. J., Allerton S. B. M. and Marshall. B. D. (1996) Applications of isotope geochemistry to the reconstruction of Yucca Mountain, Nevada, Paleohydrology – status of investigations. U.S. Geological Survey, Open-file report 98-83.
- Whelan J. F., Moscati R. J., Allerton S. B. M. and Marshall. B. D. (1998) Applications of isotope geochemistry to the reconstruction of Yucca Mountain, Nevada, Paleohydrology – status of investigations. U.S. Geological Survey, Open-file report.
- Whelan J. F., Paces J. B., Neymark L. A. and Peterman, Z. E. (2000) Thermochronology of fluid inclusions in Secondary Calcite from the Unsaturated Zone at Yucca Mountain, Nevada. U.S. Geological Survey Fiscal Year 2000 Status Report.
- Whelan J. F., Roedder E. and Paces J. B. (2001) Evidence for an unsaturated-zone origin of secondary minerals in Yucca Mountain, Nevada, *Proc. Conf. High Level Rad. Waste Mgmt.*, N1.
- Whelan J. F., Paces J. B. and Peterman Z. E. Paragenetic Relations and Evidence for Secondary Mineral Formation in Unsaturated-zone Tuffs at Yucca Mountain, Nevada. *Applied Geochemistry*, (in press).
- Wilson N. S. F., Cline J. S. and Amelin Y. (2002) Thermochronological Evolution of Calcite Formation at the Potential Yucca Mountain Repository Site, Nevada: Part 2, Fluid Inclusion Analyses and U-Pb Dating, *Companion report submitted to DOE*.
- Winograd I. J. (1981) Radioactive waste disposal in thick unsaturated zones. *Science* **212**, 1457-1464.
- Winograd I. J., Coplen T. B., Landwehr J. M., Riggs A. C., Ludwig K. R., Szabo B. J., Kolesar P. T. and Revesz K. M. (1992) Continuous 500,000-year climate record from vein calcite in Devils Hole, Nevada. *Science* **258**, 255-260.

FIGURE AND TABLE CAPTIONS

- Fig. 1** Simplified location and geological map and cross section of Yucca Mountain, Nevada (adapted from Day et al., 1998 and Paces et al., 2000). Cross section shows the underground location of the potential repository. Stratigraphic units are after Buesch et al. (1996). Approximate locations of the water table, unsaturated zone and saturated zone are also shown.
- Fig. 2** Location of samples collected from the Exploratory Studies Facility (ESF), ECRB Cross Drift (ECRB), and exploratory alcoves. Unfilled circles indicate samples from a LC, whereas filled circles indicate samples from a fracture or breccia occurrence. To simplify discussion in the text the site has been divided into the following zones; North portal and ramp (NPR), Lithophysal Cavity Zone (LCZ), Intensely Fractured Zone (IFZ), South Portal and Ramp (SPR), and ECRB Cross Drift (ECRB).
- Fig. 3** Images of standard polished sections (~ 3.5 cm wide) illustrating the variation of open space secondary minerals in LC (A – C), fractures (D – F), and breccias (G – I). Arrows in the lower left corners indicate the growth direction of secondary minerals. Sample ESF 48+11 (D) contains multiple slices of a thin mineral crust; in all cases the crusts precipitated towards the top of the section. Sample ECRB 12+90 (G) contains two sections of the mineral crust mounted on the same slide. The bases of the crusts are at the top and bottom of the section. The white arrows in (H) highlight thin layers of calcite that rim open pores and are suggestive of meniscus textures commonly found in the vadose zone. Abundant open spaced is preserved in all LC, fracture, and breccia occurrences. (Cdy = Chalcedony, Qtz = Quartz, C = Calcite, O = Opal)
- Fig. 4** Composite photomicrographs illustrating mineral and textural relationships in secondary mineral crusts. The large arrows indicate the growth direction of the mineral crusts. Photomicrographs were taken in plane-polarized light (PPL), crossed polarized light (XPL), or partially crossed polarized light (PXPL). All sections were 100 μm thick resulting in higher order interference colors. The dashed white lines mark the boundary between MGSC and earlier minerals. (A) Photomicrograph in PPL of finer-grained calcite at the base of a LC, overgrowing tridymite (T) and being overgrown by bladed calcite (slender crystals) in the LCZ. Early bladed calcite consists of smaller slender blades on the scale of a few millimeters while later calcite blades are longer. (B) Early blocky, dark calcite in PPL that encompasses vapor-phase tridymite (T) and tuff pieces at the base of a LC. (C) Bladed calcite (PXPL) overgrown by MGSC and opal at the outer edge of a LC crust. The white arrows indicate growth zones in MGSC. Note that opal is concordant (opal layers) and discordant (outer opal) with respect to the growth zoning. (D) Fracture sample from the NPR in PPL containing tridymite (T), overlain by chalcedony, and then, in turn, by brown opal and MGSC. (E) Photomicrograph (PPL) of opal layers and hemispheres within MGSC from a LC crust. Opal hemispheres highlight previous depositional surfaces. MGSC and opal overgrew earlier 'nail head' calcite (see Fig. 5C). (F) Chalcedony layer (XPL) within a calcite crust from a LC. Vapor-phase tridymite (T) is overgrown by basal calcite and some dissolution of this calcite was followed by precipitation of chalcedony. Chalcedony is overgrown by clear, bladed

calcite that is in turn, overgrown by MGSC. (G) Layered calcite (PPL) at the contact of the secondary minerals with the wall rock from a fracture occurrence in the IFZ. (H) Fracture / breccia sample (PPL) from the IFZ containing fluorite growing around the host tuff and overlain by a number of generations of calcite. The layered calcite, which occurs adjacent to the wall rock in G occurs within open space fillings and is overgrown by later secondary minerals. This indicates that older material fell into the breccia and was cemented by younger minerals. Outer non-descript calcite overgrows the host rock and is the youngest secondary mineral in the sample. This section shows that paragenetically early material, including fluorite and host tuff, can be spatially but not temporally related to paragenetically late minerals. (I) Fracture sample (PXPL) from the NPR containing calcite (Cal) replaced by chalcedony. White arrows indicate anhedral calcite remnants in the chalcedony and black arrows highlight an early calcite cleavage pseudomorphed by chalcedony. Chalcedony contains inclusions of fluorite and is overgrown by quartz, which in turn is overgrown by MGSC and brownish opal (O). (J) Chalcedony-brown opal-quartz layers (XPL) in a LC crust. Chalcedony occurs as a number of discrete layers and commonly contains euhedral quartz crystals on the outermost edges of the growths. (K) Quartz (PPL) at the basal part of a fracture crust from the NPR containing small cubic crystals and nodules of fluorite (Fl). (L) Cathodoluminescence in basal calcite, from the IFZ, illustrating detailed oscillatory growth zoning. Growth zones are typically planar or rounded and approximately 50 μm thick. Truncated growth zoning highlights breaks in precipitation.

Fig. 5 Pairs of backscatter electron (BSE; left) images and Mg X-ray maps (right) illustrating the presence and absence of Mg in calcite. In the Mg maps the lighter color indicates higher concentrations of Mg. Quantitative analyses (in wt. %) for Mg are indicated on the maps. (A) Map from the basal part of a LC crust with vapor-phase tridymite overgrown by fluorite (Fl) and then by early calcite. Calcite growing around tridymite and fluorite contains patchy Mg-enriched calcite (PMC). Calcite from the center of the map does not contain detectable Mg. (B) Map of LC calcite crust (shown in Fig. 5F) from tridymite at the base outward to basal calcite and a chalcedony layer, to bladed calcite and MGSC (top). PMC occurs around the tridymite and adjacent to the wall rock and is not clearly related to crystal growth. The majority of the crust, including bladed calcite, does not contain detectable Mg. Bladed calcite is overgrown by MGSC containing clearly visible individual growth zones. Textures indicating dissolution of calcite at the base of the chalcedony are visible in the BSE image. (C) Map across a LC crust from basal calcite to outer MGSC. In BSE imaging irregular calcite at the base of the section is overgrown by clear calcite and then by MGSC associated with opal. Opal layers mark the boundary between basal and intermediate calcite and approximately mark the boundary between intermediate calcite and MGSC. The Mg map clearly shows that MGSC occurs only on the outermost part of the sample. The preexisting depositional surface for MGSC is indicated by the dashed white line and delineates the distinctive 'nail head' crystals. The dashed line also indicates that MGSC and intermediate calcite cannot be distinguished based on petrography alone, and that opal layers dated from within MGSC (see Wilson et al., 2002) formed after MGSC had begun precipitating.

- Fig. 6 Detailed X-ray map for Mg (up to 1 wt. %) illustrating the complex enriched and depleted Mg growth zoning present in MGSC (fracture sample ESF 78+41). Growth zones are locally discontinuous and cannot be traced across the sample. Bright spots are edge effects and do not represent high levels of Mg.
- Fig. 7 Plot of $\delta^{13}\text{C}$ versus $\delta^{18}\text{O}$ for micro-milled calcite samples. Calcite samples are grouped according to calcite morphologies and/or paragenetic position in secondary mineral crusts. Filled symbols indicate samples that contained 2-phase fluid inclusions (see Wilson et al., 2002).
- Fig. 8 Schematic illustration shows the paragenetic sequence of secondary minerals at Yucca Mountain. The left side of the figure represents fracture and breccia occurrences, and the right side illustrates LC crusts. Although there are significant differences, consistent mineral relationships are observed in LC and fracture and breccia occurrences. The figure illustrates the variable and heterogeneous nature of early secondary minerals, which contrasts significantly with the consistent presence of MGSC \pm opal as the youngest, outermost minerals.

Table 1. C and O stable isotope data for calcite samples and calibration standards.

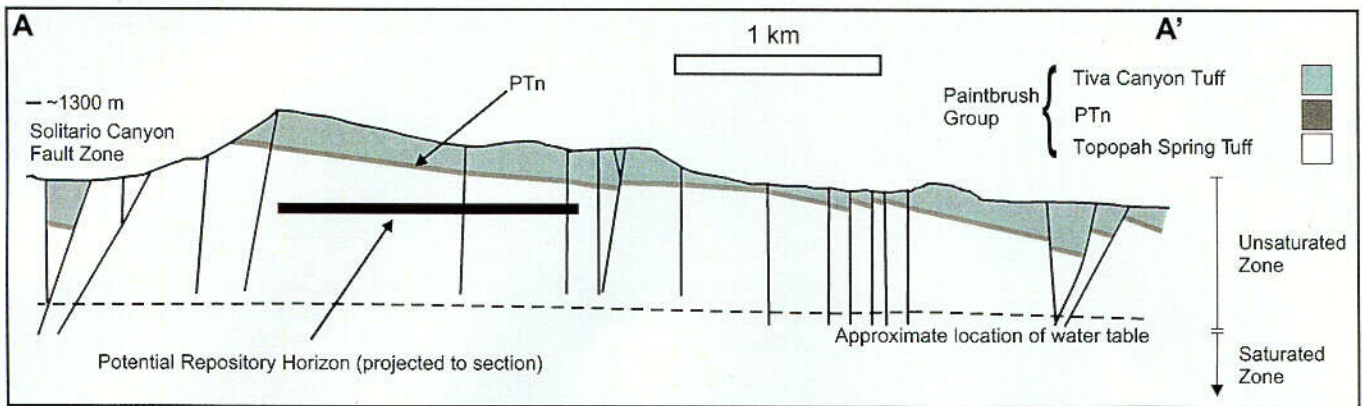
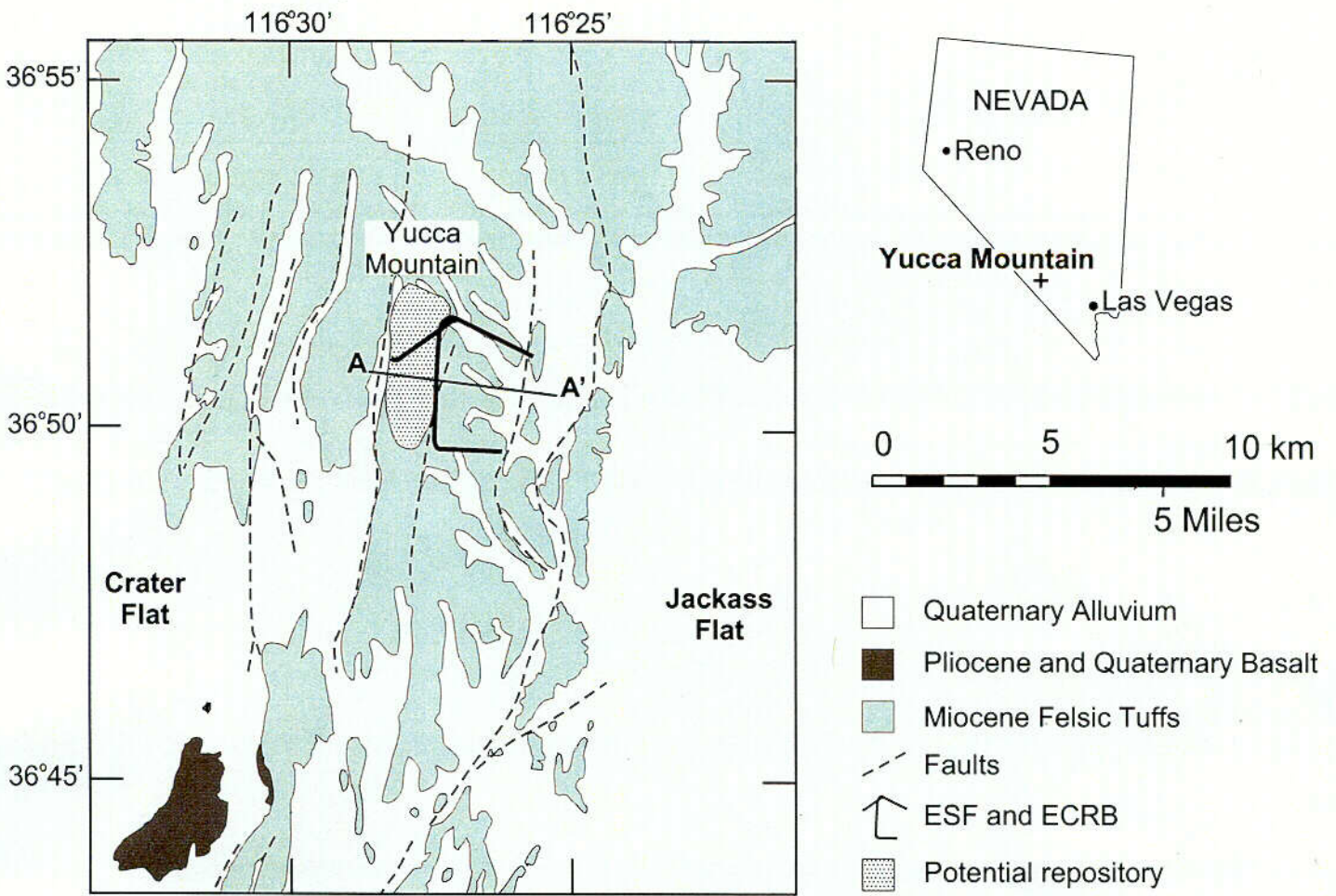


Figure 1

col

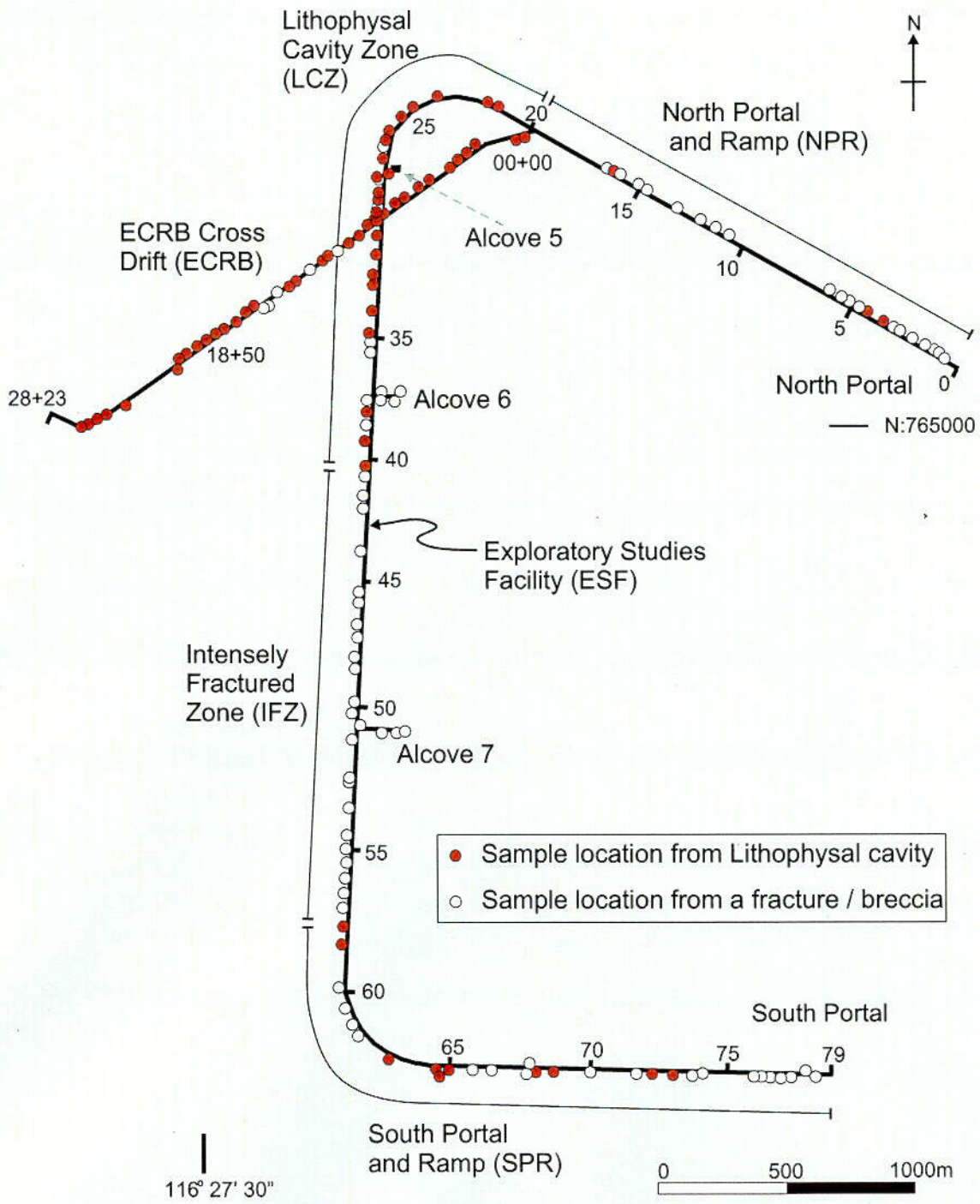
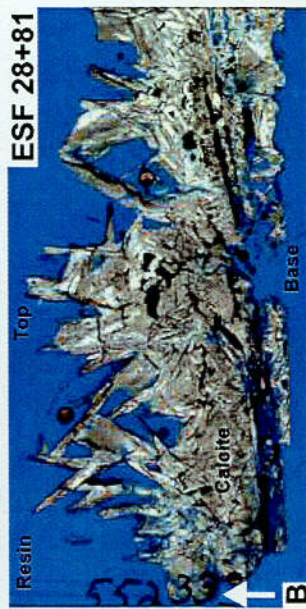
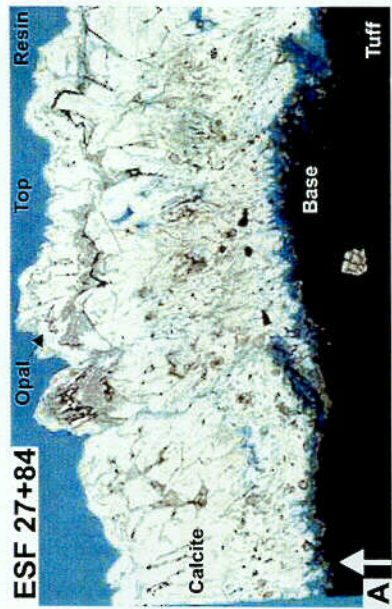


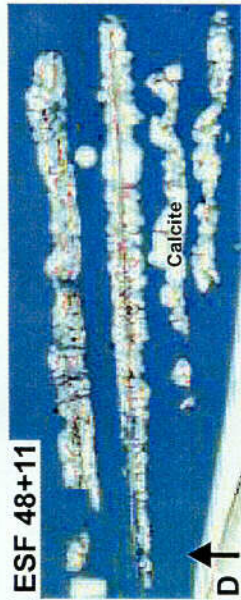
Figure 2

COZ

Lithophysal Cavities



Fractures



Breccias

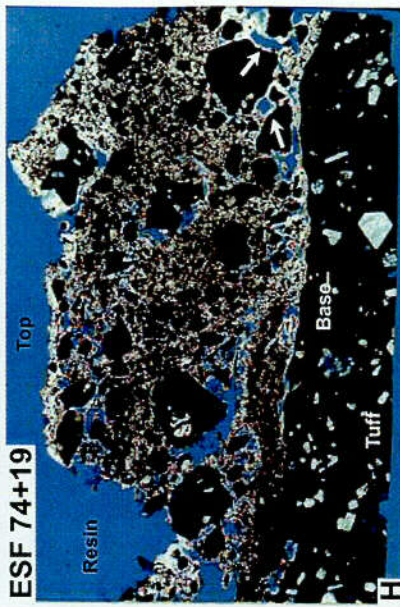
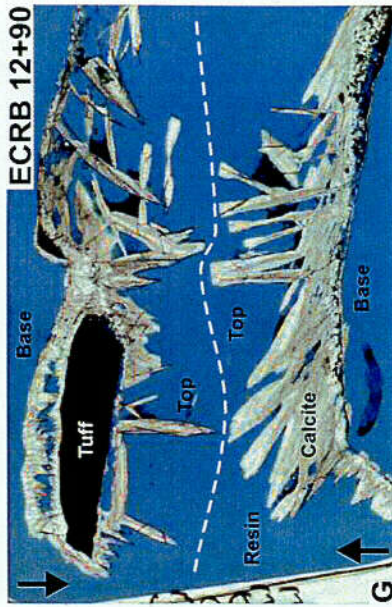


Figure 3

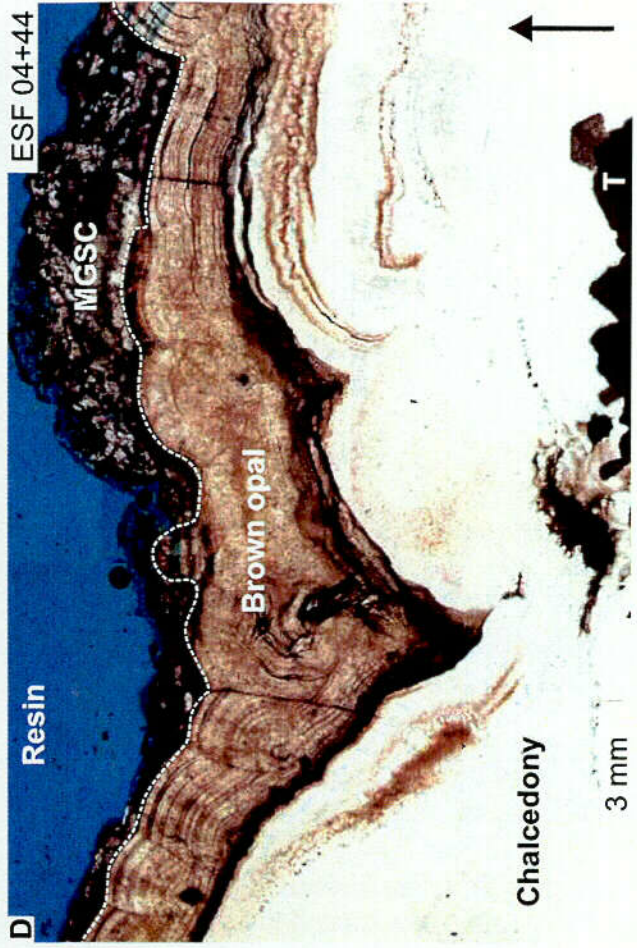
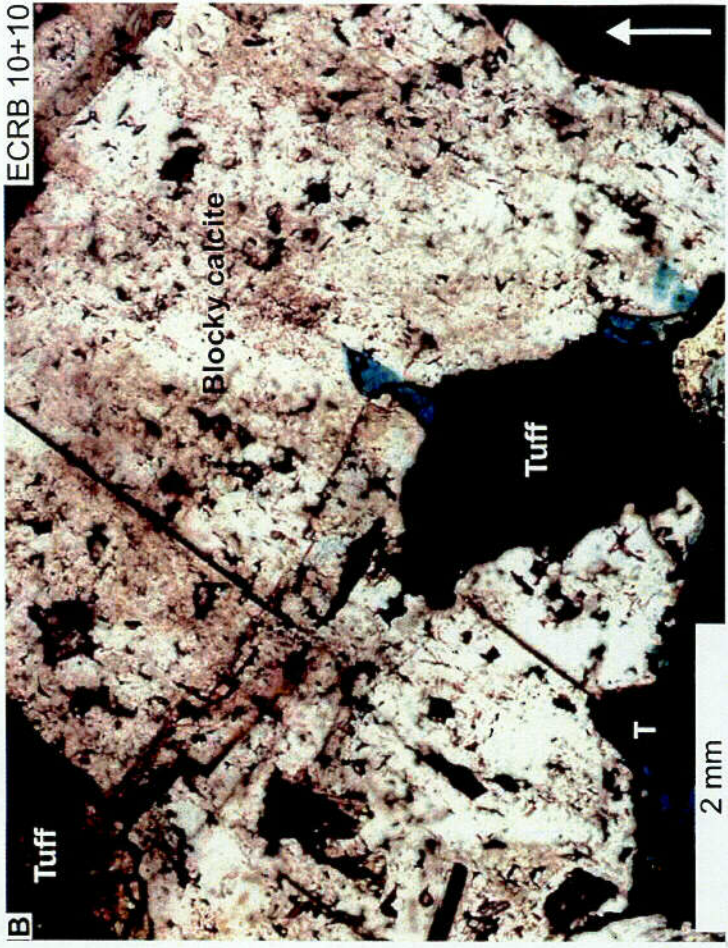
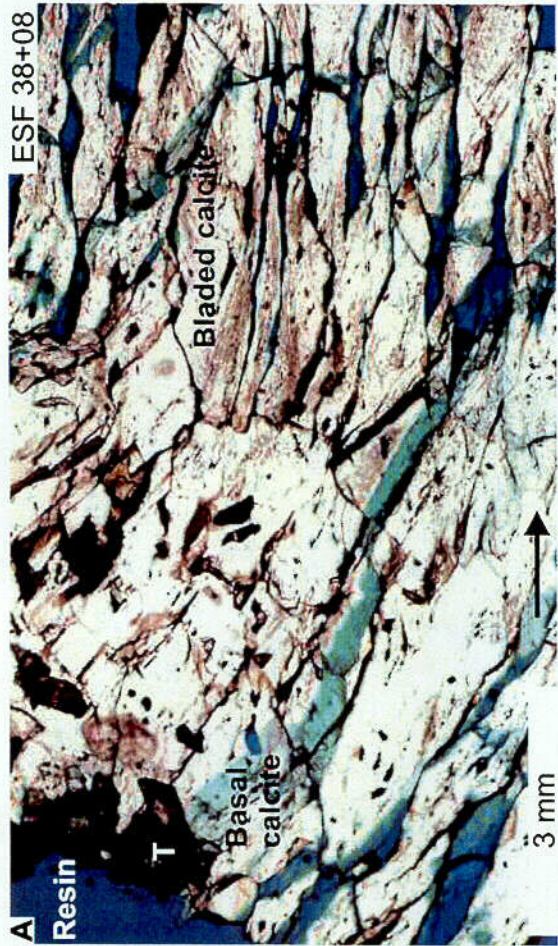


Figure 4

C04

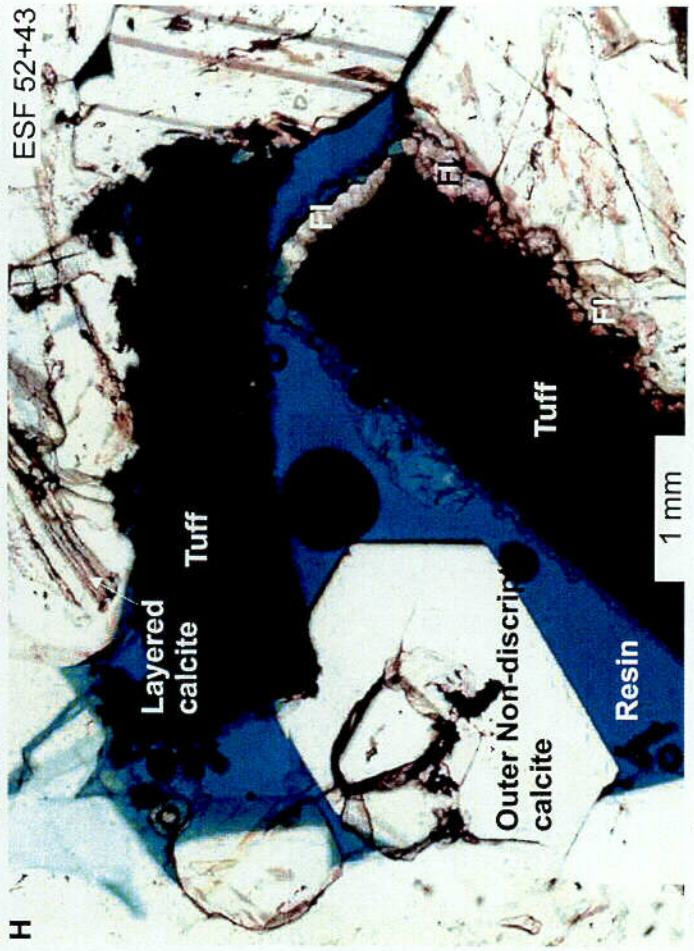
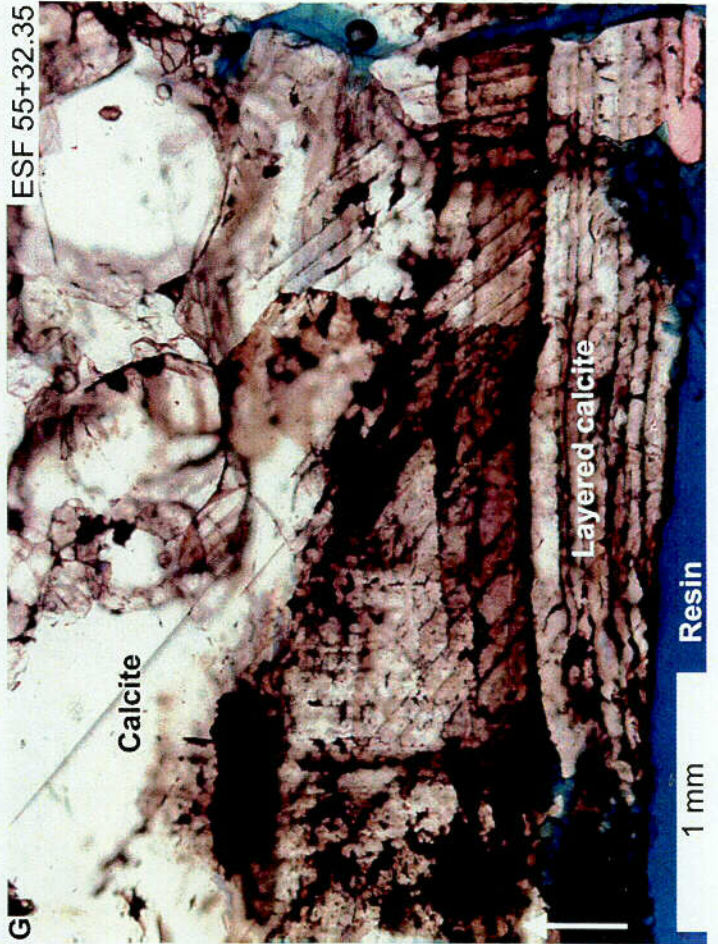
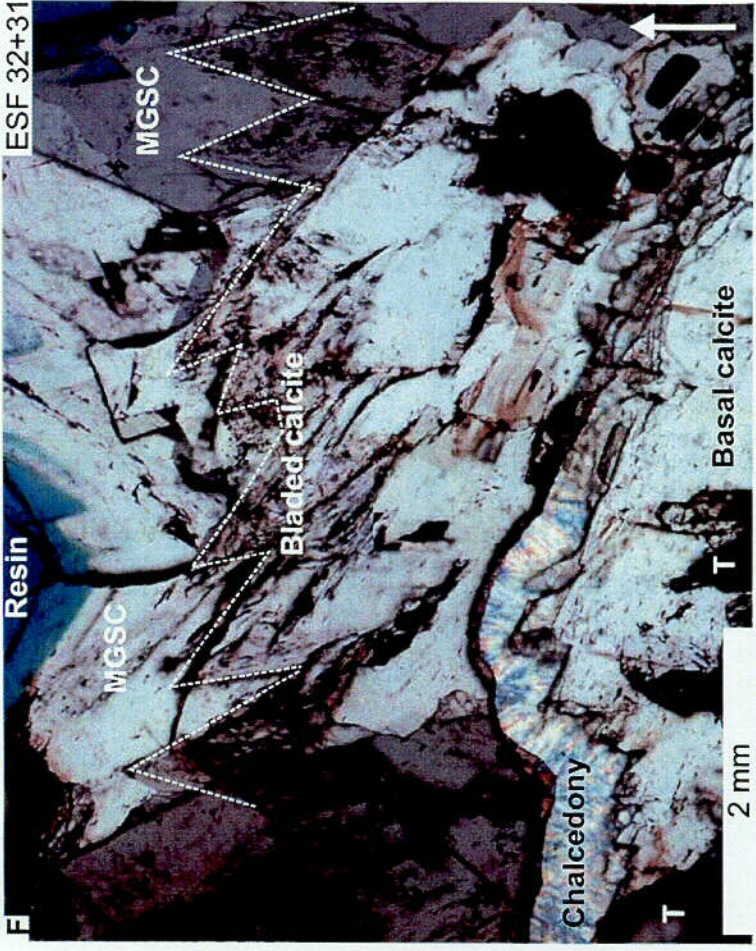
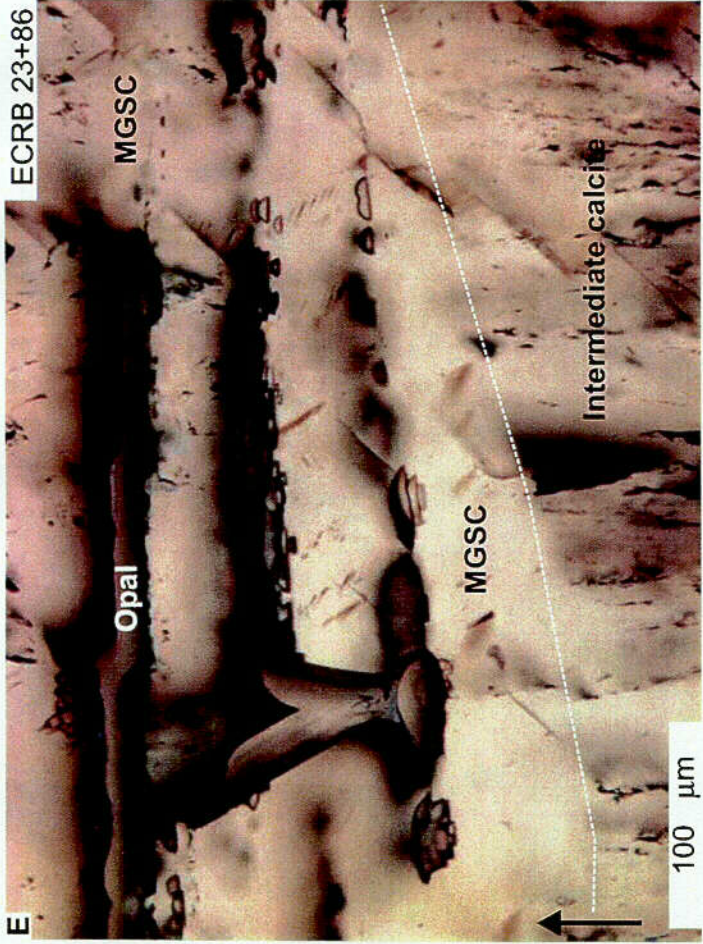
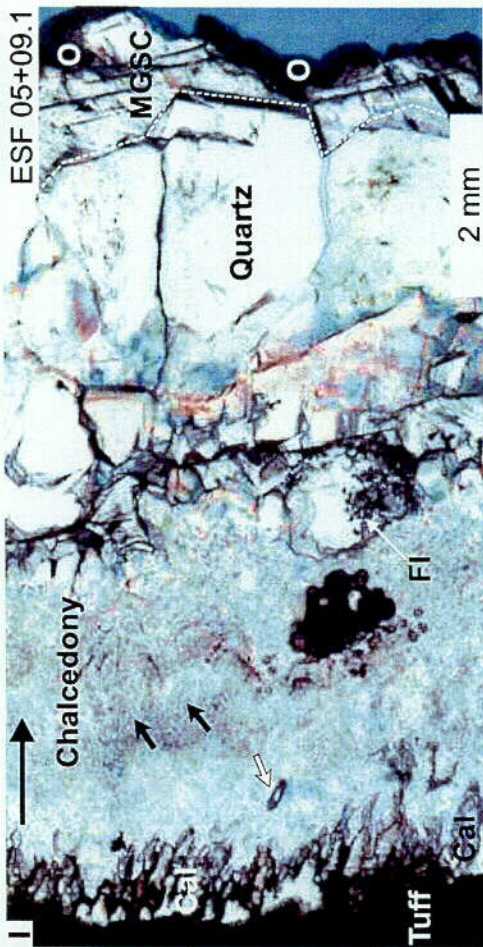


Figure 4

Figure 4



J

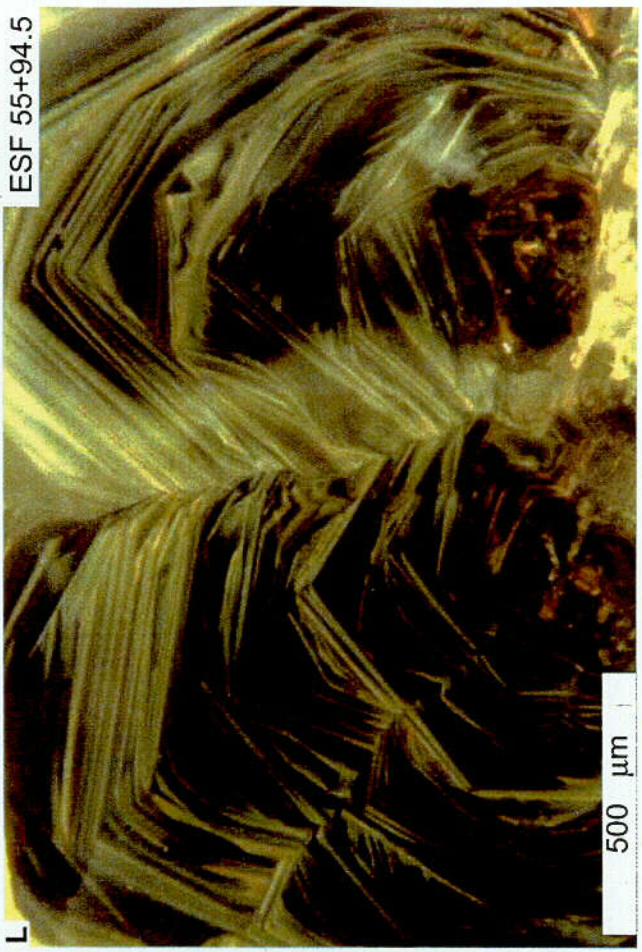
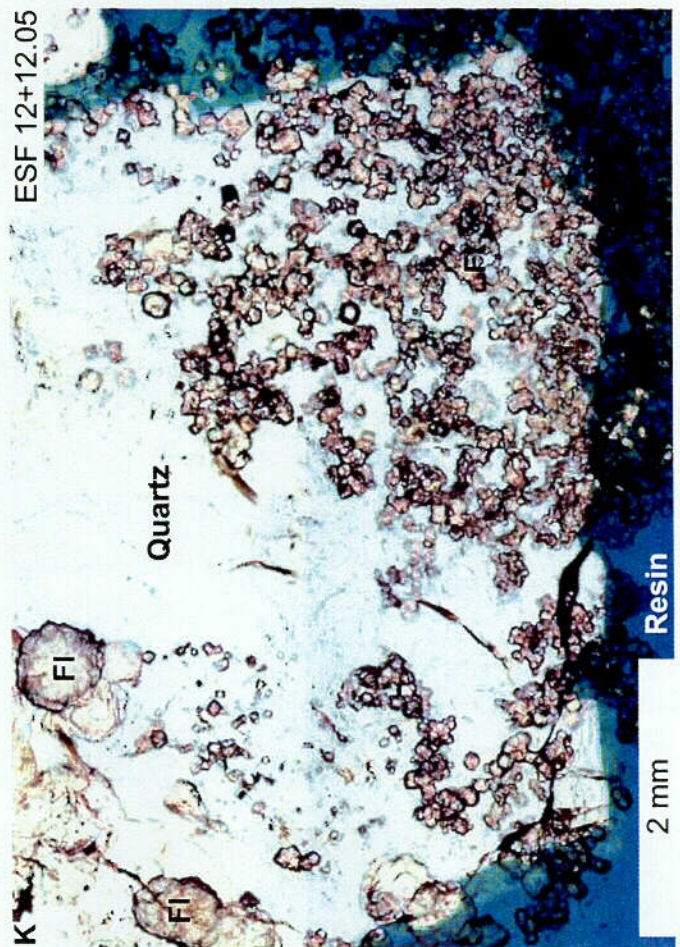
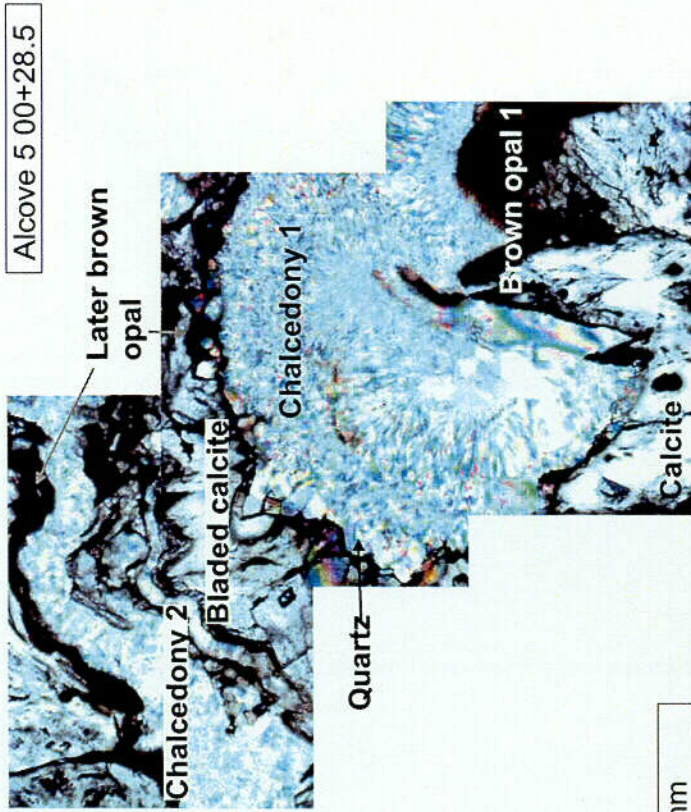
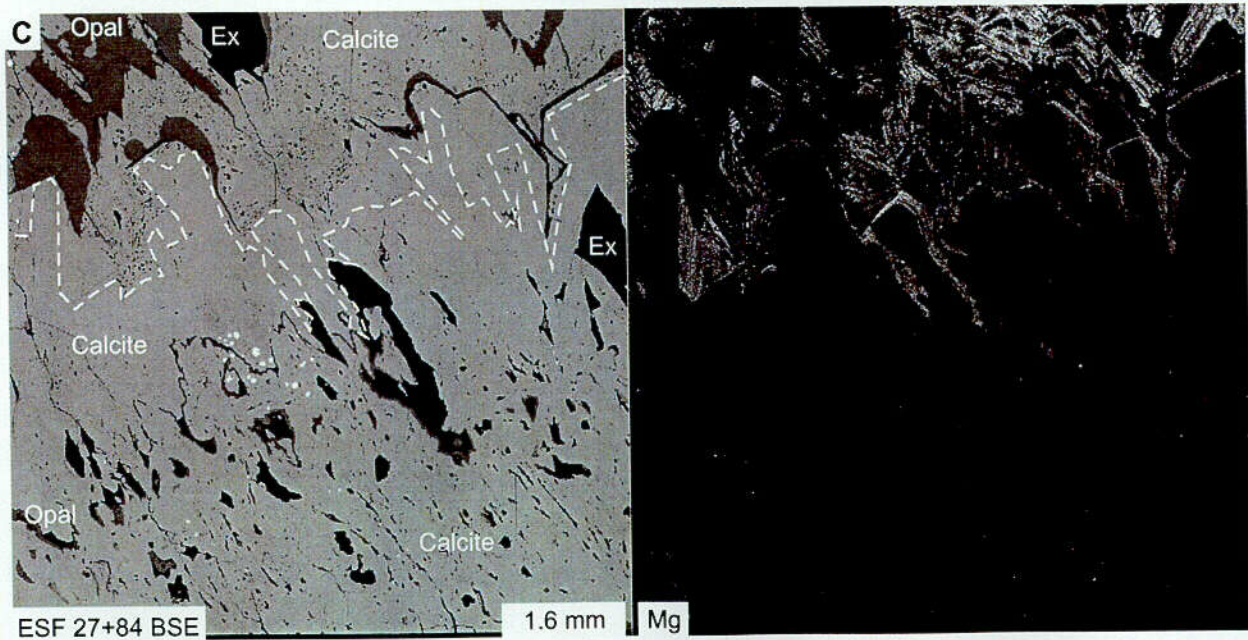
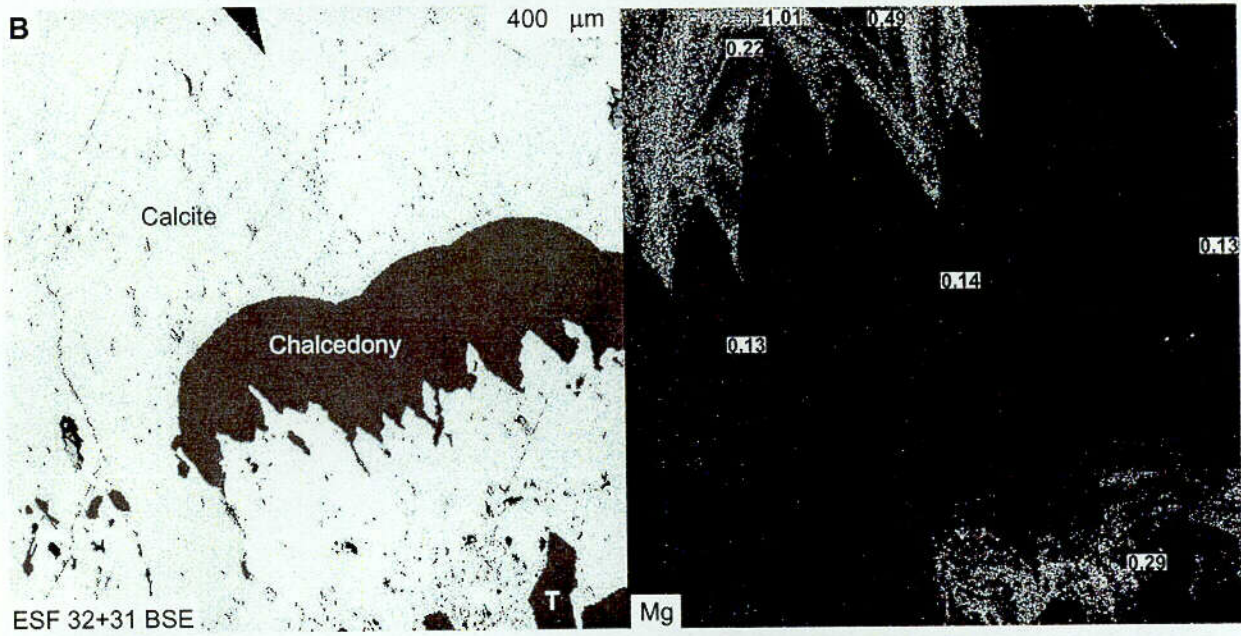
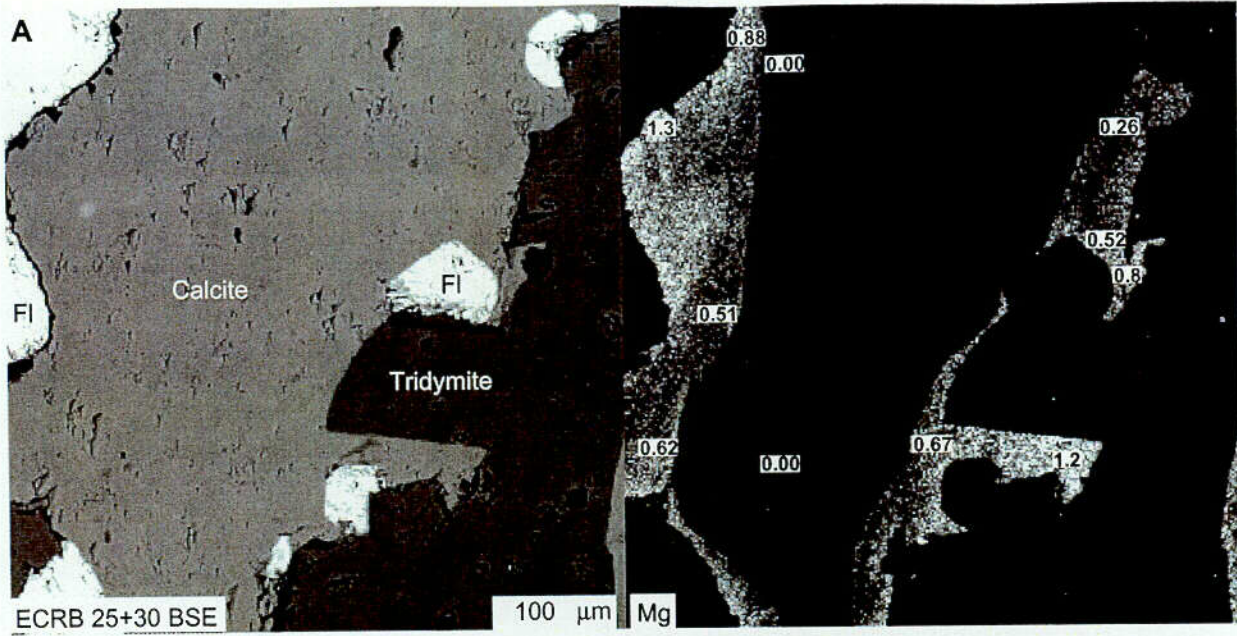
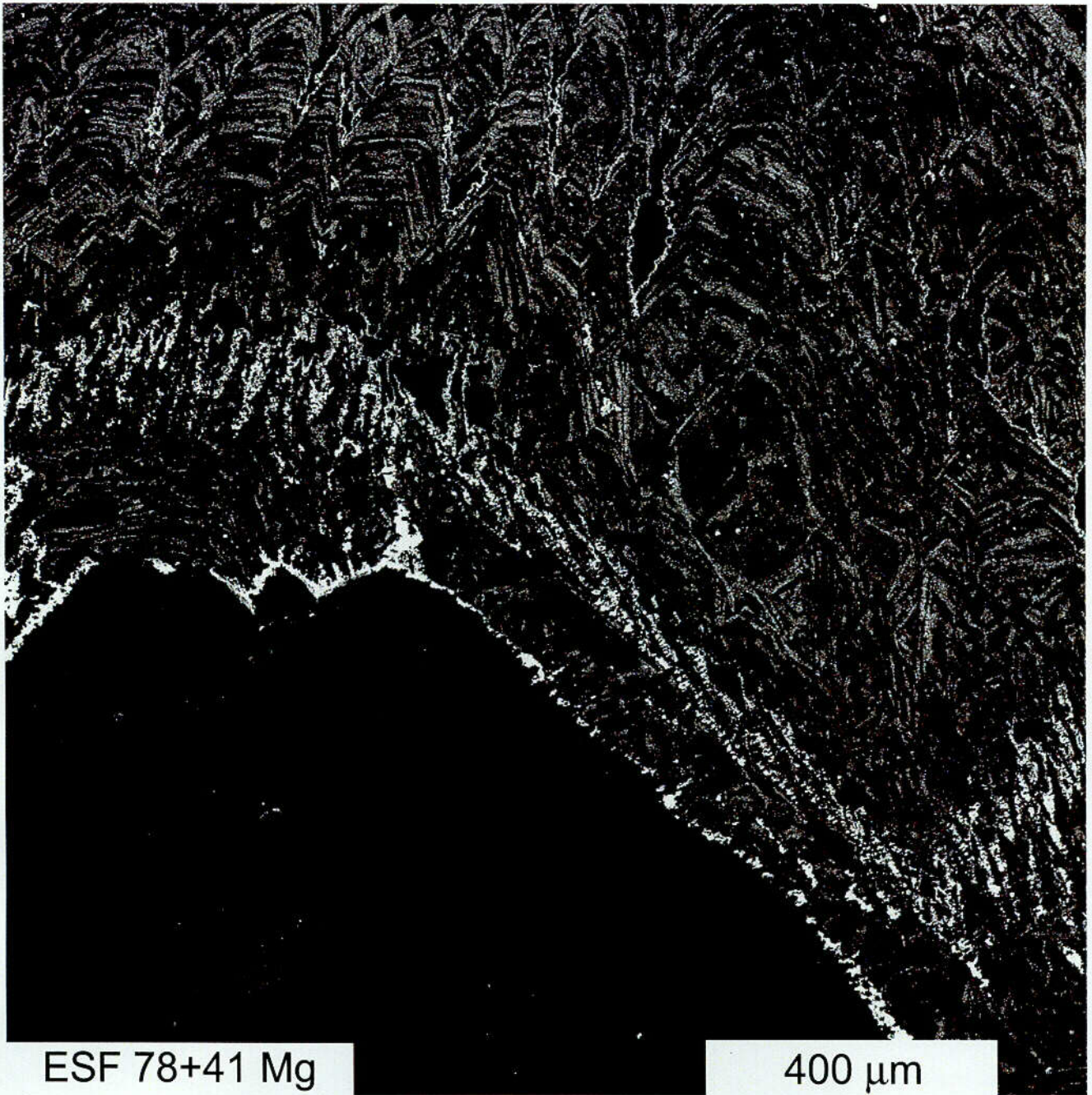


Figure 5



C07



ESF 78+41 Mg

400 μm

Figure 6

C08

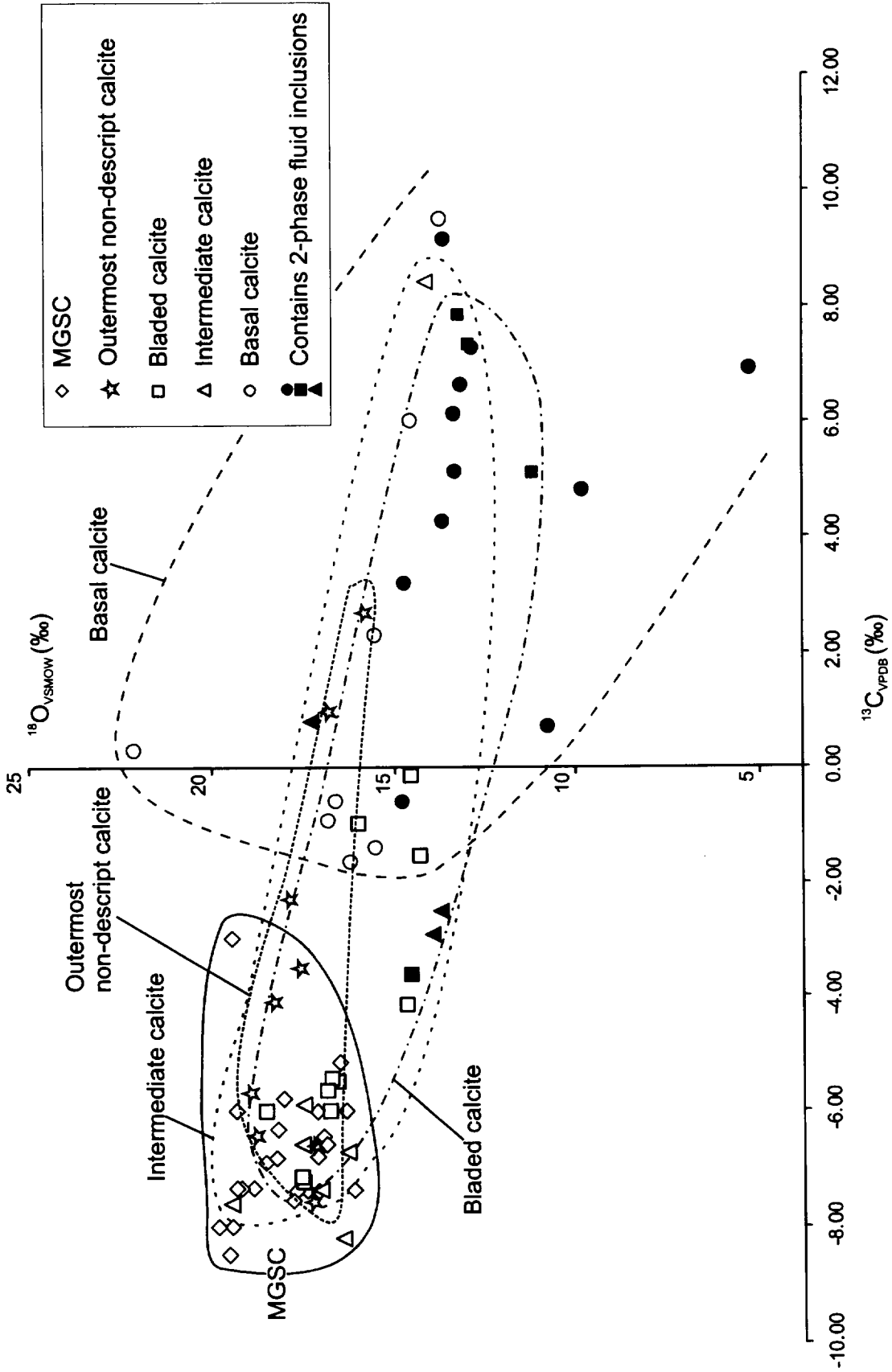


Figure 7

Fracture / Breccia | Lithophysal Cavities



Figure 8

C09

Table 1. C and O isotope data for calcite samples and calibration standards

Sample	Sample Split	Sample description	$\delta^{13}\text{C}$ (‰)	$\delta^{18}\text{O}$ (‰)
ECRB 04+87	B17	Basal calcite	-1.4	15.5
ECRB 04+87	B16	Bladed calcite	-4.2	14.7
ECRB 04+87	A2	Bladed calcite	-5.5	16.6
ECRB 04+87	A3	MGSC	-7.3	17.4
ECRB 12+90*	A1	Basal calcite	9.1	13.6
ECRB 12+90	B11	Bladed calcite	-1.0	16.0
ECRB 12+90	A2	Intermediate calcite	-6.6	17.6
ECRB 12+90	A3	MGSC	-6.4	17.0
ECRB 12+90	B12	MGSC	-6.6	16.9
ECRB 14+69	A1	Basal calcite	3.9	15.3
ECRB 14+69	A2	Outer basal calcite	-1.6	16.2
ECRB 14+69	A4	MGSC	-6.6	17.1
ESF 01+62.3*	A1	Basal calcite	0.7	10.9
ESF 01+62.3*	A2	Intermediate calcite	0.8	17.1
ESF 01+62.3	A3	Outer non-descript calcite	-4.1	18.3
ESF 01+62.3	A4	Outer non-descript calcite	-5.7	19.0
ESF 04+73.4*	B10	Basal calcite	6.8	5.2
ESF 04+73.4	A3	MGSC	-6.0	19.4
ESF 05+09.1	A1	outer sparry calcite	-3.0	19.5
ESF 13+19	A2	outer clear calcite above fluorite and quartz	-2.3	17.9
ESF 14+75.8*	A4	Basal calcite	4.8	9.9
ESF 27+84*	B6	Basal calcite	5.1	13.3
ESF27+84*	C17	Central basal calcite	-0.6	14.8
ESF 27+84	B8	Intermediate calcite	-6.7	16.3
ESF 27+84	A1	Intermediate calcite	-8.2	16.4
ESF 27+84	A2	MGSC	-7.3	16.2
ESF 27+84	A3	MGSC	-7.3	17.1
AL#5 00+28.5*	C10	Basal calcite	7.2	12.9
AL#5 00+28.5*	C11	Outer basal calcite	4.2	13.7
AL#5 00+28.5*	C12	Intermediate calcite	-2.5	13.4
AL#5 00+28.5*	C15	Intermediate calcite	-2.9	13.7
AL#5 00+28.5*	C16	Bladed calcite	-3.6	14.4
ESF 28+81*	A3	Bladed calcite	7.3	13.0
ESF 28+81*	A2	Bladed calcite	5.1	11.2
ESF 28+81*	A1	Bladed calcite	7.9	13.2
ESF 28+81	A4	Outer bladed calcite	-0.1	14.4
ESF 28+81	A5	Outer bladed calcite	-1.5	14.2
ESF 29+11	C8	MGSC	-5.2	16.5
ESF 29+11	C9	MGSC	-6.8	17.2
ESF 32+31	C6	Basal calcite	9.5	13.8
ESF 32+31	C7	MGSC	-6.0	17.2
ESF 34+86.5	B9	Basal calcite	6.0	14.5

Table 1. Continued.

Sample	Sample Split	Sample description	$\delta^{13}\text{C}$ (‰)	$\delta^{18}\text{O}$ (‰)
ESF 34+86.5	A5	Bladed calcite	-5.4	16.7
ESF 34+86.5	A6	Bladed calcite	-6.0	16.9
ESF 34+86.5	A3	MGSC	-6.0	16.4
ESF 34+86.5	A7	Bladed calcite	-5.6	16.9
ESF 43+83.5	A2	Basal calcite	-0.6	16.6
ESF 43+83.5	A3	Intermediate calcite	-5.9	17.5
ESF 43+83.5	A4	Outer non-descript calcite	-7.5	17.3
ESF 46+79*	B13	Basal calcite	3.2	14.9
ESF 46+79	B14	Basal calcite	2.3	15.4
ESF 46+79	B15	Outer non-descript calcite	-3.5	17.6
ESF 48+11	A1	Basal calcite	-0.9	16.8
ESF 48+11	A2	Outer non-descript calcite	-6.6	17.2
ESF 52+65.2	A3	Outermost non-descript calcite	2.7	15.7
ESF 52+65.2	A2	Outermost non-descript calcite	1.0	16.8
ESF 52+65.2	A1	Outer non-descript calcite	-6.4	18.8
ESF 60+52.5	A3	MGSC	-6.3	18.2
ESF 60+52.5	A2	MGSC	-6.9	18.6
ESF 64+95*	E2	Basal calcite	6.1	13.5
ESF 64+95*	E3	Basal calcite	6.6	13.2
ESF 64+95	E4	Bladed calcite	-7.2	17.5
ESF 64+95	E5	MGSC	-7.3	17.8
ESF 64+95	E1	MGSC	-7.5	17.8
ESF 64+95	A2	Bladed calcite	-7.1	17.6
ESF 67+81	C4	Basal calcite	0.3	22.1
ESF 67+81	C5	MGSC	-6.8	18.3
ESF 72+25	C13	Bladed calcite	-6.0	18.5
ESF 72+25	C14	MGSC	-5.8	18.1
ESF 77+03	B18	Intermediate calcite	8.4	14.1
ESF 76+59.5	C2	Intermediate calcite	-7.6	19.5
ESF 76+59.5	C3	MGSC	-7.3	18.9
ESF 78+05.2	B1	MGSC	-7.3	19.2
ESF 78+05.2	B5	MGSC	-7.3	19.4
ESF 78+05.2	B4	MGSC	-8.0	19.5
ESF 78+05.2	B2	MGSC	-8.0	19.9
ESF 78+05.2	B3	MGSC	-8.5	19.6
Standards				
NBS 18		Carbonatite (n=7)	-5.0 to -4.9	7.0 to 7.2
NBS 19		Marble (n=7)	1.9 to 2.0	28.6 to 28.8
NBS 20		Solenhofen Lst (n=3)	-1.1 to -1.0	26.6 to 26.7
LIPS		A1 (n=1)	1.1	24.9
YULE		Marble (n=1)	-2.7	23.9

* Sampled calcite contained 2-phase fluid inclusions.

Document No.: TR-02-005.2

Document Title: Thermochronological Evolution of Calcite Formation at the Potential Yucca Mountain Repository Site, Nevada: Part 2, Fluid Inclusion Analyses and U-Pb Dating

Document Revision: 0

Originators: Nicholas S. F. Wilson and Jean S. Cline; Department of Geoscience, University of Nevada Las Vegas, 4505 Maryland Parkway, Box 454010, Las Vegas, Nevada, USA 89154-4010; and Yuri Amelin, Royal Ontario Museum, Ontario, Canada

PI (Jean S. Cline) signature: Jean S. Cline

Date: 5/20/02

QA Manager (Amy Smolecinski) signature: Amy J. Smolecinski

Date: 5/20/02

Technical Reviewer: Robert Bodnar, Virginia Tech, Blacksburg, Virginia

Technical Reviewer signature: Robert J. Bodnar

Date: 05/17/02

Table of Contents

Table of Contents.....	2
Table of Abbreviations	3
Abstract.....	4
1. Introduction.....	6
2. Background and Previous Research.....	6
2.1. Geological Background	6
2.2. Fluid Inclusion Studies	8
2.3. U–Pb and U–series Studies.....	8
3. Sampling and Analytical Methods.....	9
3.1. Sample Collection.....	9
3.2. Fluid Inclusion Petrology and Microthermometry	9
3.3. δD Composition of Inclusion Fluids.....	10
3.4. U–Pb and U-series Dating	10
4. Fluid Inclusion Analyses.....	11
4.1. Fluid Inclusion Petrography.....	11
4.2. Spatial Distribution of 2-Phase FIAs	13
4.3. Fluid Inclusion Microthermometry.....	13
4.4. Fluid Inclusion Ice Melting Temperatures.....	16
4.5. δD Compositions of Fluid Inclusion Fluids.....	16
5. U–Pb Dating.....	16
5.1. Results.....	17
6. Discussion.....	21
6.1. How Widespread, Within the Repository Site, was the Influx of Fluids with Elevated Temperatures?.....	21
6.2. What Temperatures do the 2–phase FIAs Represent?	22
6.3. When Were 2–phase FIAs Trapped?	23
6.4. Origin of the Fluids.....	24
6.5. Genetic Models for the Formation of Secondary Minerals	24
6.6. Model for the Formation of Secondary Minerals	24
7. Conclusions.....	25
References.....	27
Figure captions.....	31
FIGURES.....	34
TABLES	46
APPENDIX – ADDITIONAL DESCRIPTIONS OF DATED SAMPLES.....	49

Table of Abbreviations

BZ	barren zone
CAZ	calcite alteration zone
CL	cathodoluminescence
DOE	Department of Energy
DPTS	doubly polished thin sections
ECRB	Enhanced Characterization of the Repository Block Cross Drift
EPMA	electron probe microanalyses
ESF	Exploratory Studies Facility
FIAs	fluid inclusion assemblages
IFZ	intensely fractured zone
LA-ICP-MS	ablation inductively coupled plasma mass spectrometry
LC	lithophysal cavities
LCZ	lithophysal cavity zone
MGSC	magnesium-enriched growth-zoned sparry calcite
NP	north portal
NPR	north portal and ramp
NR	north ramp
PMC	patchy Mg-enriched calcite
PTn	Paintbrush Tuff nonwelded
ROM	Royal Ontario Museum
SMOW	standard mean ocean water
SPR	south portal and ramp
SZ	saturated zone
UCCSN	University and Community College System of Southern Nevada
USGS	United States Geological Survey
UZ	unsaturated zone
WDS	wavelength dispersive spectrometry

Abstract

The presence of two-phase fluid inclusions in thin secondary mineral crusts at the potential Yucca Mountain nuclear waste repository has raised questions regarding the origin, timing, and temperature of past fluid flow through the repository horizon. The geologically recent passage of fluids with high temperatures would call into question the suitability of the site for the storage of high level nuclear waste. This study determined the thermal history of fluid flow through the site using fluid inclusion analyses and constrained the timing of thermal fluids by dating silica minerals spatially associated with the fluid inclusions using U-Pb techniques. Results provide a detailed time-temperature history of fluid migration through primary and secondary pore spaces during the past 8 to 9 million years.

One hundred and fifty-five samples were collected in the unsaturated zone from the C-shaped Exploratory Studies Facility (ESF), the ECRB cross drift which crosses the potential repository horizon, and exploratory alcoves. Detailed petrographic and paragenetic studies indicated that the oldest secondary minerals consisted of heterogeneously distributed calcite with lesser chalcedony, quartz, opal, and fluorite. The oldest secondary minerals were overgrown by intermediate bladed calcite. The youngest secondary minerals include chemically distinct Mg-enriched, growth-zoned sparry calcite (MGSC) and intergrown U-enriched opal.

Fluid inclusion petrography indicated that 50 % of the samples ($n = 78$) contained fluid inclusion assemblages with two-phase fluid inclusions, and that assemblages of liquid-only fluid inclusions represent > 96% of all fluid inclusions within the secondary minerals. Assemblages of two-phase inclusions also contain liquid-only inclusions that did not nucleate a vapor-bubble owing to formation at relatively low temperatures. Virtually all two-phase fluid inclusions occur in paragenetically old calcite; rare two-phase inclusion assemblages were observed in old fluorite ($n = 3$) and quartz ($n = 2$). Rare two-phase fluid inclusions were observed in early-intermediate calcite; sparse, irregularly shaped liquid-only inclusions form the only fluid inclusion assemblages observed in late-intermediate minerals and young MGSC. Homogenization temperatures for calcite across the site are generally 45 – 60 °C, but higher temperatures reaching 83 °C were recorded in the north portal and ramp of the ESF and cooler temperatures of ~ 35 – 45 °C were recorded in the intensely fractured zone. Samples from lithophysal cavities in the ESF and ECRB contain multiple populations of two-phase inclusions. Inclusion temperatures are highest in early calcite (> 45 °C) and cooler in paragenetically younger early calcite, indicating cooling with time. The cooler temperatures coincide with temperatures recorded in the intensely fractured zone and indicate that secondary minerals in the intensely fractured zone began to precipitate later than secondary minerals in other locations. Freezing point depressions determined for inclusions range from -0.2 to -1.6 °C indicating trapping of a low salinity fluid. A small number of fluid inclusions in fluorite and quartz were identified and evaluated. Four inclusions in these minerals homogenized at temperatures higher than those recorded for calcite (91 ° - 95 °C).

Two approaches were used to constrain the timing of thermal fluids at Yucca Mountain. First, the age of MGSC was determined, and it provides a minimum age for fluids with elevated temperatures owing to the presence of only liquid-only inclusions in MGSC. Results indicate that MGSC began to precipitate across the site between 2.90 ± 0.06 Ma and about 1.95 ± 0.06 Ma, and MGSC has continued to precipitate to within the last half million years. These ages constrain fluids with elevated temperatures to have accessed the site more than about 2.90 Ma. Second, more precise temporal constraints were determined for samples in which datable opal or

chalcedony occur in the intermediate or older parts of the mineral crusts, or are spatially related to 2-phase fluid inclusions. Such ages indicate that two-phase fluid inclusions are older than 5.32 ± 0.02 Ma, and that fluids with elevated temperatures were present at Yucca Mountain before this time.

Results from this study are consistent with a model of descending meteoric water that infiltrated the cooling tuff sequence, became heated, and precipitated secondary minerals within the vadose zone. Fluid inclusions indicate that fluids with elevated temperatures were present during the early history of Yucca Mountain. Sparse, liquid-only fluid inclusions in late-intermediate to young calcite indicate that secondary minerals were precipitated from low temperature fluids during the past 5 million years. This study demonstrates that the hypothesis of geologically recent upwelling hydrothermal fluids is untenable and should not disqualify Yucca Mountain as a potential nuclear waste storage site.

1. INTRODUCTION

Yucca Mountain is unique among potential nuclear waste repository sites owing to its location underground, in the unsaturated zone (UZ), above a deep water table (Winograd, 1981). Nevertheless, the potential for dispersion of radionuclides by fluid flow through the UZ is of great concern, and site characterization has focused on constraining this flow, in part, by determining the origin of open space, secondary minerals that occur within the host Miocene tuffs. Secondary mineral crusts occur in lithophysal cavities, fractures, and breccias in the host tuffs, but the majority of the primary and secondary pore spaces contains no secondary mineral record (Whelan et al., in press).

Previous fluid inclusion studies of secondary calcite documented the presence of two-phase fluid inclusions with homogenization temperatures of 35 – 85 °C (Dublyansky, 1998; Dublyansky et al., 2001). These authors concluded that hydrothermal fluids flooded the host rocks and, as a result, they questioned the suitability of Yucca Mountain as a potential high-level nuclear waste repository. However, the timing of the presence and trapping of fluids with elevated temperatures and their sources were not known.

A major goal of this study was to determine when fluids with elevated temperatures were present at Yucca Mountain. Ambient temperatures at Yucca Mountain are about 27 °C. However, we do not know what past ambient temperatures were at Yucca Mountain. Two-phase, liquid-vapor fluid inclusions form because trapped fluids cooled and contracted. Therefore, two-phase fluid inclusions clearly document the former presence of fluids with elevated temperatures. In this study we documented two-phase fluid inclusions that homogenized at temperatures of 35 °C and higher, and we consider fluid temperatures of about 35 °C and higher to be elevated.

To conduct this study, samples were collected from the Exploratory Studies Facility (ESF), Enhanced Characterization of the Repository Block Cross Drift (ECRB), and exploratory alcoves (Fig. 1), and detailed petrographic, geochemical, and isotopic studies were conducted. Initial work focused on constructing a paragenetic sequence for secondary mineral occurrences across the site (Wilson and Cline, 2002). Subsequent work, reported here, integrates the paragenetic study with fluid inclusion and geochronology studies to address four specific questions: 1) Did fluids with elevated temperatures invade the repository site? If an influx of fluids with elevated temperatures occurred, 2) how widespread within the repository site was this influx? 3) what were the temperatures of the fluids that invaded the site? and 4) when did these fluids invade the site?

2. BACKGROUND AND PREVIOUS RESEARCH

2.1. Geological Background

Yucca Mountain was originally identified as a possible high-level geologic nuclear waste repository for a number of reasons. In particular, this region has an arid climate with less than 25 cm of rain per year (U.S. DOE, 1988), and a deep unsaturated zone with a water table 400 – 600 m below the present day surface (Winograd, 1981). The mountain is located 90 miles northwest of Las Vegas at the western edge of the Nevada test site, within the Southwest Nevada Miocene volcanic field (Christiansen et al., 1977). Comprehensive discussions of the geology at Yucca

Mountain are given by Sawyer et al. (1994), Buesch et al. (1996), and Stuckless and Dudley (in press), and have been briefly summarized by Wilson and Cline (2002).

Yucca Mountain is composed of a 1 – 3 km thick sequence of shallowly eastward dipping felsic welded and non-welded volcanic tuffs of the Paintbrush Group (Sawyer et al., 1994; Wilson and Cline, 2002; their Fig. 1). The Paintbrush Group comprises the Topopah Spring, Pah Canyon, Yucca Mountain, and Tiva Canyon Tuffs (Sawyer et al., 1994). The Topopah Spring Tuff, dated at 12.8 Ma, directly overlies bedded rhyolite tuffs of the Calico Hills Formation and is overlain by the thin Pah Canyon and Yucca Mountain Tuffs (Sawyer et al. 1994), collectively known as the PTn. The Tiva Canyon Tuff, dated at 12.7 Ma, overlies the PTn (Sawyer et al., 1994). Younger faulting related to Basin and Range extension (e.g. Stewart, 1988) cuts the tuff sequence. Basaltic eruptions formed flows and cones during the late Tertiary in Crater Flat with the most recent episode creating the Lathrop Wells Cone about 75 Ka (Heizler et al., 1999).

To enhance site characterization, two tunnels were excavated into the mountain near the potential repository (Fig. 1). The ESF crosses the Topopah Spring, Pah Canyon, Yucca Mountain, and Tiva Canyon Tuffs; the ECRB was excavated entirely within the Topopah Spring tuff about 15 m above the potential repository horizon. All samples used in this study were collected from the ESF, ECRB, and exploratory alcoves in the UZ. The UZ extends from the surface to a depth of around 500 – 700 m where the water table is encountered and the saturated zone (SZ) begins. The potential repository is to be situated in the lower member of the Topopah Spring Tuff, ~ 300 m below the surface and above the water table.

Within the UZ, primary and secondary porosity occur as lithophysal cavities (LC), fractures, and breccias. LC are roughly parallel to bedding and formed as gas exsolved from the cooling tuff sequence. This gas exsolution led to early high-temperature vapor-phase alteration along the margins of LC and cooling fractures. Alteration produced bleached margins and secondary minerals that are sub-parallel to bedding (vapor-phase partings) and include predominantly tridymite, cristobalite, alkali feldspar, and hematite (Carlos, 1994; Levy et al., 1996).

The majority of primary and secondary pore spaces in tuffs at Yucca Mountain remain open and contain no secondary mineral record (Whelan et al. 1996; Whelan et al., in press; Wilson and Cline, 2002). Where present, secondary minerals are restricted predominantly to the footwalls and bases of LC, fractures, and breccias (Whelan et al. 1996; Wilson and Cline, 2002). Paragenetic studies by two groups (Whelan et al., in press; Wilson and Cline, 2002) led to similar conclusions in regards to the sequence of secondary mineral precipitation following deposition of vapor-phase minerals. Early minerals were represented by calcite with lesser chalcedony, quartz, opal, and fluorite and were heterogeneously distributed across the site. These minerals were overgrown by intermediate minerals composed primarily of distinctive calcite blades. Outer 'late stage' calcite observed by Whelan et al. (in press) was typically clear and had distinctive C and O isotopic signatures and the authors concluded that this calcite could be correlated across the site based on a combination of petrography and C and O isotopic signatures (Paces et al., 1997). Wilson and Cline (2002) observed that the outer late stage calcite represented the most recently deposited secondary mineral at Yucca Mountain. They further determined that this calcite is chemically distinct and contains fine growth zones containing up to ~ 1 wt.% Mg. Termed Mg-enriched, growth-zoned sparry calcite (MGSC), this layer can be distinguished from all other calcite by its chemistry and growth zoning, is associated and intergrown with clear opal, occurs in > 65 % of the samples studied, and can be correlated across the site.

2.2. Fluid Inclusion Studies

Previous fluid inclusion studies of secondary mineral crusts have led to conflicting interpretations. Initial studies of UZ calcite from drill core samples were published by Bish and Aronson (1993) and Roedder et al. (1994). Bish and Aronson (1993) focussed on SZ calcite which contained 2-phase inclusions that formed at temperatures up to 250 °C. Roedder et al. (1994) observed primary inclusions in calcite from drill core with variable liquid-vapor ratios and the majority of inclusions were either all liquid or all vapor. They concluded that the inclusions were trapped at near surface temperatures in the vadose zone. Roedder and Whelan (1998) presented additional data from samples from the ESF and drew similar conclusions. Dublyansky and co-authors, however, produced several reports (e.g. Dublyansky, 1998; Dublyansky et al., 1998; Dublyansky et al., 2001) in which they concluded that secondary minerals formed in a phreatic environment. They suggested that calcite precipitated from upwelling hydrothermal fluids that flooded the repository horizon on multiple occasions, including during the recent geologic past. Dublyansky (1998) showed that fluid inclusion assemblages (FIAs) in calcite contained both two-phase inclusions with consistent liquid-vapor ratios and liquid-only inclusions. Several FIAs exhibited consistent homogenization temperatures over a range of 35 – 85 °C, temperatures that are higher than the present day temperature of the water table (~ 32 °C) (Dublyansky et al., 2001). Freezing point depressions of 0 °C to -1.25 °C indicated inclusion salinities that the authors concluded were too high for vadose zone waters.

The lack of recognition of FIAs containing two-phase fluid inclusions in early studies by Roedder et al. (1994) and Roedder and Whelan (1998) may be related to handling of the samples used in these studies (Whelan et al., in press). The inclusions in the samples may have homogenized during collection, storage, or section preparation (Whelan et al., in press) and, as they do not readily renucleate a vapor bubble after homogenization, two-phase fluid inclusions would not have been available for identification. More recent work by Whelan et al. (in press) based on samples that were properly handled, recognizes the presence of FIAs with consistent liquid-vapor ratios in secondary minerals at Yucca Mountain.

The limited petrographic information presented in studies by Dublyansky and coworkers precludes placing the reported fluid inclusion data in any temporal context. The current study was initiated to confirm the presence of FIAs containing fluids with elevated temperatures and to constrain the ages of these fluid inclusions and the timing of fluid access to Yucca Mountain.

2.3. U–Pb and U–series Studies

Secondary opal and chalcedony intergrown with calcite locally contain high U and very low common Pb and ²³²Th. These trace element concentrations make micro-samples of opal and chalcedony suitable for precise U-Pb (Neymark et al., 1998) and U-Series dating (Neymark and Paces, 1996, 2000; Paces et al., 1996, 1998a, Neymark et al., 1998, Neymark et al., 2000). Geochronological studies were previously conducted to investigate the timing of secondary mineral deposition and the depositional rate, which are, in turn related to fluxes through the UZ (Neymark et al., 1998). Opal and chalcedony were dated using U-Pb and have provided ages ranging from 0.1 – 10 Ma, indicating that secondary mineral formation initiated within 2 Ma of tuff emplacement; sequentially younger ages were obtained for outermost opals (Neymark et al., 1998). Chalcedony at the base of some mineral crusts gave the oldest ages of 8 – 10 Ma, whereas clear opals, typically in intermediate to youngest stratigraphic positions, have younger ages. The

older ages from chalcedony were interpreted to be consistent with late-stage magmatic activity in the Timber Mountain caldera (Neymark et al., 1998). Neymark et al. (1998) suggested that depositional rates of 1 – 4 mm/Ma in the potential repository horizon were consistent throughout the Neogene and Quaternary and have not varied substantially during the last 8 million years. These depositional rates are consistent with U-series data and led to a model describing continuous secondary mineral deposition at a constant, slow rate to the present (less than 5 mm/Ma; Neymark and Paces, 2000). Data derived from in-situ SHRIMP analyses of opal growth zones (Paces et al., 2000) indicate similar growth rates.

3. SAMPLING AND ANALYTICAL METHODS

3.1. Sample Collection

One hundred and fifty-five samples of secondary minerals and adjacent wall rock were collected from LC, fracture, and breccia occurrences from the ESF, ECRB, and exploration alcoves at Yucca Mountain (Fig. 1). All styles of secondary mineral occurrences identified within the site were sampled. Samples were maintained at temperatures between 0 – 35 °C during sampling, transportation, thin section preparation, and storage, according to UCCSN Quality Assurance (QA) procedures, so as not to adversely affect the fluid inclusions.

The tunnels and alcoves have been divided into six zones (Fig. 1) based on local differences in secondary minerals, mineral occurrences, and fluid inclusion homogenization temperatures. Samples from the north portal (NP) and north ramp (NR) are fracture and breccia occurrences and typically contain more silica minerals than samples from other areas of the site. Samples from the lithophysal cavity zone (LCZ) and the ECRB are primarily from LC occurrences and contain predominantly calcite with some chalcedony-quartz and clear opal. The intensely fractured zone (IFZ) contains steeply dipping fractures that contain calcite with minor early fluorite. South portal and ramp (SPR) samples are from LC, fracture, and breccia occurrences and contain variable amounts of calcite, chalcedony and opal. These zones are similar to zones presented by Wilson and Cline (2002) except that the north portal and north ramp are separated in this report, rather than being combined into a single zone.

3.2. Fluid Inclusion Petrology and Microthermometry

Doubly polished thick sections (DPTS) for fluid inclusion studies were prepared so as to limit heating and fracturing of the samples (Wilson and Cline, 2002). A critical component of this study was the selection of fluid inclusions for analysis that were identified as comprising fluid inclusion assemblages (FIAs) (Goldstein and Reynolds, 1994). An FIA is a petrographic classification that describes a group of fluid inclusions that were formed at the same time and, therefore, at the same temperature and pressure. All inclusions that are part of an FIA may not homogenize at the same temperature owing to post trapping modification of some inclusions. Fluid inclusions in an FIA may also exhibit different phase relations. Most fluid inclusions examined in this study were determined to be primary, based on their occurrences within growth zones; a small number of fluid inclusion assemblages occurred in fractures indicating they are secondary. Fluid inclusion petrography was integrated with the secondary mineral paragenesis;

genetic relationships between primary FIAs and various stages of secondary minerals were determined and provided relative ages for primary FIAs.

Homogenization and ice melting measurements were collected on a Linkam THMSG 600 heating and freezing stage attached to a CI 93 programmer and LNP cooling pump. The equipment was controlled by LinkSys software version 1.83. The Linkam stage is mounted on an Olympus BX60 microscope and a Polaroid DCM IE digital camera was used to capture images. Synthetic fluid inclusions were used to calibrate the stage at 374.1 °C, 0.0 °C, and -56.6 °C and stage calibration was checked each day prior to analysis. Chips from the DPTS were left attached to glass slides during microthermometry, because the samples tended to break apart if removed from the slide.

Homogenization temperatures for selected inclusions in an FIA in each chip were determined during a single heating run beginning at 35 °C. During each run temperatures were cycled by increasing the temperature 2 °C above the temperature of the previous cycle, and then cooling the sample a few degrees. Homogenization was assumed for each inclusion in which the vapor bubble was no longer present after heating. Freezing studies were conducted after heating studies to avoid freeze-stretching of the fluid inclusions (Lawler and Crawford, 1983). Since the two-phase fluid inclusions did not renucleate a vapor bubble on cooling following inclusion homogenization, the chips were heated to ~ 150 °C to stretch the inclusions for ice melting determinations. Stretching increased the possibility of generating vapor bubbles in the inclusions for freezing studies to estimate fluid inclusion salinities. Ice melting temperatures were determined by monitoring the expansion and contraction of the vapor bubble as temperatures were cycled at sub-zero temperatures. In the majority of samples examined, vapor bubbles did not nucleate and salinities could not be determined because ice-melting temperatures in the absence of a vapor bubble cannot be used to determine salinity (Roedder, 1984).

3.3. δ D Composition of Inclusion Fluids

Hydrogen isotope signatures were determined for selected fluid inclusion assemblages following the method of Sharp et al. (2001). Sample material was removed from billets from which the examined polished sections were prepared, from equivalent slices of secondary mineral crusts. Only samples that contained consistent single fluid inclusion populations were analyzed. Examination of as many as five polished sections from a single sample showed that samples were consistent from section to section, indicating that material examined in section could be collected from the billet for analysis. Calcite samples were thermally decrepitated using a CO₂ laser and evolved H₂O from the fluid inclusions was reduced to H₂ by glassy carbon at 1450 °C in a He carrier gas. H₂ was separated in a gas chromatograph and analyzed by a Finnigan MAT Delta^{Plus} XL mass spectrometer. The instrument and analytical setup were calibrated using NBS and other secondary standards for H. Results have a precision of ± 2 ‰ and are reported relative to Vienna SMOW.

3.4. U-Pb and U-series Dating

Opal and chalcedony used for dating were hand picked under a binocular microscope from pieces of DPTS that were soaked in acetone to allow easy separation of opal from calcite. Darker opal and chalcedony were generally collected from layers and irregular growths in paragenetically older parts of mineral crusts. Clear opal samples are generally present in and

were collected from thin continuous or discontinuous layers within paragenetically younger layers of the mineral crusts.

U–Pb and ^{230}Th –U analyses were carried out using the technique described by Neymark et al. (2000) at the Jack Satterly Geochronology Laboratory, Royal Ontario Museum (ROM), Toronto, Canada. The samples were spiked with the mixed ^{205}Pb – ^{229}Th – ^{233}U – ^{236}U tracer solution prior to dissolution, and U–Pb and U–series isotopic data were obtained from the same aliquot. Isotopic compositions of U, Th and Pb were measured using thermal ionization mass-spectrometer VG–354, recently equipped with ion counting Daly photomultiplier detectors. Ion counting provides improved precision in the analyses of small and low–U samples compared to the previously used analog Daly detectors (Neymark et al. 2000).

Isotopic analyses were corrected for procedure blanks measured with each batch of samples. Concentrations of Pb, U, and Th in procedure blanks used in the sample data reduction were taken from the blank measurements performed together with the same batch of samples or from the immediate preceding batch. In those cases where more than one blank measurement was taken with the same batch of samples, the blank values were averaged for sample data reduction. The total procedural blanks measured during this study varied between 0.3 – 0.9 pg Pb and 0.3 – 2.0 pg U and Th. The representative blank Pb isotopic composition values were obtained as weighted averages of the ROM Geochronology Lab blank database over the period of 1996 to 2000 as 18.76 ± 0.21 ($^{206}\text{Pb}/^{204}\text{Pb}$), 15.58 ± 0.094 ($^{207}\text{Pb}/^{204}\text{Pb}$), and 38.02 ± 0.27 ($^{208}\text{Pb}/^{204}\text{Pb}$). The blank Pb isotopic compositions measured together with the silica samples are consistent with the database average values.

The precision and accuracy of the $^{234}\text{U}/^{238}\text{U}$ and $^{230}\text{Th}/^{238}\text{U}$ activity ratio measurements were additionally checked using a solution of a secular equilibrium material (~70 Ma old uranium ore, Ludwig et al., 1985). The results of repeated analyses (Fig. 2) are reproducible within the 2σ error limits, and weighted means of the $^{234}\text{U}/^{238}\text{U}$ and $^{230}\text{Th}/^{238}\text{U}$ activity ratios are within analytical error of unity. The Pb isotopic compositions used in the initial common Pb corrections, and the decay constant values are the same as reported previously.

4. FLUID INCLUSION ANALYSES

4.1. Fluid Inclusion Petrography

Three types of fluid inclusions are present at Yucca Mountain. 1) Liquid-only inclusions are the most abundant fluid inclusions in secondary minerals and they constitute more than 96 % of all inclusions observed. 2) Two-phase, liquid-plus-vapor inclusions are sparse (< 3 %) and 3) vapor-only inclusions are rare (< 1 % of inclusions). A small number of assemblages (< 1 %) of liquid plus vapor inclusions contain inclusions with variable liquid-vapor ratios. Most two-phase inclusions have small vapor bubbles, exhibit consistent liquid-vapor ratios, and coexist in FIAs with liquid-only inclusions. The two-phase and liquid-only inclusions in these assemblages were trapped at the same time under the same conditions, constituting a valid FIA; however, because of the relatively low trapping temperatures, some of the inclusions did not nucleate a vapor bubble on cooling. Most of these inclusion populations are in calcite (>99 %), but a small number of FIAs containing liquid plus vapor inclusions were identified in quartz and fluorite. These low-temperature FIAs that contain the liquid plus vapor and liquid-only inclusions are referred to as 2-phase FIAs in this report, distinguishing them from assemblages of liquid-only

inclusions. Although these 2-phase FIAs are not abundant, they are relatively common in some mineral layers in some samples.

FIAs of liquid-only inclusions, the most abundant inclusions at Yucca Mountain, occur in early to early-intermediate calcite (Fig. 3) in some samples. These inclusions are typically primary, and inclusions are aligned along growth zones (Fig. 4a). Liquid-only inclusions comprise the only inclusion assemblages in bladed calcite and MGSC, and the abundance of inclusions is significantly decreased in this calcite. The liquid-only inclusions are irregularly shaped and are elongated along growth zones (Fig. 4b). Outermost MGSC is commonly clear and generally contains no inclusions, but locally exhibits dark micropores between growth zones. Some of these pores contain rare, primary liquid-only inclusions.

Sparse 2-phase FIAs are most abundant in calcite, are generally primary, and are usually aligned along growth zones in three-dimensional arrays in the cores of crystals or in calcite blades (Fig. 4c). Primary inclusions illustrated in Figure 4c are typical of 2-phase FIAs found in calcite and evaluated using microthermometry. A few 2-phase FIAs lie along fracture planes and are secondary or are of unknown origin. Typically, the homogenization temperatures of the 2-phase FIAs are consistent and temperatures are always less than 100 °C. Some inclusions with inconsistent liquid-vapor ratios (vapor-bubbles ~10 – 80 volume %) and large vapor bubbles (Fig. 4d) occur within an FIA in which the large majority of the inclusions show consistent liquid-vapor ratios and consistent homogenization temperatures. These textural relationships suggest that the inclusions with large bubbles and inconsistent liquid-vapor ratios have leaked.

Figure 3 summarizes the paragenetic sequences of secondary minerals observed by Wilson and Cline (2002) at Yucca Mountain and incorporates the distribution of fluid inclusion populations. Two-phase FIAs occur in paragenetically early calcite around and adjacent to the wall rock at the base of secondary crusts, often within a few millimeters of the wall rock. A small number of 2-phase FIAs were identified in the basal parts of bladed calcite, generally where blades are small and growth zones are broad (Fig. 3). Vapor bubbles are slightly larger in 2-phase FIAs in basal calcite and are smaller in paragenetically younger calcite. The paragenetically youngest 2-phase FIAs observed were identified in a single sample in calcite that precipitated with early-intermediate opal. Two-phase FIAs do not occur in the central and outermost parts of calcite blades, or in the larger and more slender intermediate-stage calcite blades. In these calcites rare liquid-only inclusions were identified (Fig. 3). In addition, no 2-phase FIAs are present in paragenetically youngest MGSC.

Rare 2-phase FIAs occur in paragenetically early to earliest intermediate quartz ($n = 2$) and fluorite ($n = 3$) (Wilson and Cline, 2002). These FIAs are in the basal parts of crusts adjacent to and around the wall rock, and are overgrown by later secondary minerals (Fig. 3). Quartz is usually clear and inclusion free but locally exhibits darker patches of small liquid-only inclusions ($< 10 \mu\text{m}$ diameter). Rare quartz contains primary 2-phase FIAs and inclusions have liquid-vapor ratios that are similar to 2-phase FIAs in adjacent calcite (vapor bubbles $< 1 \%$ volume). Two generations of fluorite have been identified. Earliest fluorite forms nodules and masses that are generally about 0.5 mm, but which may reach one or more millimeters, and which may contain 2-phase FIAs. Some of the 2-phase FIAs are primary and occur in the cores of crystals; others are of unknown origin. Small fluorite cubes, in which 2-phase FIAs have not been observed, are present in early to intermediate secondary minerals (Wilson and Cline, 2002).

Vapor-only inclusions are locally present at the base of some of the mineral crusts (Fig. 3). Some of these inclusions are large and “faceted,” exhibiting near-negative crystal shapes. Two-phase inclusions with variable liquid-vapor ratios and dark vapor bubbles are present in a

number of samples. These inclusions are commonly spatially associated with 2-phase FIAs at the base of crusts (Fig. 4d). The two-phase inclusions with the dark vapor bubbles occur dominantly at the base of lithophysal cavity crusts and have been observed in calcite, but not in other minerals. During heating the liquid-vapor ratios and dark vapor-bubbles did not noticeably change. It is unclear whether these inclusions formed by heterogeneous trapping or by leaking after trapping. Owing to the ambiguous origin of these inclusions and their restriction to the oldest parts of the mineral crusts in a small number of samples, they are not discussed further.

4.2. Spatial Distribution of 2-Phase FIAs

Two-phase FIAs have been observed in 78 of 155 samples (~ 50 %). The FIAs are present in secondary minerals from sample locations across the site (Fig. 1) and occurrences are split almost evenly between LC (~ 51 %) and fractures / breccias (~ 49 %). Two-phase FIAs are most common in the LCZ and the eastern part of the ECRB, and are rarer in the NP and SPR. Approximately half of the samples in the IFZ contain 2-phase FIAs. The distribution of 2-phase FIAs indicates that fluids with elevated temperatures accessed pore spaces that contain secondary minerals across the site. However, the distribution is erratic and samples that contain 2-phase FIAs are commonly adjacent to sample sites that lack 2-phase FIAs.

4.3. Fluid Inclusion Microthermometry

Sixty-one of the 78 samples that contain 2-phase FIAs were examined using microthermometry and more than 2500 inclusions were heated to determine homogenization temperatures. The temperatures determined for 2-phase FIAs in calcite across the site have a range of 35 – 83 °C (Fig. 5). Two-phase FIAs from all occurrences (LC, fractures, and breccias) in the LCZ, SPR, and ECRB provided homogenization temperatures of 35 – 67 °C. Inclusions in calcite from the NP and NR have homogenization temperatures that reach 83 °C and 75 °C, respectively, whereas most inclusions in the IFZ homogenize below 50 °C. Stratigraphic reconstructions at Yucca Mountain indicate that there has been minimal erosion since the volcanic rocks were deposited (S. Levy, personal communication, 1999) and it is generally accepted that no more than 100 m of overlying rocks have been eroded from the surface of Yucca Mountain. Such a low erosion rate indicates that the inclusions were trapped at depths of less than 400 m and, as a result, homogenization temperatures approximate inclusion trapping temperatures and do not require a pressure correction. Note that if the inclusions were trapped in a vadose environment the homogenization temperatures equal the trapping temperatures and no pressure correction is needed (Roedder and Bodnar, 1980).

Primary 2-phase fluid inclusions in individual FIAs (Fig. 4c) provided consistent homogenization temperatures. In many samples, multiple FIAs produced nearly identical data. Inclusions in most FIAs homogenized within a range of about 10 °C and in many FIAs, all inclusions homogenized over a range of about 6 °C. Figure 6 illustrates the consistency of homogenization temperatures for 181 fluid inclusions in sample ESF 01+62.3 from the NP. Most inclusions homogenized from 61 – 67 °C, a temperature range of 6 °C. Data include all homogenization temperatures from one chip and data from six FIAs identified in a second chip. These results show that a single FIA is representative of all data from this sample.

During microthermometry a few inclusions in measured FIAs homogenized at somewhat scattered, higher temperatures than the bulk of the data. Such temperatures probably reflect

stretching of calcite during heating. These data are not shown in Figure 5 and their removal does not change the mode or the range of the majority of the data. The consistency of homogenization temperatures for inclusions of different sizes reinforces the conclusion that the evaluated inclusions are part of an FIA (Goldstein and Reynolds, 1994), that the 2-phase FIAs trapped a single homogeneous fluid, and that the inclusions were not heated or perturbed by subsequent events.

Two-phase FIAs in calcite from lithophysal cavities in the Topopah Spring Tuff in the LCZ and ECRB exhibit bimodal distributions of homogenization temperatures. Samples from the LCZ have modes at 47 – 57 °C and 39 – 41 °C; samples from the ECRB have modes at 49 – 57 °C and 43 – 47 °C (Fig. 5). Higher temperature fluids were trapped in older calcite whereas lower temperature fluids were trapped by paragenetically younger calcite indicating a cooling trend with time. The low temperature modes are similar to homogenization temperatures of inclusions in fracture and breccia occurrences in the IFZ (Fig. 5), which have a mode of 41 – 49 °C. The low homogenization temperatures in samples from the IFZ suggest that fracture- and breccia-related calcite probably had not precipitated when the earliest, higher temperature fluids invaded the site. The lack of vapor phase minerals in these samples is consistent with their later formation. These observations suggest that the various temperature ranges recorded across the site reflect fluid fluxes that occurred at different times, and are consistent with a temperature decline over time.

Inclusions in calcite samples from lithophysal cavities, fractures, and breccias from the SPR exhibit a single mode of homogenization temperatures at about 53 – 59 °C. This mode is slightly higher than modes determined for the LCZ and ECRB (Fig. 5).

The highest homogenization temperatures in calcite were recorded in samples from the NP and NR. Inclusions in two samples from the Tiva Canyon Formation in the NP (Figs. 1 and 5) have homogenization modes of about 73 – 79 °C and 61 – 67 °C. In both samples 2-phase FIAs are paragenetically early and are overgrown by younger calcite that contains rare, liquid-only FIAs. Many samples from the NP contain calcite; however, very few samples from this locality contain 2-phase FIAs. This distribution highlights the localized presence of 2-phase FIAs and especially, the localization of these highest homogenization temperatures. Inclusions in samples from the NR (Fig. 5) exhibit a large mode of homogenization temperatures from about 51 – 65 °C with temperatures extending to 75 °C. Secondary mineral distribution in this zone is quite variable with some samples containing more silica than calcite. Secondary mineral crusts also have variable thicknesses, and cemented breccias are locally present. Inclusion homogenization temperatures were consistent across the breccia samples indicating that there was little variation in temperature as the cementing calcite was deposited. The data for the NR indicate that, where 2-phase FIAs are present, the calcite in these samples precipitated at temperatures slightly greater than temperatures recorded over most of the Yucca Mountain site (Fig. 5).

In samples that contain multiple 2-phase FIAs that provide different ranges of homogenization temperatures, temperatures consistently decline with age of the inclusions and host minerals. Relatively simple crusts, in which calcite precipitated layer by layer from the base of the section outward, most clearly show this relationship. Basal calcite in sample ESF 27+84 from a lithophysal cavity (Fig. 7a) contains 2-phase inclusions at the base that homogenized from 48 – 53 °C. In younger calcite, inclusion homogenization temperatures become lower and temperatures from 37 – 43 °C were recorded in the outmost layer that contains 2-phase FIAs. Younger calcite in this sample contains only liquid-only inclusions. Sample Al#5 00+28.5 (Fig.

7b) exhibits a similar trend of decreasing temperature in paragenetically younger calcite. It is somewhat more difficult to identify the precipitation sequence of secondary minerals in fracture and breccia samples especially in samples in which multiple tuff clasts are cemented and rimmed by calcite. Nevertheless, even these samples (Figs. 7c and 7d) show a decline in temperature from identifiable older basal layers to younger layers; MGSC containing only liquid-only inclusions forms the youngest layers.

Two-phase FIAs were only observed in two samples of quartz and three samples of fluorite and the limited data are presented in Figure 8. The small number of homogenization temperatures is generally consistent with data obtained from calcite. The highest homogenization temperatures were obtained from inclusions in a sample from the NP. Inclusions in quartz from this sample have homogenization temperatures that range from 73 – 95 °C and are less consistent than temperatures typically obtained from calcite. Two-phase inclusions in paragenetically early fluorite from the same sample leaked during heating. Both quartz and fluorite in this sample (ESF 05+57.1) are present at the base of the mineral crusts, are overgrown by chalcedony, and are paragenetically old. Although the temperature range for quartz is rather large for an FIA (e.g. Goldstein and Reynolds, 1994) the data indicate that quartz and probably fluorite in the NP formed at temperatures similar to and slightly higher than temperatures obtained for calcite in this locality. Inclusions in quartz and fluorite from other localities provided lower homogenization temperatures, similar to calcite. Sample ESF 22+19 contains primary 2-phase inclusions in quartz that homogenized from 53 – 71 °C (Fig. 8). Inclusions in calcite adjacent to the quartz homogenized at 53 – 57 °C (n = 10). Sample ESF 53+35.5 contains paragenetically early fluorite that precipitated on wall rock. This fluorite contains 2-phase FIAs that have homogenization temperatures of 43 – 53 °C, identical to homogenization temperatures obtained in adjacent calcite. In sample ECRB 25+30 fluorite that precipitated on wall rock contains 2-phase FIAs, all but two of which homogenized at 69 – 81 °C (n = 21; 2 assemblages). Calcite surrounding this fluorite contained only liquid-only inclusions indicating formation at lower temperatures.

The integrated secondary mineral paragenesis, fluid inclusion petrography, and heating studies demonstrate the presence of a single, consistent cooling trend with time. Two-phase FIAs with the highest homogenization temperatures occur in secondary minerals growing around the wall rock or in minerals spatially associated with wall rock at the base of mineral crusts. The high temperatures recorded in NP and NR samples are in paragenetically old material and may record the earliest fluid fluxes through the Yucca Mountain site. Two-phase FIAs with lower homogenization temperatures occur in early-intermediate secondary minerals, and are the only inclusions trapped in secondary minerals associated with fractures and breccias in the IFZ. In samples that contain modes of both higher and lower homogenization temperatures, the higher temperature inclusions are always present in paragenetically older minerals. Intermediate bladed calcite and youngest MGSC only contain liquid-only inclusions, demonstrating continuation of the cooling trend to youngest calcite. As most of the evaluated inclusions are primary, these homogenization temperatures reflect declining temperature conditions across the site as the secondary minerals precipitated.

Homogenization temperatures are clearly not related to a paleogeothermal gradient and are, in fact, inversely related to depth. Samples containing the fluid inclusions with the highest observed homogenization temperatures are from the NP, which is at a current depth of 0 – 55 m. The LCZ and ECRB are located at depths below the surface of greater than 185 m and inclusions in both areas trapped fluids with intermediate to low temperatures. Samples from the IFZ that

trapped only the coolest fluids are from the deepest part of the ESF (215 – 270 m). These temperatures, furthermore, are not related to a lateral temperature gradient across the site because the temperature variations occurred at different times. The distribution of fluid inclusion homogenization temperatures is related to precipitation of secondary minerals from fluids that declined in temperature over time.

4.4. Fluid Inclusion Ice Melting Temperatures

Ice melting temperatures were obtained for 129 inclusions from 2-phase FIAs in calcite from 30 samples across the site (Fig. 9). The data are limited owing to the difficulty in nucleating vapor bubbles necessary for the analyses. Temperatures range between -0.2 and -1.6 °C, and the majority of the temperatures are between -0.4 and -0.9 °C. These temperatures indicate a salinity range of 0.35 to 2.74 wt.% NaCl equivalent (Bodnar, 1993), with the majority of the data ranging from 0.71 to 1.57 wt.% NaCl equivalent. Given that the inclusions are trapped in calcite, trace CO₂ in the fluid is contributing to the freezing point depression.

There is no systematic relationship between homogenization and ice melting temperatures. For example, ice melting temperatures for inclusions in fluorite (ECRB 25+30) are between -0.6 °C and -0.7 °C and homogenization temperatures range from 69 – 81 °C. These ice melting determinations are the same as the majority of the data for calcite, including samples from the IFZ that formed at < 50 °C. Results indicate that the 2-phase FIAs consistently trapped a low-salinity fluid.

4.5. δD Compositions of Fluid Inclusion Fluids

Three calcite samples were analyzed to determine the δD composition of the fluids trapped by various inclusion populations (Table 1). Samples were collected from intermediate calcite that contained 2-phase FIAs and was well constrained by U-Pb dating, and from MGSC that contained rare all liquid inclusions. δD compositions varied between -90 ‰ and -131 ‰. Intermediate calcite (AL#5 00+28.5) had a composition of -90 ‰ to -120 ‰, and the youngest MGSC (ESF 27+84, ESF 60+52.5) had isotopic signatures of -110 ‰ to -131 ‰. These data indicate that the inclusions trapped meteoric fluids.

5. U-Pb DATING

Opal and chalcedony in the secondary mineral layers were dated using U-Pb and U-series methods to constrain the ages of the 2-phase FIAs. Based on the distribution and availability of datable minerals in the sections, the strategy of the geochronology study was to 1) determine the age of MGSC, which provides a minimum age for the 2-phase FIAs, and 2) place more precise constraints on the ages of 2-phase FIAs in samples where dateable minerals are spatially related to the FIAs. Because 2-phase FIAs are not present in MGSC (Fig. 3), ages of earliest MGSC precipitation provide a minimum age for the FIAs. The majority of opal that can be dated is intergrown with MGSC and the age of formation of MGSC was well constrained. The ages of primary FIAs can be constrained by dating material that is demonstrably paragenetically older and younger than a spatially related FIA. However, minerals that could be dated were commonly not spatially associated with 2-phase FIAs, limiting temporal constraints in many samples.

Nevertheless, opal and chalcedony in the older parts of some of the mineral crusts provided older constraints on the ages of 2-phase FIAs.

5.1. Results

Forty-one U-Pb and U series ages were obtained from 18 sample locations across the site (Fig. 1; Tables 2 and 3). The ages that best constrain the formation of the MGSC and the FIAs are discussed below. Additional dates and their significance, locations of the dated sample material, and detailed thin section maps are provided in the Appendix.

5.1.1. U-Pb dating of minerals in case of radioactive disequilibrium

The conventional method of calculating $^{206}\text{Pb}^*/^{238}\text{U}$ and $^{207}\text{Pb}^*/^{235}\text{U}$ isotopic ages (asterisks denote radiogenic Pb) assumes that activities of all intermediate daughter isotopes were in secular equilibrium (activities of all daughter isotopes are equal to that of the parent) at the time of mineral formation. Previous U-series studies of the Yucca Mountain opals from outermost surfaces of calcite-silica coatings revealed large initial excesses of ^{234}U and absence of ^{230}Th (Paces et al., 2000; Neymark and Paces, 2000; Neymark et al., 2000). Therefore, a more general form of the age equations for a closed system had to be applied (Bateman, 1910). Principles of U-Pb dating in case of initial radioactive disequilibrium and their application to secondary silica mineralization were discussed by Neymark et al. (2000). Equations used for the current work are applicable to systems older than 1000 years (that is, only daughter isotopes with half-lives greater than 1 yr are considered), emphasize initial disequilibrium of ^{234}U , and assume negligible initial ^{231}Pa , ^{227}Ac , ^{230}Th , ^{226}Ra , ^{210}Pb (Ludwig, 1977). The absence of these isotopes in minerals precipitated from aqueous solutions is suggested by their low solubility and short residence time in ground waters (Gascoyne, 1992), and is substantiated by very low contents of ^{232}Th and common Pb in the analyzed silica minerals (Neymark et al. 2000, 2001; Table 2).

The isotopic ratios $^{206}\text{Pb}^*/^{238}\text{U}$ and $^{207}\text{Pb}^*/^{235}\text{U}$ correspond to two independent apparent ages obtained from two different radioactive decay systems. Concordance of these ages is an important check on the closed-system behavior of the material analyzed. The age calculation from $^{206}\text{Pb}^*/^{238}\text{U}$ requires that the ($^{234}\text{U}/^{238}\text{U}$) initial activity ratio must be known. Previous U-series data indicate that initial ($^{234}\text{U}/^{238}\text{U}$) for opal and calcite from the ESF range from 2 to 10 Ma (Paces et al., 2001; Neymark and Paces, 2000). Growth of radiogenic Pb from variable excesses of ^{234}U is described by a family of concordia curves for different initial ($^{234}\text{U}/^{238}\text{U}$), shown in Figure 10. The shape of the concordia curves reflects the fast growth of radiogenic $^{206}\text{Pb}^*$ derived from the excess ^{234}U during the first 1 m.y. after mineral deposition. Then ^{234}U reaches radioactive equilibrium with ^{238}U and the curves became parallel to each other.

In contrast to the ^{238}U decay chain, the ^{235}U decay chain contains neither daughter uranium isotopes nor any other water-soluble long-lived isotopes. The $^{207}\text{Pb}/^{235}\text{U}$ age therefore is not dependent on the unknown initial ($^{234}\text{U}/^{238}\text{U}$). The disequilibrium $^{207}\text{Pb}/^{235}\text{U}$ ages, assuming the absence of initial ^{231}Pa and ^{227}Ac , are considered the best approximation for the timing of silica precipitation and are used in the following sections of this paper (Table 3, column d). The difference between conventional and disequilibrium $^{207}\text{Pb}/^{235}\text{U}$ ages is between 46 – 50 ka.

The ($^{234}\text{U}/^{238}\text{U}$) and ($^{230}\text{Th}/^{238}\text{U}$) activity ratios (Tables 2 and 3; Fig. 11) vary between ~ 1 and ~ 3.7. Young opals with $^{207}\text{Pb}/^{235}\text{U}$ disequilibrium ages less than 1.5 Ma have elevated ($^{234}\text{U}/^{238}\text{U}$) and ($^{230}\text{Th}/^{238}\text{U}$) ratios that are negatively correlated with the age. This is consistent

with deposition of silica from water with high ($^{234}\text{U}/^{238}\text{U}$) (Paces et al., 1998). Opal fractions with $^{207}\text{Pb}/^{235}\text{U}$ disequilibrium ages older than 1.5 – 2.0 Ma have both ($^{234}\text{U}/^{238}\text{U}$) and ($^{230}\text{Th}/^{238}\text{U}$) closer to unity. However, many of these older fractions contain small (up to 6 %, not considering two imprecise analyses) excesses of ^{234}U and ^{230}Th . This suggests relatively recent addition of uranium from the water, either by exchange between old silica and young fracture water, or, more likely, by small additional opal growth (Neymark et al. 2000; in press).

5.1.2. The role of possible multi-stage opal growth

Slightly elevated ($^{234}\text{U}/^{238}\text{U}$) and ($^{230}\text{Th}/^{238}\text{U}$) activity ratios in opals older than 1.5 – 2.0 Ma suggests mixing of small amounts of young opal with older opal. In this case the $^{207}\text{Pb}/^{235}\text{U}$ disequilibrium age would represent a minimum age of deposition for the older opal component (Neymark et al., in press). Replicate analyses of such “mixed” opals allow us to estimate the ages of the older components. Fragments of opal for replicate analyses are taken from different portions of the same opal layers, and are likely to contain variable proportions of the “old” and “young” end members. Duplicate analyses of samples ESF 27+84 Op-2, ESF 28+80 Op-2, and ESF 60+52.5 Op-1, and triplicate analysis of the sample ESF 27+84 Op-1 show variable and negatively correlated $^{207}\text{Pb}/^{235}\text{U}$ ages and ($^{234}\text{U}/^{238}\text{U}$), in agreement with two-component mixing between the “old” and “young” end members. Assuming that the “old” end member is in secular equilibrium and the end member compositions in replicate fractions are identical, we can extrapolate the ($^{234}\text{U}/^{238}\text{U}$) versus $^{207}\text{Pb}/^{235}\text{U}$ age line to ($^{234}\text{U}/^{238}\text{U}$) = 1 and get the “age of the older end member” at the axis intersection (similar for the ($^{230}\text{Th}/^{238}\text{U}$) versus $^{207}\text{Pb}/^{235}\text{U}$ age relationship). The estimated “ages of the old components” are 1.21 – 1.24 Ma for ESF 27+84 Op-2, 0.76 – 1.15 Ma for ESF 28+80 Op-2, and 1.17 – 1.26 Ma for ESF 60+52.5 Op-1. These values should be considered tentative semi-quantitative estimates, because linear extrapolation and two-component mixing are over-simplifications. Nevertheless, these estimates show that the true depositional ages of opals containing admixtures of young silica can be 0.2 – 0.7 m.y. older than their apparent $^{207}\text{Pb}/^{235}\text{U}$ ages.

Most of the studied opals have ($^{234}\text{U}/^{238}\text{U}$) and ($^{230}\text{Th}/^{238}\text{U}$) activity ratios much closer to unity than the young opals used in the above modeling. Accordingly the differences between the ages of the “old component” and the apparent $^{207}\text{Pb}/^{235}\text{U}$ ages would be smaller. The triplicate analysis of a more representative sample ESF 27+84 Op-1 yielded the estimates “age of the older end member” from 1.97 ± 0.06 to 2.05 ± 0.21 Ma, within error of the $^{207}\text{Pb}/^{235}\text{U}$ ages of 1.89–1.95 Ma. For samples older than 2 m.y. with similar or lower ($^{234}\text{U}/^{238}\text{U}$) and ($^{230}\text{Th}/^{238}\text{U}$) activity ratios, the bias in the $^{207}\text{Pb}/^{235}\text{U}$ age due to the possible presence of “young” admixture is insignificant.

5.1.3. Age of MGSC

To determine the age of MGSC, opal samples were collected from polished sections from below, within, and on top of the MGSC layer. All samples were X-ray mapped using the electron microprobe to identify MGSC and determine the paragenetic relationship between the sampled material and MGSC. The ages and the relationships between dated material and MGSC are summarized in Figure 12.

The obtained ages show that MGSC began to precipitate at Yucca Mountain between about 2.9 – 1.9 Ma. Opal collected along the boundary between bladed calcite and MGSC (ESF

72+25; Fig. 7e) gave an age of 2.90 ± 0.06 Ma, and provides a maximum age for MGSC precipitation. Opal (ESF 27+84; Fig. 7a) collected from just within MGSC near the contact between MGSC and underlying calcite provided three ages from 1.89 ± 0.09 to 1.95 ± 0.07 Ma (Table 3, column d), and indicates that MGSC began to precipitate before about 1.9 Ma. A second opal from this layer provided an age of 1.97 ± 0.04 Ma (Fig. 7a), confirming this timing. The ages determined from these two samples bracket the initial precipitation of MGSC. Additional ages, including ages younger than 1 Ma for opal from the outermost parts of crusts, show that MGSC and intergrown opal have continued to precipitate to at least within the last few hundred thousand years (Figs. 7 and 12; Appendix). A few samples of paragenetically older material consistently demonstrate that MGSC is younger than 3 – 9 Ma.

Ages determined for opal collected from the base of the MGSC in samples from other localities, for example ECRB 14 + 49 (Appendix), indicate that MGSC began to precipitate around 1.22 ± 0.02 Ma (Fig. 12, left pointing arrow at 1.0 - 1.5 Ma). This age indicates that MGSC did not start precipitating at the same time across the site and, furthermore, shows that the MGSC layer does not represent an absolute timeline. These various ages are consistent with petrographic observations and X-ray mapping that clearly show that MGSC did not precipitate in every site and that MGSC layers can vary in thickness and be discontinuous within a single sample and between adjacent samples sites (Fig. 3; Wilson and Cline, 2002). In spite of these discontinuities, the similarity in the range of ages obtained from opal associated with MGSC, as well as the distinctive chemistry and growth zoning in MGSC, permit this layer to be correlated across the site. Observations and analyses show that various sample sites recorded different components of the larger MGSC event which occurred between ~ 2.9 Ma and the last few hundred thousand years.

5.1.4. Ages of 2-phase FIAs

In some samples, calcite that precipitated before MGSC is intergrown with opal and chalcedony. Ages obtained for these samples place tighter constraints on the ages of some 2-phase FIAs. In a sample from a LC in the LCZ (Fig. 7a; ESF 27+84), primary 2-phase FIAs occur in fine mottled calcite at the base of the section. Calcite in the central part of the crust is clear and is overgrown by clear and dark MGSC. Both the central calcite and outer MGSC only contain rare liquid-only inclusions. A discontinuous clear opal layer at the boundary between the basal calcite and the central clear calcite has an age of 5.32 ± 0.02 Ma, indicating that fluids with elevated temperatures were present more than about 5.3 Ma. A discontinuous opal layer within MGSC confirmed that MGSC began to precipitate before 1.9 Ma. Opal from the outermost part of the sample gave U-Pb ages of 0.72 ± 0.42 to 0.99 ± 0.02 Ma indicating deposition of this outer layer within the last million years.

In a sample from alcove 5 (AL#5 00+28.5; Fig. 7b) in the LCZ, primary 2-phase FIAs are distributed throughout the lower and central portions of a LC crust, but are not present in outermost calcite. This youngest calcite is not MGSC and this sample does not contain the youngest mineral layer. Two-phase FIAs exhibit a clear decrease in temperature from older to younger layers in the sample. Chalcedony in the central portion of the sample gave an age of 6.29 ± 0.08 Ma, indicating that inclusions with homogenization temperatures greater than about 45 °C, which are located below this chalcedony, are older than this age. Calcite between this chalcedony and outer opal contains 2-phase FIAs that homogenize from about 37 – 43 °C. Opal paragenetically younger than these inclusions gave two ages of 5.78 ± 0.30 and 1.37 Ma showing

that these inclusions are between about 6.3 – 5.8 Ma in age. Two-phase FIAs that homogenize at 35 – 41 °C are in calcite adjacent to and outboard of the opal, and are younger than 5.8 Ma. These inclusions were the youngest 2-phase inclusions identified in this study and a minimum age for these inclusions could not be determined. However, near the outermost surface of these samples 2-phase FIAs were not observed and liquid-only inclusions are present. These liquid-only inclusions are in calcite that is older than MGSC.

A NR sample from a fracture occurrence (Fig. 7c; ESF 13+19) contains primary 2-phase FIAs with homogenization temperatures that reach 75 °C. The inclusions are in calcite adjacent to the wall rock fragments, and are overgrown by calcite, fluorite, chalcedony-quartz, and MGSC. U-Pb ages determined for chalcedony indicate that the 2-phase FIAs are older than 4.00 ± 1.46 Ma. Outer brown opal associated with MGSC has an age of 1.70 ± 0.02 Ma. Note that sparse MGSC occurs sporadically on the outermost surface of the sample and requires microprobe X-ray mapping for identification.

A sample from a shallowly dipping fracture occurrence in the LCZ contains relatively sparse 2-phase FIAs at the base and in the central part of the crust (Fig. 7d; ESF 28+80). Central calcite is overgrown by MGSC that only contains liquid-only inclusions. Two-phase FIAs near the base of the crust homogenize at temperatures of 49 – 55 °C, but other calcite that precipitated on a tuff clast contains inclusions that homogenize at 39 – 45 °C. Two-phase FIAs in the basal and central parts of the crust have generally similar homogenization temperatures between 35 – 45 °C. Opal that is younger than the 2-phase FIAs has ages between 3.29 ± 0.08 Ma and 3.88 ± 0.11 Ma, indicating that fluids with elevated temperatures were present more than about 3.9 Ma. Calcite that is not MGSC directly overlies the dated opal, confirming that MGSC is younger than 3.9 Ma. Outermost opal associated with MGSC gave ages of 0.32 ± 0.02 and 0.38 ± 0.02 Ma.

The oldest age constraint for 2-phase FIAs was obtained from a fracture occurrence in the NP (ESF 04+73.4; Fig. 7f). Several 2-phase FIAs with homogenization temperatures that reach 83 °C occur in dark calcite that is younger than basal brown opal that occurs within chalcedony, and which was dated at 9.06 ± 0.08 Ma. The dark calcite contains solid inclusions of chalcedony-quartz and is overgrown by clear calcite and MGSC that contain liquid-only inclusions. This sample indicates that the 2-phase FIAs are younger than 9 Ma and older than about 2.9 Ma. The association of chalcedony-quartz with the calcite and the light $\delta^{18}\text{O}$ composition of this calcite (~ 5 ‰; Wilson and Cline, 2002) suggest that the calcite that contains these high temperature FIAs is paragenetically early. The age of 9.06 ± 0.08 Ma is similar to ages of 7.79 ± 0.67 Ma obtained for brown opal at the base of a LC crust in the SPR (ESF 76+59.5; Appendix), and 7.94 ± 0.22 Ma obtained for chalcedony from a LC crust from the LCZ (ESF 32+31; Appendix). Two-phase FIAs with homogenization temperatures from 43 – 53 °C are present in calcite that is lateral to, but which encompasses the dated opal (Appendix). These temperatures are consistent with temperatures in older calcite.

These ages, collectively, show that 2-phase FIAs were trapped prior to 4.0 Ma, and probably prior to 5.3 Ma. The youngest identified 2-phase inclusions were trapped in calcite adjacent to and paragenetically younger than opal dated at about 5.8 Ma. These inclusions homogenize at temperatures ≤ 41 °C.

6. DISCUSSION

This study addressed the spatial extent and timing of the passage of fluids with elevated temperatures through the Yucca Mountain site. The presence of spatially related, liquid plus vapor fluid inclusions that provide consistent homogenization temperatures demonstrates that fluids with elevated temperatures did pass through the site. The paragenesis, microthermometry, and geochronology studies conducted as part of this project have provided the spatial relationships, temperatures, and timing of the inclusions to answer the posed questions.

Fluid inclusion petrography and microthermometry on polished sections prepared for this study and a parallel study by the USGS indicate that equivalent sections have identical paragenetic sequences but vary in mineral abundance (J. Whelan, personal communication; 2000). The parallel studies also show that fluid inclusion petrography is identical between sections, but there are variations in the abundance of 2-phase FIAs. Distribution maps for 2-phase FIAs and homogenization temperatures determined from fewer samples in a parallel study (Whelan et al., 2000) were almost identical to the data presented in this study. Earlier data collected by State of Nevada scientists (Dublyansky, 1998; Dublyansky et al. 2001) from a small number of samples are also consistent with results reported here.

Paragenesis and fluid inclusion studies indicate that fluids with elevated temperatures traveled through open spaces and precipitated secondary minerals at localities throughout the ESF and ECRB. However, secondary minerals are present in only about 10% of the available open space. The remaining 90 % contains no secondary mineral record indicating fluid flow. The secondary mineral record is a function of the amount of fluid input, porosity, permeability and connectivity of individual precipitation sites, and the time of formation of the precipitation sites relative to the fluid flux. Flow paths for early fluids may have become blocked by mineral precipitation leading to cessation of precipitation in one site and initiation of mineral precipitation in a new site. Studies of the site, however, have shown that most of the tuff is relatively porous and fluid flow through fractures and rock matrix have been demonstrated (e.g. Stuckless and Dudley, in press). Given that the rocks are porous and permeable, the general lack of secondary minerals and sparse record of fluids with elevated temperatures is most likely related to input of only small amounts of a fluid that is transporting small quantities of dissolved components.

6.1. How Widespread, Within the Repository Site, was the Influx of Fluids with Elevated Temperatures?

The passage of fluids with elevated temperatures as indicated by the presence of 2-phase FIAs is recorded in half of the secondary mineral samples collected from about 10% of the pore spaces across the ESF and ECRB. Significantly, half of the collected samples do not contain a record of these fluids, and samples that recorded the highest temperatures occur adjacent to samples that did not record elevated temperatures, or which are barren of secondary minerals. The record of elevated temperatures is more prevalent in some areas of the site (LCZ, eastern ECRB) and is sparse in other areas (SPR, western ECRB). These features show that fluids with elevated temperatures were not pervasive throughout Yucca Mountain.

The distribution of fluid temperatures is related to the timing of mineral precipitation at various sites. Where present, elevated temperatures are recorded in early to early-intermediate calcite, and the presence or absence of this record is related to whether or not early fluids with

elevated temperatures reached precipitation sites. Some of the LC that formed contemporaneously with the rock recorded the presence of higher temperature fluids. Other precipitation sites particularly fractures and breccias, probably did not exist when the earliest and highest temperature fluids were present. Fracture and breccia occurrences are interpreted to represent cooling joints and recorded the passage of later fluids with lower temperatures. The youngest calcite recorded only the presence of cool fluids, represented by liquid-only inclusions.

Variations in inclusion homogenization temperatures in the ECRB, which traverses above the potential repository horizon in the Topopah Spring Tuff, are minimal compared to the rest of the site. Petrographically the ECRB is extremely consistent; fine-grained calcite is overgrown by bladed calcite and capped by MGSC. Although many samples in the ECRB do not contain 2-phase FIAs, fluid inclusion petrography and microthermometry are similar between LC, fracture, and breccia occurrences that do. This consistency indicates a similar fluid flux across the ECRB and suggests a similar history of fluid flow for the part of the site that may host the repository.

It is noteworthy that temperatures recorded across the Yucca Mountain repository horizon do not exhibit a central hot plume and large lateral thermal gradients that are present in geothermal and epithermal systems (Henley, 1985). The lack of a significant temperature gradient and presence, instead, of relatively uniform temperatures argues against an upwelling hot fluid model.

6.2. What Temperatures do the 2-phase FIAs Represent?

Fluid inclusion petrographic and microthermometric data show that evaluated fluid inclusions comprise valid assemblages according to the criteria outlined by Goldstein and Reynolds (1994). Consistent homogenization temperatures, generally within 10 °C, show that inclusions trapped homogeneous fluids and demonstrate that the inclusions were not perturbed after they formed.

The highest temperature fluids in calcite, from about 70 – 80 °C, were only identified in the NP, in paragenetically old calcite. Fluids with temperatures reaching 70 °C were identified in the NP and NR, again in paragenetically old calcite in the welded Tiva Canyon Tuff. Interestingly no samples from the NP and NR have bimodal distributions and only recorded early fluids. Early, high temperature fluids were restricted to welded Tiva Canyon Tuff and did not extend to deeper areas. The Tiva Canyon is underlain by the PTn, an important hydrogeologic barrier that impedes downward flow as permeability changes from being fracture-controlled to matrix-controlled at the Tiva Canyon-PTn contact (e.g. Stuckless and Dudley, in press). The high temperature inclusions are found in the northeastern part of the ESF where it intersects the Tiva Canyon Tuff. High temperature fluids may have been restricted to this part of the site, or may have infiltrated Tiva Canyon Tuff elsewhere above the level of the ESF and ECRB. However, high temperature fluids were not identified in Tiva Canyon Tuff in the south portal of the ESF. The PTn tapers out between the North and South portal, and the South ramp and portal area is cut by numerous faults offsetting lithologies exposed in the ESF. High temperature fluids may not have reached this region owing to the lack of a hydrologic barrier, such as the PTn, to focus the early high temperature fluid flow along the PTn Tiva Canyon Tuff contact.

Subsequently, fluids with temperatures up to about 60 °C infiltrated the western (NR, LCZ, ECRB) and southern (SPR) part of the site. These fluids did not access the NP, suggesting that fluid flow was inhibited in this part of the site when these fluids were present. The greater abundance of silica minerals found dominantly in the NP may have reduced fluid access to this

area. These fluids also were not recorded in the IFZ because fractures had not formed at this time and there are fewer LC in this region.

As fluids cooled to less than 50 °C, fluid movement was restricted to the ECRB, LCZ, and IFZ. The majority of samples from the LCZ and ECRB recorded this lower temperature fluid plus earlier higher temperature fluids, and demonstrate fluid cooling with time (Figs. 5 and 7). Such evidence of cooling is restricted to samples from the Topopah Spring Tuff and is not observed in samples from the NP, NR, and SPR. Secondary minerals in the IFZ occur in steeply dipping fractures and recorded only cooler, < 50 °C fluids. The lack of vapor-phase mineralization, early calcite, and high temperature fluid inclusions in the IFZ support the interpretation that fractures in the IFZ formed after passage of the higher temperature fluids. Samples from this part of the ESF provide a record of intermediate and young calcite.

As more than 65 % of samples from across the site contain MGSC, the youngest, low temperature event is recorded across Yucca Mountain. Late, low temperature fluids deposited MGSC in less than 10 % of the available open space, but accessed some pore spaces across the entire site.

Rare, liquid-only inclusions are the only fluid inclusions present in outer intermediate calcite and MGSC. The presence of liquid-only inclusions has been generally accepted to indicate that the inclusions formed at < 100 °C (Roedder, 1984). However, all 2-phase and liquid-only inclusions observed in this study formed at < 100 °C. As shown in Figure 5, many 2-phase inclusions were trapped at < 50 °C. During one of the heating runs, 2-phase inclusions from the IFZ homogenized at 32 – 33 °C, below the first heating step of 35 °C, demonstrating that fluids trapped at temperatures as low as 32 °C can form 2-phase FIAs. These observations provide some of the strongest evidence that secondary minerals that contain only liquid-only fluid inclusions, which includes most intermediate calcite and MGSC, formed at temperatures below 35 °C.

The range of trapping temperatures for fluorite and quartz demonstrates that they formed over a range of temperatures at Yucca Mountain, and also shows that fluorite can precipitate at relatively low temperatures. Some homogenization temperatures from inclusions in fluorite and quartz are slightly higher than homogenization temperatures from associated calcite. The high temperatures and paragenetic positions of these minerals suggest that they formed very early, possibly during vapor phase alteration (Wilson and Cline, 2002).

Freezing point depressions for most inclusions range from -0.4 to -0.9 °C indicating a salinity range of 0.7 to 1.6 wt.% NaCl equivalent with no systematic relationship between homogenization and ice melting temperatures. These results show that regardless of fluid temperature, fluid salinity was low and inclusions may have trapped a fluid that cooled over time.

6.3. When Were 2-phase FIAs Trapped?

Paragenetic studies and fluid inclusion petrography show that 2-phase FIAs occur in early to earliest-intermediate calcite. Two-phase FIAs have not been observed in late-intermediate calcite or in outer MGSC. Therefore, based on these observations, fluids with elevated temperatures were probably not present in the recent geologic past.

Integration of fluid inclusion petrography, microthermometry and U-Pb dating establishes that elevated temperature fluids were present only during the early history of Yucca Mountain. The oldest age constraint obtained for the fluid inclusions is 9.06 ± 0.08 Ma (ESF 04+73.4; Fig.

7f), and 2-phase FIAs are younger than this age. Two-phase FIAs with temperatures $> 45\text{ }^{\circ}\text{C}$ are older than $5.32 \pm 0.02\text{ Ma}$ (Fig. 7a), $6.29 \pm 0.30\text{ Ma}$ (Fig. 7b), $4.00 \pm 1.46\text{ Ma}$ (Fig. 7c), and $3.88 \pm 0.11\text{ Ma}$ (Fig. 7d) and therefore fluids with temperatures $> 45\text{ }^{\circ}\text{C}$ were present in the site prior to $6.29 \pm 0.30\text{ Ma}$. Fluids with temperatures around $35 - 45\text{ }^{\circ}\text{C}$ can be constrained to being older than $5.32 \pm 0.02\text{ Ma}$ (Figs. 7a and b). Secondary minerals determined to be less than $5.32 \pm 0.02\text{ Ma}$ contain only single-phase fluid inclusions and, therefore, precipitated from fluids $\leq 35\text{ }^{\circ}\text{C}$. Mg-enriched growth-zoned sparry calcite began to precipitate between about 2.9 and 1.9 Ma from fluids of $\leq 35\text{ }^{\circ}\text{C}$.

These results show that there is no fluid inclusion evidence for an influx of thermal waters into the repository site during the past 5.3 m.y. The integrated petrography, paragenetic studies, geochemistry (Wilson and Cline, 2002), fluid inclusion, and geochronological studies provides no evidence for recent hydrothermal activity.

6.4. Origin of the Fluids

The most plausible environment for secondary mineral formation is in the vadose zone (Wilson and Cline, 2002). The low δD signatures of fluid inclusion fluids (e.g. $\leq -105\text{ }_{\text{‰}}$; Table 1) indicate that intermediate calcite and MGSC could only have been derived from meteoric fluids.

6.5. Genetic Models for the Formation of Secondary Minerals

Results presented in this paper and by Wilson and Cline (2002) are compatible with models proposed by U.S. Geological Survey geologists (Paces et al., 1996; 1998a; 1998b, 2001; Whelan et al., 1996; in press; Marshall and Whelan, 2000) that involve infiltration by descending meteoric fluids. Results are not consistent with models proposed for the formation of secondary minerals by upwelling hydrothermal fluids in the phreatic zone (Dublyansky 1998; Dublyansky et al., 1998; 2001).

U.S. Geological Survey scientists concluded that secondary minerals formed in the vadose zone and the following model is summarized from Whelan et al., (in press). A small amount of meteoric water percolated through the soils and infiltrated the UZ at Yucca Mountain. Although much of this water moved as matrix flow, some flow occurred along fracture pathways and open spaces. Highly porous vapor-phase alteration provided a pathway that diverted flow to the base of lithophysal cavities where thin water films were unevenly distributed. Water was drawn up the faces of growing crystals by surface tension, and the removal of CO_2 and H_2O via the gas phase precipitated calcite and silica (Whelan et al., in press). Fluid inclusion temperatures of $35 - 85\text{ }^{\circ}\text{C}$ are interpreted to be common in the early stage, rare in the intermediate age, and absent in the late stage (Whelan et al., in press; Wilson et al., 2000). Early high temperatures coincided with reduced $\delta^{18}\text{O}$ compositions and cooling of the fluid with time is compatible with a progressive increase in $\delta^{18}\text{O}$ during the early and intermediate stages (Whelan et al., 2000).

6.6. Model for the Formation of Secondary Minerals

Early – early intermediate secondary minerals ($> 5.32\text{ Ma}$)

After deposition of the host tuff sequence and vapor-phase alteration descending meteoric fluids percolated into the warm tuff sequence ($> 50\text{ }^{\circ}\text{C}$) and precipitated secondary minerals (calcite, quartz, fluorite) that contained 2-phase FIAs and chalcedony and brown opal in the vadose zone.

Elevated temperatures within the sequence could be expected for a few m.y. following intrusion of the Timber Mountain at around 10 Ma (Marshall and Whelan, 2000) consistent with the secondary minerals record. The NP recorded localized elevated temperatures that were not recorded in the underlying tuff units. Fluids greater than 50 °C were present at the site more than 6.29 Ma and later, cooler fluids of 35 – 45 °C were present as recently as 5.32 Ma. These temperatures indicate that the sequence was above current day ambient temperature of 27 °C for a considerable time after tuff deposition at 12.7 Ma.

Late intermediate secondary minerals (5.32 – ~2.9 Ma)

Meteoric fluids percolated into the tuff sequence at temperature less than 35 °C and temperatures within the site have not varied significantly from the present day temperature. No 2-phase FIAs were recorded in the minerals that precipitated. Only rare liquid-only inclusions were trapped. Principally calcite was deposited during this stage with rare clear opal, and very minor chalcedony-quartz. Long bladed calcite crystals formed as overgrowths on early smaller bladed calcite crystals and comprise the majority of intermediate calcite. In other sites, where space was at a premium, other calcite habits formed. δD compositions of inclusion fluids indicate formation from meteoric fluids.

Late precipitation of MGSC (~2.9 Ma to present)

The deposition of MGSC across the site was related to a change in fluid flux from that responsible for earlier secondary minerals. This change can be correlated to a climatic change in southern Nevada that resulted in cyclical increases and decreases in the Mg/Ca ratio of the meteoric fluids percolating into the site (see discussion in Wilson and Cline, 2002). MGSC precipitated from small inputs of fluids, resulting in fine Mg-enriched and depleted growth zones. Precipitation by small fluid inputs is supported by ages determined for this layer that confirm minimal or no precipitation over a significant period of time. Rare liquid-only inclusions are consistent with MGSC forming from thin films of fluid and indicate that MGSC formed at < 35 °C. The presence of MGSC across the site suggests that the processes responsible for formation of this calcite occurred across the site and that the site has been stable, on conservative estimates, for the last few million years.

7. CONCLUSIONS

Two-phase FIAs indicative of elevated temperatures are present in secondary mineral crusts at the proposed Yucca Mountain nuclear waste repository. These 2-phase FIAs occur predominantly in paragenetically early calcite around the wall rock at the base of mineral crusts. Rare 2-phase FIAs occur in the earliest intermediate minerals but they are not present in late intermediate calcite and the youngest Mg-enriched growth zoned sparry calcite (MGSC). Only rare liquid-only inclusions are present in late intermediate minerals and outer MGSC.

Homogenization temperatures obtained from calcite across the site are 35 – 83 °C. Rare fluorite and quartz contain 2-phase FIAs that typically had homogenization temperatures similar to adjacent calcite. The majority of samples across the site recorded fluids of 45 – 60 °C. Some calcite from the North portal formed at higher temperatures than calcite elsewhere, and recorded fluid temperatures up to 83 °C in one sample. These localized high temperatures were also recorded by 2-phase FIAs in quartz and fluorite. Samples from the IFZ recorded cooler

temperatures of 40 – 50 °C. The majority of samples collected from the Topopah Spring Tuff, mainly from LC occurrences, indicate a cooling trend with time; homogenization temperatures at the base of the crusts formed at temperatures > 50 °C and paragenetically younger basal calcite formed at temperatures of 35 – 45 °C. The timing relationships suggest that the 35 – 45 °C inclusions are equivalent to the low temperature 2-phase FIAs observed in the IFZ. Only rare liquid-only inclusions are observed in paragenetically younger calcite. The presence of liquid-only FIAs indicates that young secondary minerals formed at temperatures less than 35 °C. Freezing point depressions of -0.2 to -1.6 °C (mode -0.4 to -0.9 °C) are consistent with formation from a low salinity fluid and suggest that secondary minerals formed from similar fluids.

Integration of fluid inclusion petrography and microthermometry with U-Pb dating indicates that fluids with elevated temperatures have not been present in the recent geologic past. Two-phase FIAs adjacent to the wall rock that trapped fluids of > 50 °C are older than 6.29 ± 0.30 Ma. Two-phase FIAs in paragenetically later, early calcite which formed from fluids of 35 – 45 °C are older than 5.32 ± 0.02 Ma. The consistent homogenization temperatures obtained for 2-phase FIAs in early minerals argues strongly that the site has not been perturbed since these fluid inclusions were trapped. There is no evidence of fluids with elevated temperatures in secondary minerals that formed during the past 5.32 m.y. The presence of MGSC across the site indicates a consistent flux from ambient temperature fluids during the past 2 to 3 m.y.

Results from this study are not consistent with models requiring formation of secondary minerals in a saturated environment at Yucca Mountain. Results, furthermore, provide no evidence for the former presence of upwelling hydrothermal fluids. Alternatively, results are consistent with infiltration of a cooling tuff sequence by descending meteoric water. This study demonstrates that the hypothesis of geologically recent upwelling hydrothermal fluids is untenable and should not disqualify Yucca Mountain as a potential nuclear waste storage site.

Acknowledgements. We would like to thank Drew Coleman (DOE-YMP) for his help during all aspects of this project, Joel Rotert for assistance during sampling and for hours of patient microthermometry, and Bob Bodnar for his technical review of this report. Bob Bodnar, Yuri Dublyanski, Bob Goldstein, Ed Roedder, Joe Whelan and Ike Winograd are thanked for discussions on all aspects of this project. Project funding was awarded to JSC under DOE Cooperative Agreement DE-FC08-98NV-12081.

All data presented in this report were collected under the University and Community College System of Nevada (UCCSN) Quality Assurance Program. Technical Data Management System data tracking number UN0203SPA004JC.001 correlates to data collected during this study. Access to electronic data was limited to task personnel and controlled with the use of passwords. Loss was prevented by use of backup files. Manual entry and file transfers were verified for accuracy. No electronic data were lost or corrupted.

REFERENCES

- Bateman H. (1910) Solution of a system of differential equations occurring in the theory of radio-active transformations. *Proc. Cambridge Phil. Soc.* 15, 423-427.
- Bish D. L. and Aronson J. L. (1993) Paleogeothermal and paleohydrologic conditions in silicic tuff from Yucca Mountain, Nevada. *Clays and Clay Minerals*, 41, 2, p. 148-161.
- Bodnar R. J. (1993) Revised equation and table for determining the freezing point depression of H₂O-NaCl solutions. *Geochim. Cosmochim. Acta*, 57, 683-684.
- Buesch D. C., Spengler R. W., Moyer T. C. and Geslin J. K. (1996) Proposed stratigraphic nomenclature and macroscopic identification of lithostratigraphic units of the Paintbrush Group exposed at Yucca Mountain, Nevada. U. S. Geological Survey Open-File Report 94-469, 47 p.
- Carlos B. A. (1994) Field guide to fracture-lining minerals at Yucca Mountain. Los Alamos National Lab. Rep. LA-12803-MS.
- Christiansen R. L., Lipman P. W., Carr W. J., Byers F. M Jr., Orkild P. P. and Sargent K. A. (1977) Timber Mountain-Oasis Valley caldera complex of southern Nevada. *GSA Bulletin* 88, 943-959.
- Data Tracking Number UN0203SPA004JC.001. Thermochronological evolution of calcite formation at Yucca Mountain. Submittal date: 03/26/2002.
- Dublyansky Y. (1998) Fluid inclusion studies of samples from the Exploratory Study Facility, Yucca Mountain, Nevada. Institute for Energy and Environmental Research, Washington.
- Dublyansky Y., Szymanski J., Chepizhko A., Lapin B. and Reutsky V. (1998) Geological history of Yucca Mountain (Nevada) and the problem of a high-level nuclear waste repository. In *Defense Nuclear Waste Disposal in Russia* (eds. M. Stenhouse and V. Kirko). NATO Series, Kluwer Academic Publishing, Netherlands, pp. 279-292.
- Dublyansky Y., Ford D. and Reutski V. (2001) Traces of epigenetic hydrothermal activity at Yucca Mountain, Nevada: preliminary data on the fluid inclusion and stable isotope evidence. *Chemical Geology* 173, 125-149.
- Gascoyne M. (1992) Geochemistry of actinides and their daughters. In *Uranium-series Disequilibrium: Applications to Earth, Marine, and Environmental Sciences*, 2nd ed., Clarendon Press.
- Goldstein R. H. and Reynolds T. J. (1994) Systematics of Fluid Inclusions in Diagenetic Minerals, SEPM Short Course 31, Tulsa, Oklahoma, 199 p.
- Heizler M. T., Perry F. V., Crowe B. M., Peters L. and Appelt R. (1999) The age of the Lathrop Wells volcanic center: an ⁴⁰Ar/³⁹Ar dating investigation. *Jour. Geophys. Res.* 104, 767-804.
- Henley, R.W. (1985) The geothermal framework of epithermal deposits. In *Geology and Geochemistry of Epithermal Systems, Reviews in Economic Geology, Vol. 2*, B.R. Berger and P.M. Bethke (eds.), 1-24.
- Lawler and Crawford (1983) Stretching of fluid inclusions resulting from a low temperature microthermometric technique. *Economic Geology* 78, 527-529.
- Levy, S., Norman D. and Chipera S. (1996) Alteration History Studies in the Exploratory Studies Facility, Yucca Mountain, Nevada, USA. In *Scientific Basis for Nuclear Waste Management XIX*, W. Murphy and D. Knecht (eds.), 783-790.
- Ludwig K. R. (1977) Effect of initial radioactive-daughter disequilibrium on U-Pb isotope apparent ages of young minerals. *J. Res. U. S. Geol. Survey* 5, 663-667.

- Ludwig K. R., Wallace A. R., and Simmons K. R. (1985) The Schwartzwalder uranium deposit, II: Age of uranium mineralization and lead isotope constraints on genesis. *Economic Geology* **80**, 1858-1871.
- Marshall B. D. and Whelan, J.F. (2000) Isotope geochemistry of calcite coatings and the thermal history of the unsaturated zone at Yucca Mountain, Nevada. GSA annual meeting, Nov. 13-16. Reno, Nevada, *Abstracts with Programs, T111*, A-259.
- Neymark L. A. and Paces J. B. (1996) Mixed isotopic ages as a consequence of very slow rates of deposition in Quaternary subsurface fracture-coatings, GSA annual meeting, Oct. 28-31. Denver, Colorado, *Abstracts with Programs, 28, N7*, A139.
- Neymark L. A. and Paces J. B. (2000) Consequences of slow growth for $^{230}\text{Th}/\text{U}$ dating of Quaternary opals, Yucca Mountain, Nevada, USA. *Chem. Geol.* **164**, 143-160.
- Neymark L. A., Paces J. B. and Amelin Y. V. (1998) Neogene to Quaternary U-Th-Pb geochronology using opal, Yucca Mountain, Nevada, USA. *Mineral. Mag.* **62A**, 1077-1078.
- Neymark L. A., Amelin Y. A. and Paces J. B. (2000) ^{206}Pb - ^{230}Th - ^{234}U - ^{238}U and ^{207}Pb - ^{235}U geochronology of Quaternary opal, Yucca Mountain, Nevada. *Geochim. Cosmochim. Acta* **64**, 2913-2928.
- Neymark L.A., Amelin Y., Paces J.B., Peterman Z.E. U-Pb ages of secondary silica and implications for paleohydrology of the unsaturated zone at Yucca Mountain, Nevada. *Applied Geochemistry*, in press.
- Paces J. B., Neymark L. A., Kwak L. M., and Peterman Z. E. (1996) U-series dating of secondary minerals as a tool for estimating paleo water flux through a thick unsaturated zone, Yucca Mountain, NV, GSA Annual meeting, October 28-31, Denver, Colorado, *Abstracts with programs*, A139-A140 (abstr.).
- Paces J. B., Marshall. B. D., Whelan, J. F. and Neymark L. A. (1997) Progress Report on Unsaturated Zone Stable and Radiogenic Isotope Studies, U.S. Geological Survey Milestone report SPC23FM4.
- Paces J. B., Neymark L. A., Marshall B. D., Whelan J. F. and Peterman Z. E. (1998a) Inferences for Yucca Mountain unsaturated zone hydrology from secondary minerals. *Proc., Intl. High-Level Rad. Waste Manag. Conf., Las Vegas, NV, May 11-14, 1998*, Amer. Nucl. Soc., 36-39.
- Paces J. B., Ludwig K. R., Peterman Z. E., Neymark L. A., and Kenneally J. M. (1998b) Anomalous ground-water $^{234}\text{U}/^{238}\text{U}$ beneath Yucca Mountain: Evidence of local recharge? *Proc., Intl. High-Level Rad. Waste Manag. Conf., Las Vegas, NV, May 11-14, 1998*, Amer. Nucl. Soc., 185-188.
- Paces J.B., Neymark L.A., Persing H. M. and Wooden, J. L. (2000) Demonstrating slow growth rates in opal from Yucca Mountain, Nevada, using microdigestion and ion-probe uranium-series dating. Geological Society of America Abstracts with Programs, vol. 32, p. A-259 (abst.).
- Paces J. B., Neymark, L. A., Marshall, B. D., Whelan J. F. and Peterman Z. E. (2001) Ages and origins of calcite and opal in the Exploratory Studies Facility Tunnel, Yucca Mountain, Nevada. U.S. Geological Survey, Water-Resources Investigations Report 01-4049, Denver, CO, 95 p.
- Roedder, E., 1984, Fluid Inclusions, Reviews in Mineralogy Volume 12: Mineralogical Society of America, VPI&SU, Blacksburg, Virginia, 644 p.

- Roedder, E. and Bodnar, R. (1980) Geologic pressure determinations from fluid inclusion studies. *Annual Review Earth and Planetary Sciences* 8, 263-301.
- Roedder E. and Whelan J. F. (1998) Ascending or descending water flow through Yucca Mountain tuffs? Fluid inclusion evidence. In *PACROFI VII; Pan-American conference on Research on fluid inclusions program and abstracts* (eds. D. A. Vanko and Cline J. S.) p. 56.
- Roedder E., Whelan J. F. and Vaniman, D. T. (1994) Fluid inclusion crushing and homogenization studies of calcite veins from Yucca Mountain, Nevada, tuffs; environment of formation, In *International Mineralogical Association, 16th general meeting abstracts*, p. 354-355.
- Sawyer D. A., Fleck R. J., Lanphere M. A., Warren R. G., Broxton D. E. and Hudson M. R. (1994) Episodic Caldera Volcanism in the Miocene Southwestern Nevada Volcanic Field: Revised Stratigraphic Framework, $^{40}\text{Ar}/^{39}\text{Ar}$ Geochronology, and Implications for Magmatism and Extension. *GSA Bulletin* 106, 1304-1318.
- Sharp Z. D., Atudorei V. and Durakiewicz, T. (2001) A rapid method for determination of hydrogen and oxygen isotope ratios from water and hydrous minerals. *Chemical Geology* 178, 197-210.
- Stewart J. H (1988) Tectonics of the Walker Lane Belt, Western Great Basin – Mesozoic and Cenozoic Deformation in a Zone of Shear. In *Metamorphism and crustal evolution of the western United States* (ed. W. G. Ernst), Vol. VII, Prentice-Hall Inc., New Jersey, p. 684-713.
- Stuckless J. S. and Dudley W. W. (2002) The Geohydrologic Setting of Yucca Mountain, Nevada. *Applied Geochemistry, in press*.
- Szymanski J. S. (1987) Conceptual Considerations of the Death Valley Groundwater System with Special Emphasis on the Adequacy of This System to Accommodate the High-Level Nuclear Waste Repository (draft). *DOE internal report*, Yucca Mountain Project Office, Las Vegas Nevada, Nov. 1987.
- Szymanski J. S. (1989) Conceptual Considerations of the Yucca Mountain Groundwater System with Special Emphasis on the Adequacy of This System to Accommodate the High-Level Nuclear Waste Repository. *DOE internal report*, Yucca Mountain Project Office, Las Vegas Nevada, July 1989.
- U.S. Department of Energy (1988) Site characterization plan, Yucca Mountain site, Nevada research and development area, Nevada. U.S. Dept. Energy Report, DOE/RW-0199-8 Volumes.
- Whelan J. F., Moscati R. J., Allerton S. B. M. and Marshall. B. D. (1996) Applications of isotope geochemistry to the reconstruction of Yucca Mountain, Nevada, Paleohydrology – status of investigations. U.S. Geological Survey, Open-file report 98-83.
- Whelan J. F., Paces J. B., Neymark L. A. and Peterman, Z. E. (2000) Status of fluid inclusion studies, U.S. Geological Survey, Water-Resource Investigation Status Report, 8191213UU5.
- Whelan J. F., Paces J. B. and Peterman Z. E. (2002) Paragenetic Relations and Evidence for Secondary Mineral Formation in Unsaturated-zone Tuffs at Yucca Mountain, Nevada. *Applied Geochemistry, in press*.
- Wilson N. S. F., Cline J. S., Rotert J. and Amelin Y. A. (2000) Timing and Temperature of Fluid Movement at Yucca Mountain, NV: Fluid inclusion and U-Pb and U-series dating, GSA Annual meeting, Nov. 13-16, Reno, Nevada, *Abstracts with programs*, A-260 (abstr.).

- Wilson N. S. F. and Cline J. S. (2002) Thermochronological evolution of calcite formation at the potential Yucca Mountain repository site, Nevada: Part 1, Secondary mineral paragenesis and geochemistry. *Companion report submitted to DOE*.
- Winograd I. J. (1981) Radioactive waste disposal in thick unsaturated zones. *Science* **212**, 1457-1464.

FIGURE CAPTIONS

- Figure 1** Sample locations in the ESF, ECRB, and exploratory alcoves. Circles mark sample locations; filled circles indicate samples that contained 2-phase FIAs. Arrows point to samples that were dated. The site has been divided into six regions that are labeled and discussed in the text.
- Figure 2** $^{230}\text{Th}/^{238}\text{U}$ and $^{234}\text{U}/^{238}\text{U}$ activity ratios in the in-house secular equilibrium standard SU-1 (Schwartzwalder uranium ore, Ludwig et al. 1985, see also Neymark et al. 2000), analyzed with the Yucca Mountain samples during the period of June to December 2000. The x-axis is equivalent to time with respect to the analyses.
- Figure 3** Schematic diagram illustrating the mineral paragenesis and spatial distribution of 2-phase FIAs in secondary mineral crusts at Yucca Mountain (adapted from Wilson and Cline, 2002). Basal calcite and the central early cores of the bladed calcite, just above the qtz-cdy layer, are considered early to early-intermediate. The left side of the figure shows the typical paragenesis for fracture and breccia samples, whereas the rest of the figure illustrates the variability in parageneses in lithophysal cavities. See text for discussion. Cdy is chalcedony, Td is tridymite, Hem is hematite, and Qtz is quartz.
- Figure 4** Fluid inclusion populations, distinguished by arrow color, under plane polarized light. Two-phase fluid inclusions are shown by black arrows, liquid-only inclusions are shown by white arrows, and 2-phase inclusions with inconsistent liquid-vapor ratios are indicated by gray arrows. **(A)** Typical primary liquid-only FIA in bladed calcite. **(B)** Primary all-liquid FIA along a growth zone in MGSC. No 2-phase FIAs have been observed in this outermost calcite. **(C)** Primary 2-phase FIA along a growth zone at the base of a LC. Microthermometry gave consistent homogenization temperatures of 43 – 53 °C (n = 43). **(D)** Primary (?) assemblage of 2-phase fluid inclusions with consistent liquid-vapor ratios and homogenization temperatures (53 – 59 °C; n = 23). Two-phase FIAs include liquid-only inclusions, 2-phase inclusions with variable liquid-vapor ratios, and vapor-only inclusions.
- Figure 5** Summary of fluid inclusion homogenization temperatures for six areas (Fig. 1) in the ESF and ECRB. The vertical dashed line represents a reference temperature of 50 °C. Note the consistency of data within each of the six areas and the differences in homogenization temperatures between areas. In samples with two modes, higher homogenization temperatures were obtained from paragenetically older calcite and lower homogenization temperatures from paragenetically younger calcite, indicating a cooling trend with time. See text for discussion.
- Figure 6** Histogram of fluid inclusion homogenization temperatures obtained from sample ESF 01+62.3 near the north portal from the welded Tiva Canyon tuff. These data were collected from 2 sample chips with the summarized data from the first chip

shown in white. Individual assemblages from the second chip have similar ranges and data are similar to the summarized data. In some assemblages (3 and 6) only a few inclusions were chosen (at random) and measured from larger FIAs. This was done to see how many inclusions were required to produce a valid distribution of data for the entire FIA. Assemblages 3 and 6 have modes and distributions similar to the larger data set and indicate that not all inclusions must be measured to obtain representative data for the samples.

Figure 7 Doubly polished sections showing the locations of primary 2-phase FIAs (black squares) and the locations of opal and chalcedony dated using U-Pb methods. Yellow filled squares indicate 2-phase FIAs that were examined using microthermometry. Homogenization temperatures are given adjacent to the squares. Opal and chalcedony are shown in black with dated areas indicated in red; ages and errors are shown adjacent to the dated material. All dated material was opal unless stated. Dashed black lines indicate the boundaries between MGSC and underlying secondary minerals. (A) Two-phase FIAs are located below, and are older than, the 5.32 ± 0.02 Ma opal layer (gray). Only liquid-only inclusions occur above this layer in intermediate calcite and outer MGSC. An outer discontinuous opal layer (dashed blue line) was precipitated within the MGSC layer. (B) Lithophysal cavity crust from the LCZ. Two-phase FIAs occur throughout most of the crust and vary from $45 - 57$ °C at the base of the sample to $35 - 41$ °C near the outer part of the sample. Dates on chalcedony near the center of the crust indicate that 2-phase FIAs with homogenization temperatures of $45 - 57$ °C are older than 6.29 ± 0.08 Ma. Opal near the outer part of the crust was dated at 5.78 ± 0.3 Ma and $35 - 41$ °C 2-phase FIAs are younger than this age. MGSC does not occur on the outermost surface indicating that young secondary minerals did not precipitate at this location. The locations of 2-phase FIAs are only shown for the left side of the section in basal calcite below the 6.29 ± 0.08 Ma chalcedony, but 2-phase FIAs are present in the basal calcite across the section. All 2-phase FIAs observed in the outer part of the crust are shown. (C) Crust from a fracture occurrence in the NR. Primary 2-phase FIAs have homogenization temperatures of $67 - 75$ °C and are older than 4.00 ± 1.46 Ma, the age of a chalcedony layer that is younger than the primary 2-phase FIAs. A younger brown opal layer associated with MGSC has an age of 1.70 ± 0.02 Ma. (D) Shallowly dipping fracture sample from the LCZ. Three ages determined for opal (Table 3, column d) indicate that 2-phase FIAs are older than 3.88 ± 0.11 Ma. (E) Lithophysal cavity crust with bladed calcite overlain by MGSC associated with opal. No 2-phase FIAs are present in this sample but opal occurs along the boundary between bladed calcite and outer MGSC and indicates that MGSC formed after 2.90 ± 0.06 Ma. (F) Lithophysal cavity crust with chalcedony with brown opal patches that have an age of 9.06 ± 0.09 Ma overlain by dark calcite that contains abundant 2-phase FIAs. This calcite is overgrown by a thin layer of younger calcite and outer layer of MGSC that contains rare liquid-only inclusions. In this sample the 2-phase FIAs, with homogenization temperatures from $69 - 83$ °C, are younger than 9.06 ± 0.09 Ma. $\delta^{18}\text{O}$ compositions are

consistent with this calcite forming early and at higher temperature (Wilson and Cline, 2002).

- Figure 8 Homogenization temperatures from fluorite and quartz. All data were obtained from paragenetically early fluorite and quartz that precipitated around and adjacent to the host tuffs. Homogenization temperatures for fluorite vary from 43 – 91 °C and for quartz from 53 – 95 °C. Homogenization temperatures for fluorite and quartz vary across the site and samples from the NP have higher homogenization temperatures than samples from other areas. Homogenization temperatures obtained for fluorite and quartz are generally similar to homogenization temperatures obtained from adjacent secondary minerals where present.
- Figure 9 Histogram of ice melting temperatures ($n = 129$) for fluid inclusions in calcite ($n = 127$) and fluorite ($n = 2$; $T_m = -0.7$ °C) from 30 samples across the site.
- Figure 10 U-Pb concordia diagram for opals. Common-lead-corrected $^{206}\text{Pb}/^{238}\text{U}$ and $^{207}\text{Pb}/^{235}\text{U}$ ratios for Yucca Mountain opals are plotted together with concordia curves corresponding to $^{234}\text{U}/^{238}\text{U}$ initial activity ratios (U_i) of 1, 3 and 10. Isochrons are shown as vertical dotted lines connecting points of equal age on the concordia curves. It is assumed that initial ^{230}Th , ^{231}Pa , and ^{227}Ac are absent. Error ellipses are 2σ . The distribution of the data indicates variations of $^{234}\text{U}/^{238}\text{U}$ initial activity ratios between values 1 and > 10 (values are shown in Table 3).
- Figure 11 Measured $^{234}\text{U}/^{238}\text{U}$ (A) and $^{230}\text{Th}/^{238}\text{U}$ (B) activity ratios versus $^{207}\text{Pb}/^{235}\text{U}$ disequilibrium ages in Yucca Mountain opals. Error bars are 2σ . Analytical points for three very young opal fractions with $^{234}\text{U}/^{238}\text{U}_{\text{activity}} > 2$ are not shown.
- Figure 12 Histogram of U-Pb ages obtained from opal (open squares) and chalcedony (filled squares). Arrows indicate the location of the dated sample within the section with respect to MGSC. Arrows pointing right indicate that the dated sample was collected from material paragenetically younger than MGSC; double arrows indicate that the dated sample was collected from within MGSC, and arrows pointing left indicate that the dated sample was collected from material paragenetically older than MGSC. The shaded bar indicates the approximate time of initial precipitation of MGSC. See text for discussion.

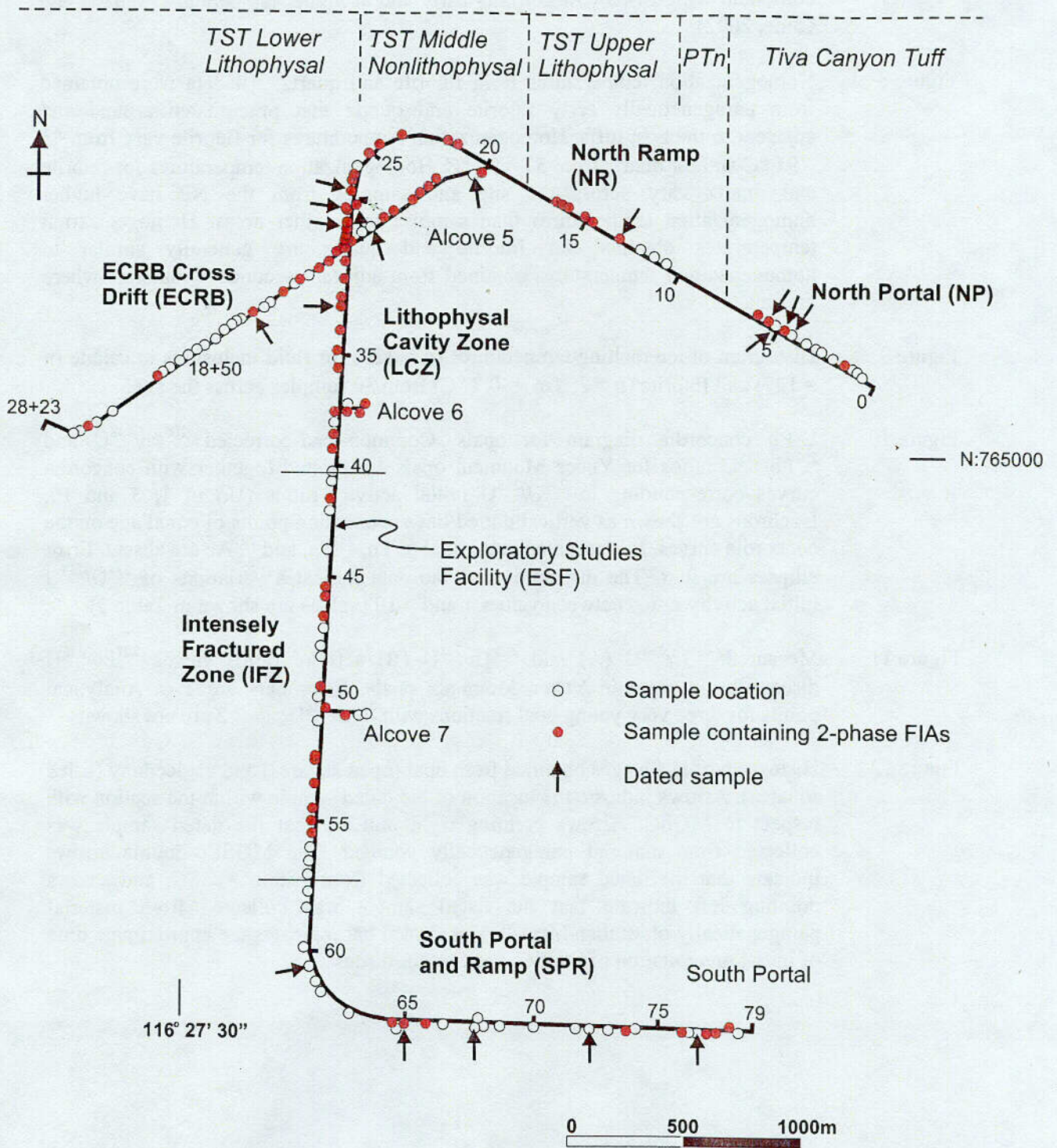


Figure 1

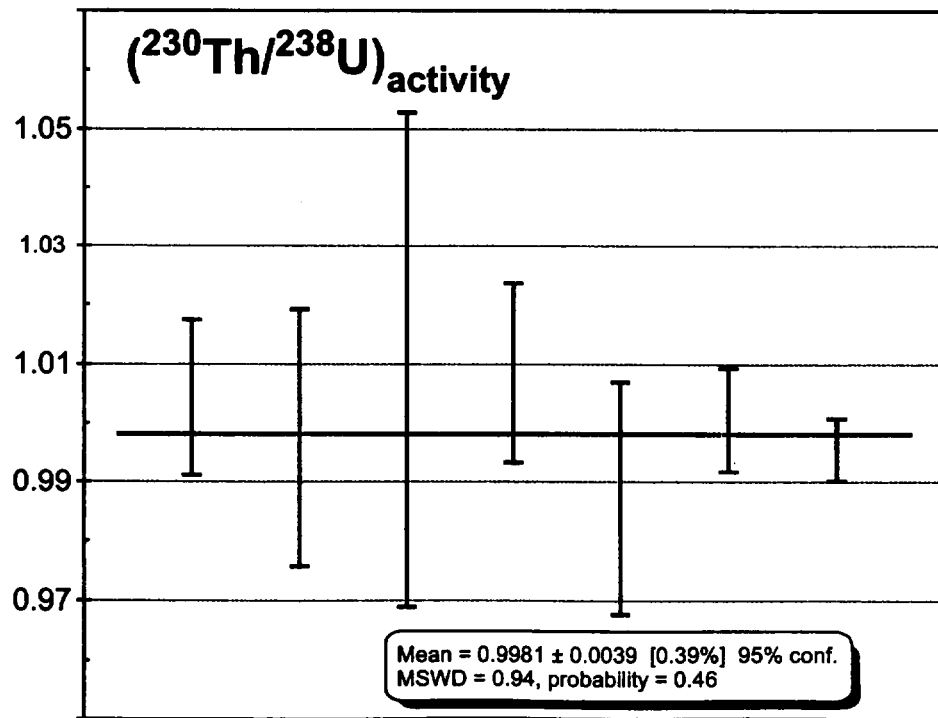
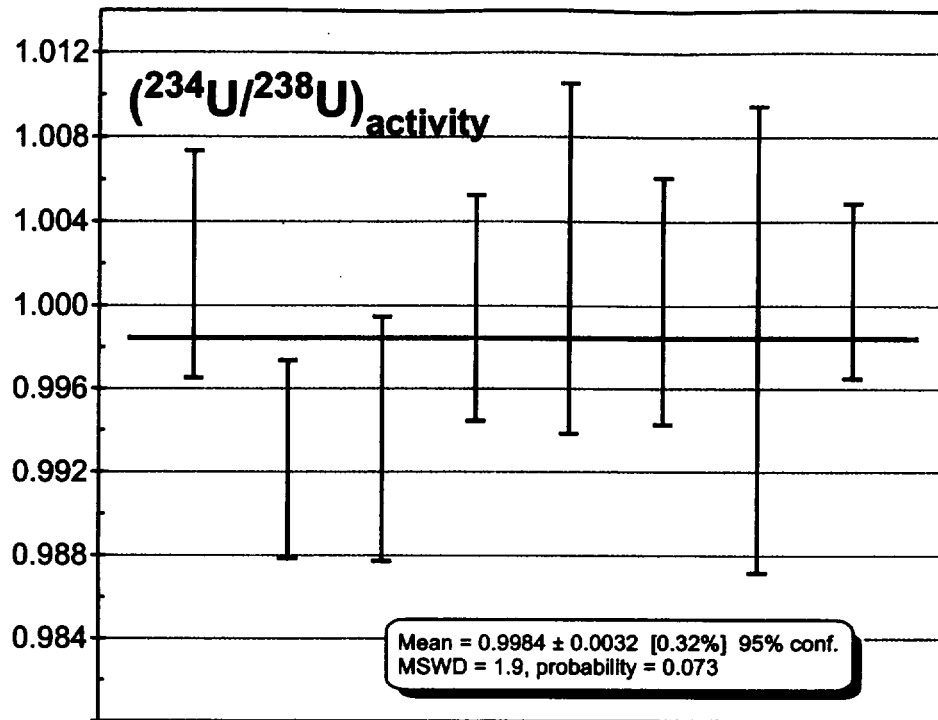


Figure 2

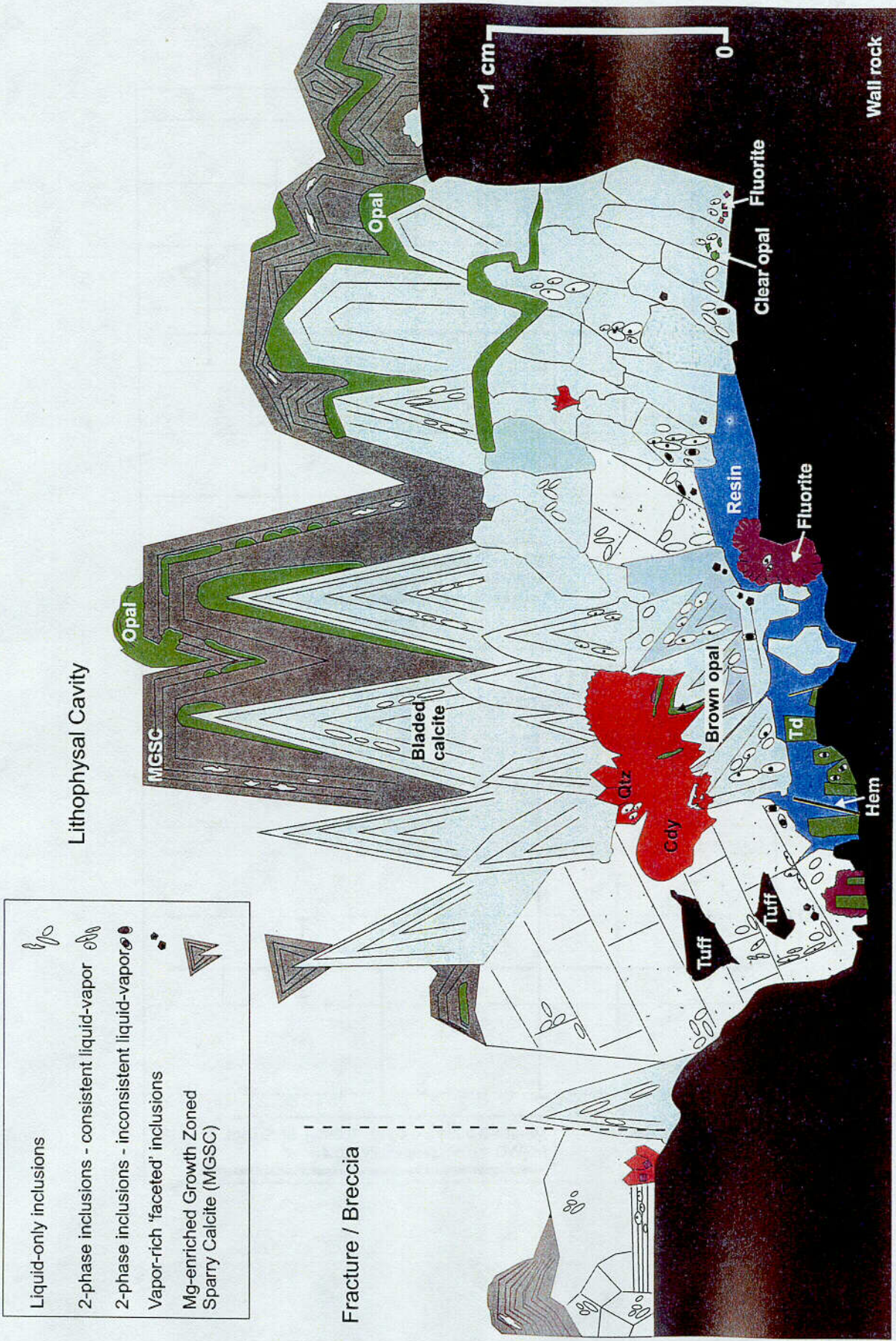


Figure 3

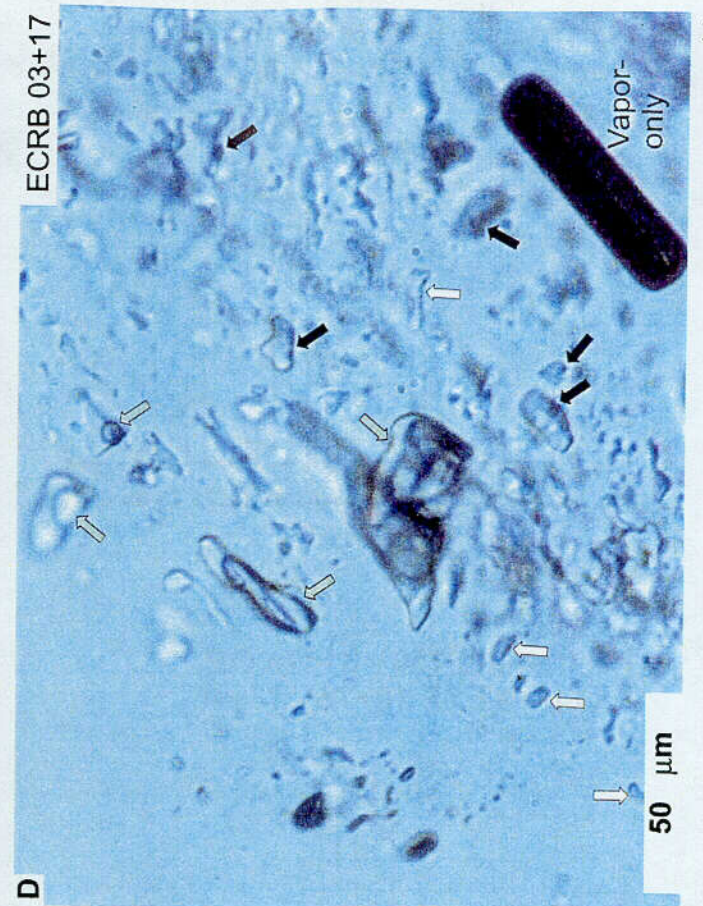
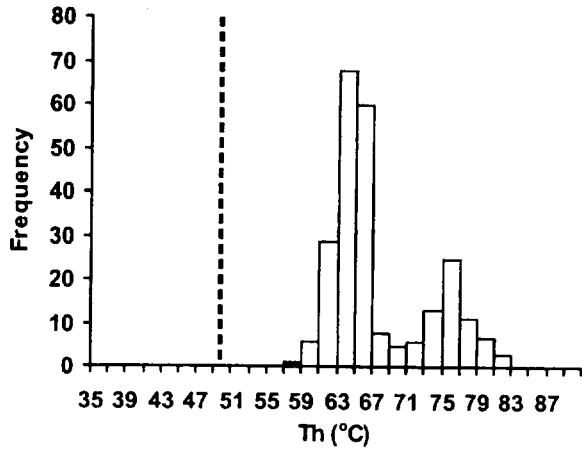


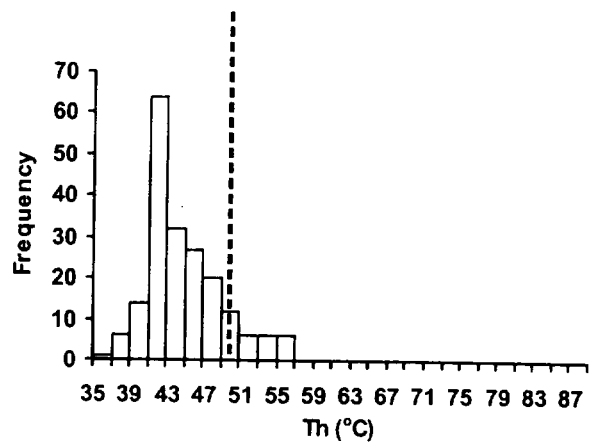
Figure 4

C12

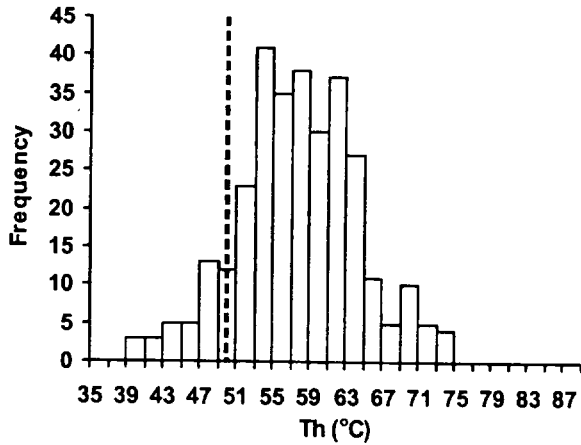
NP (n=242; 0-55 m OB)
Samples ESF 00+00 - 06+11.5



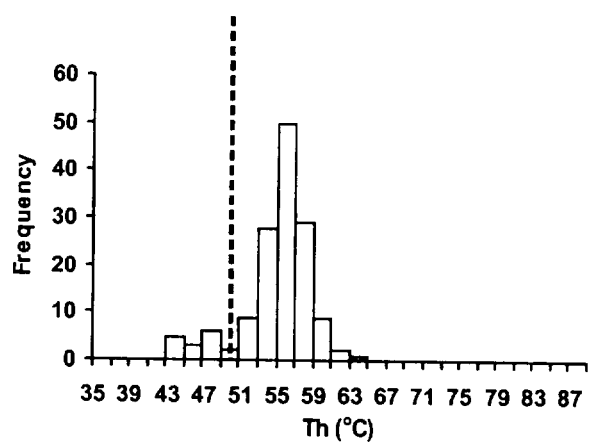
IFZ (n=194; 215 - 270 m OB)
Samples ESF 40+68 - 57+00



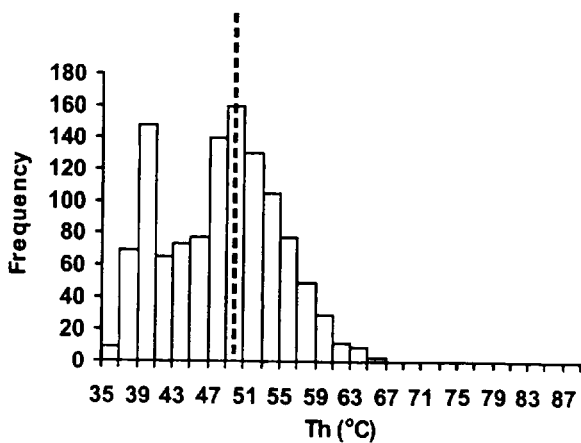
NR (n=307; 150 - 210 m OB)
Samples ESF 10+75 - 16+46



SPR (n=144; 0 - 225 m OB)
Samples ESF 57+70 - 78+41



LCZ (n=1161; 180 - 310 m OB)
Samples ESF 21+61 - 40+21



ECRB (n=342; >185 OB)
All ECRB samples

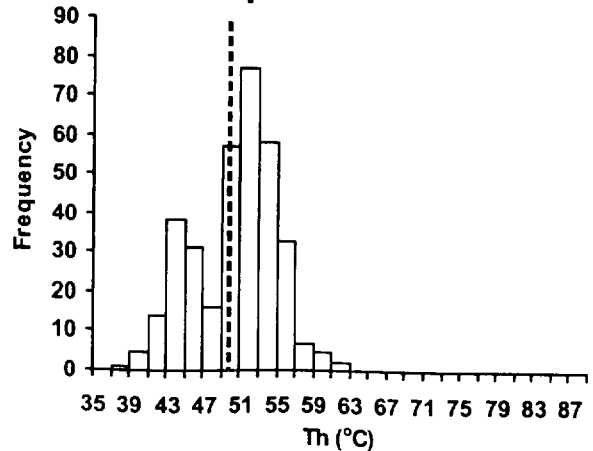


Figure 5

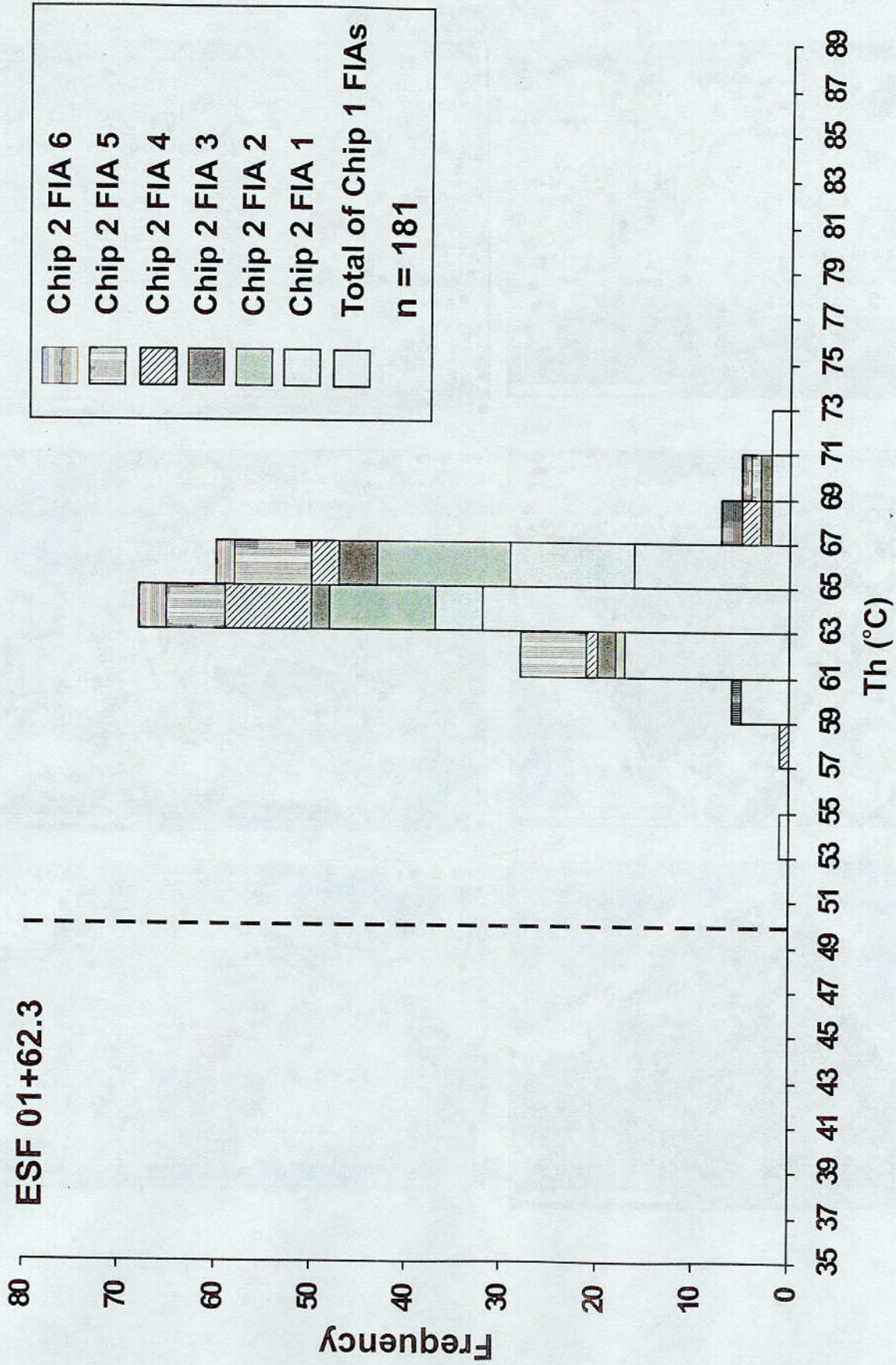


Figure 6

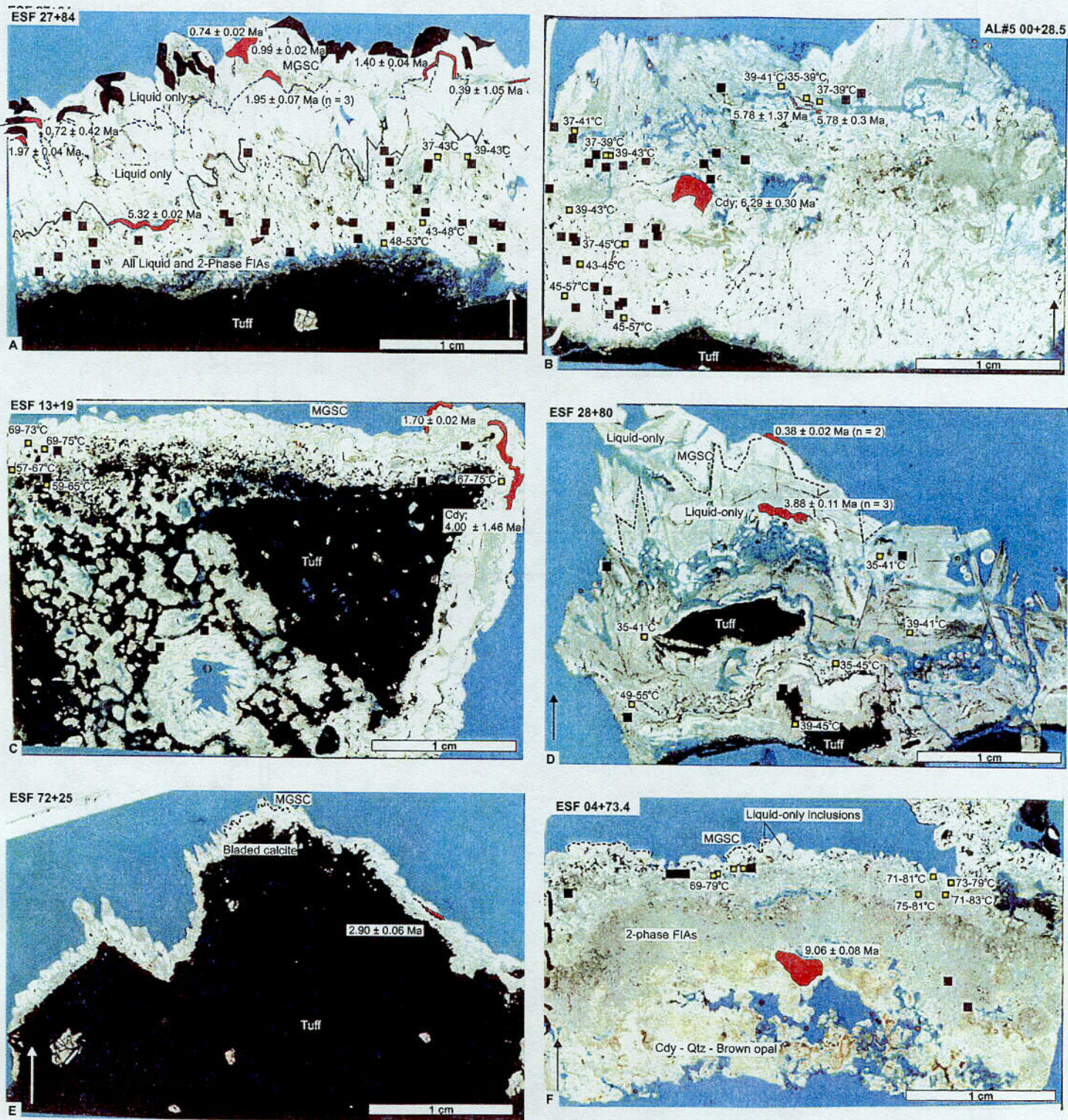


Figure 7

C14

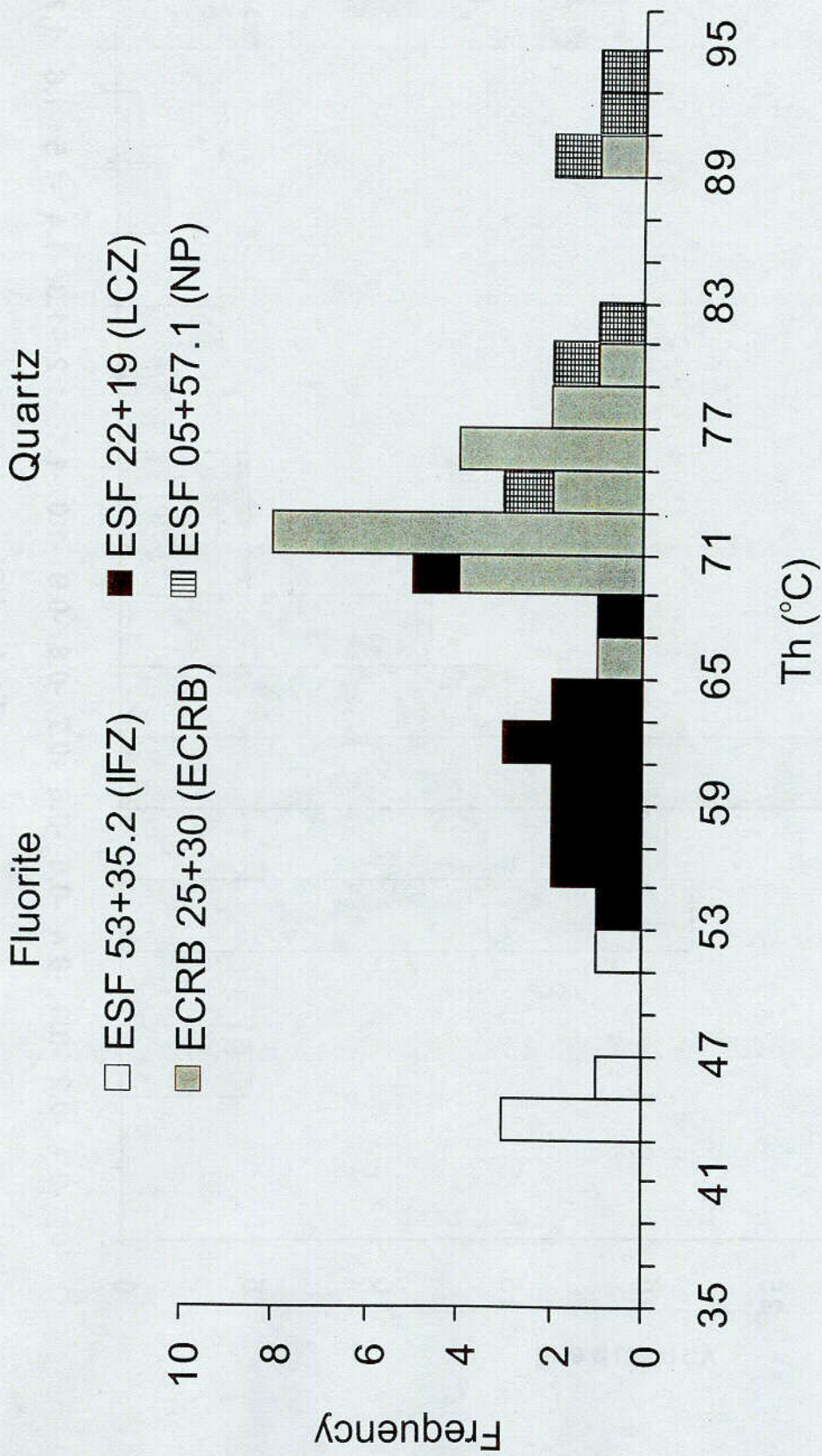


Figure 8

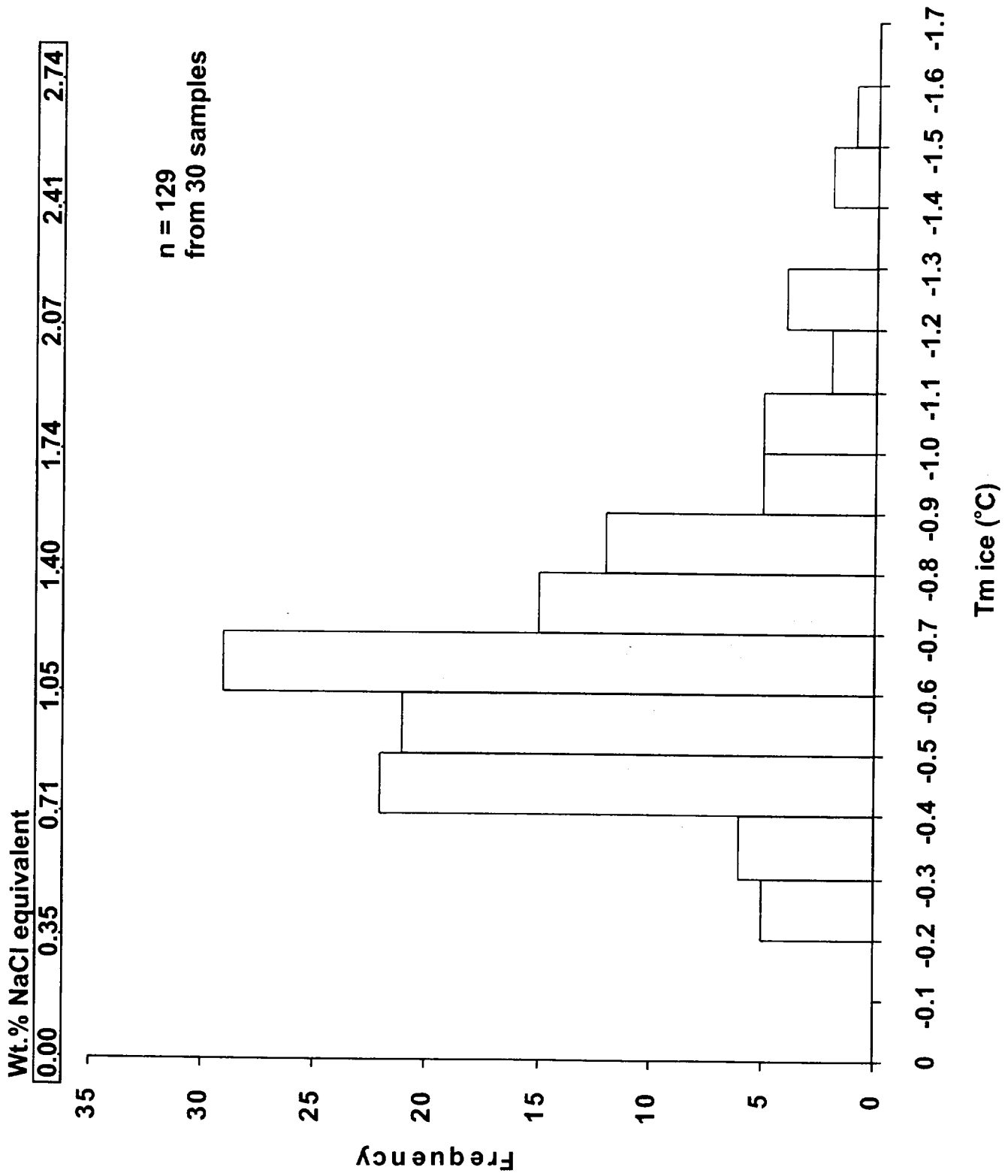


Figure 9

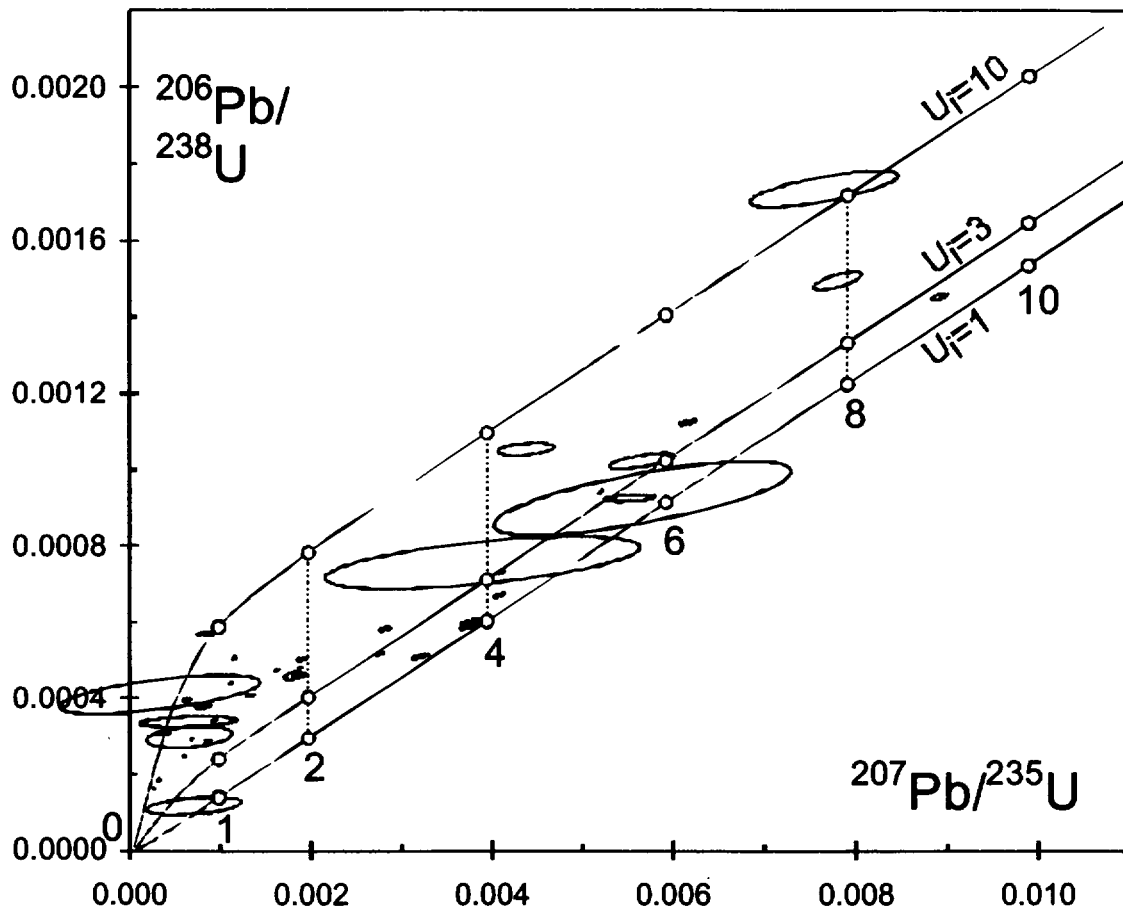


Figure 10

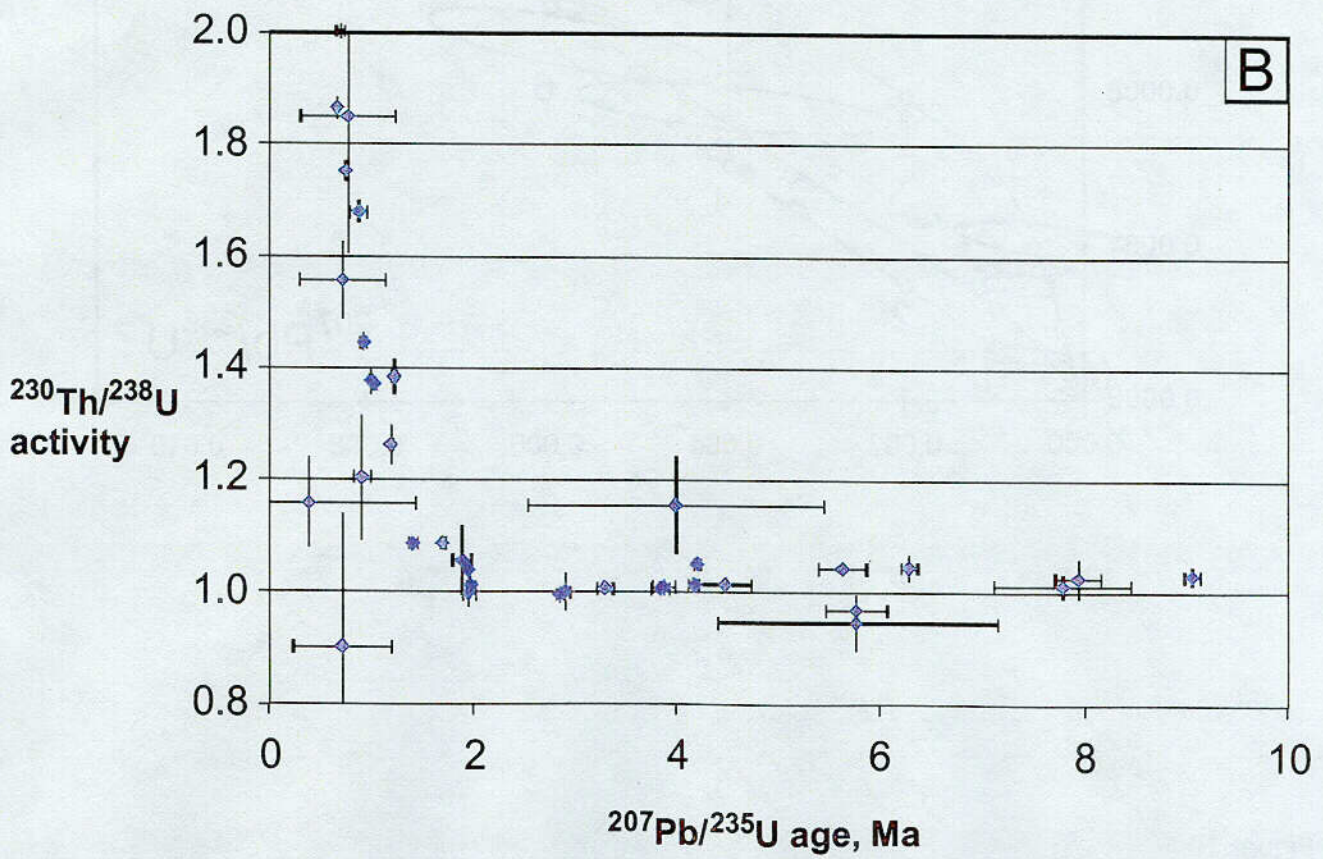
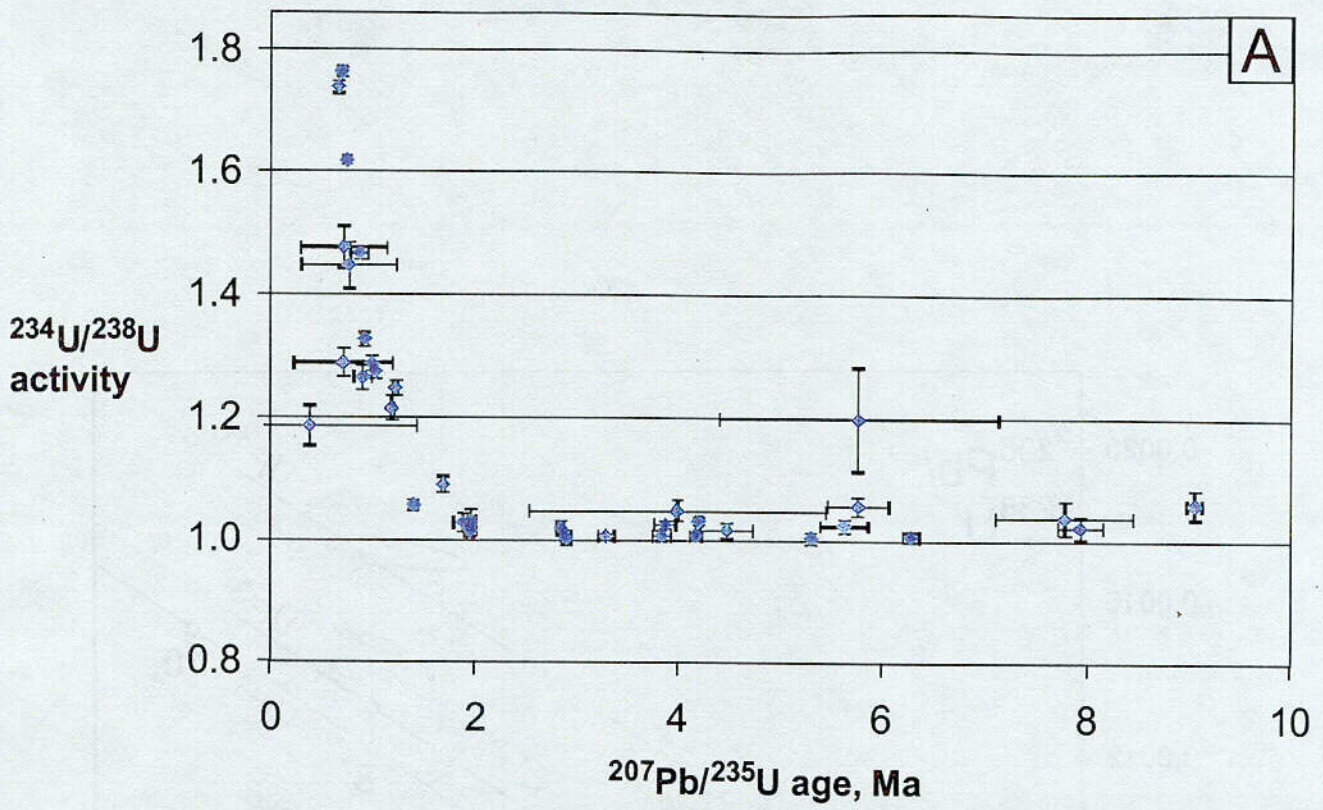


Figure 11

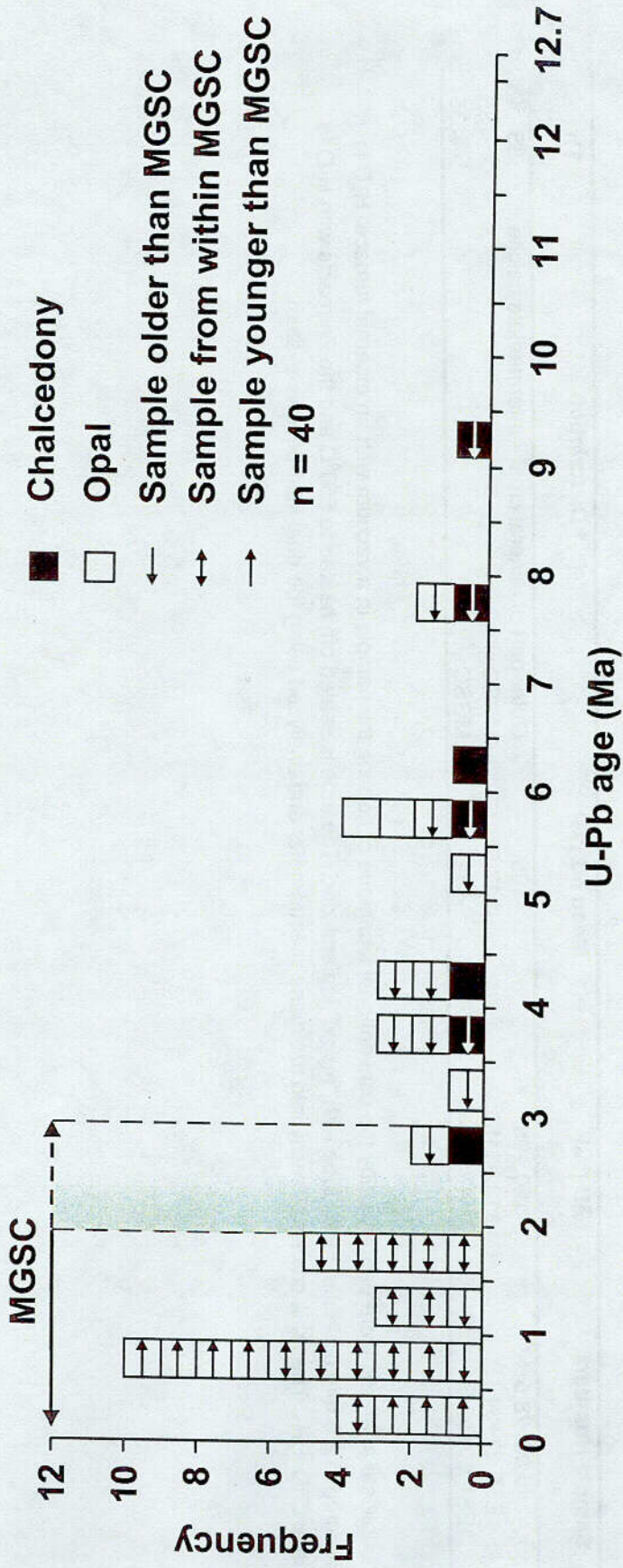


Figure 12

Table 1. δD compositions of fluid inclusion fluids

Sample Number	δD (‰)	Mean δD (‰)	Description	Th (°C)
AL#5 00+28.5	-120, -90	-105	Outer part of mineral crust - Intermediate calcite	35 - 45
ESF 27+84	-110, -115*	-112.5	MGSC	< 35
ESF 60+52.5	-131*	-131	MGSC	< 35

* Duplicate analyses were performed by the conventional technique of heating the sample in a vacuum with an external furnace. H_2O is collected in a 6 mm diameter Pyrex tube with "magic" Indiana zinc. The tube is sealed off, heated to 550°C and the Zn reacts with H_2O to make $ZnO + H_2$. The H_2 is cracked directly into the mass spectrometer and analyzed using the dual inlet-bellows system.

Table 2. U-Th-Pb isotopic data.

No	Sample, fraction	Fraction weight (mg)	ppm U	ppb Th	Th/U	Com Pb	²⁰⁶ Pb/ ²³⁸ Pb	²⁰⁶ Pb/ ²³⁸ Pb	2σ% err	²⁰⁶ Pb/ ²³⁸ Pb	²⁰⁶ Pb/ ²³⁸ Pb	2σ% err	²³⁵ U/ ²³⁸ U	²³⁵ U/ ²³⁸ U	2σ% err	²³⁰ Th/ ²³² Th	2σ% err
			(a)	(b)	(c)	(d)	(e)	(f)	(g)	(h)	(i)	(j)	(k)	(l)	(m)	(n)	(o)
1	AL#5 00+28.5 Cdy-1(1)	1.505	28.5	0.64	2.2E-05	15.8	215.7	0.15	218.9	0.40	23.58	39.29	177.877	1.0062	0.82	1.0453	2.38
2	AL#5 00+28.5 Op-1a(1)	0.111	32.7	b.d.l.	n.d.	4.91	69.1	0.31	73.0	1.75	17.79	38.09	52.948	1.0557	1.52	0.9692	2.79
3	AL#5 00+28.5 Op-2a(1)	0.030	49.4	b.d.l.	n.d.	9.70	58.8	0.22	28.4	0.45	16.04	37.81	10,346	1.1983	7.11	0.9471	5.24
4	ECRB 01+25 Op-1(1)	0.028	26.5	48.49	1.8E-03	0.40	55.9	2.20	78.6	64.3	18.27	36.10	514,770	1.4480	2.64	1.8498	13.23
5	ECRB 07+40.5 Op-1(1)	0.124	156	54.55	3.5E-04	0.64	693.8	0.98	1283	17.90	41.44	37.37	3,685,500	1.2745	0.95	1.3711	0.90
6	ECRB 07+40.5 Op-2(1)	0.336	77.5	2.24	2.9E-05	0.92	472.2	0.79	683.6	9.65	27.55	36.33	2,702,410	1.7366	0.58	1.8656	1.14
7	ECRB 14+49 Op-1(1)	0.041	316	119.6	3.8E-04	0.33	1303	2.00	15375	223	270.18	54.12	30,299,600	1.2476	1.02	1.3833	2.39
8	ECRB 04+73.4 Op-1(1)	0.518	373	64.50	1.7E-04	25.3	375.9	0.18	380.8	0.31	30.37	38.35	495,379	1.0305	0.55	1.0503	0.92
9	ESF 04+73.4 Op-1(1)	2.685	21.5	2.28	1.1E-04	13.4	419.5	0.53	428.5	0.71	33.82	38.35	281,460	1.0594	2.23	1.0313	1.55
10	ESF 05+09.1 Op-1(1)	0.150	39.5	10.09	2.6E-04	1.27	196.0	0.98	243.1	5.95	18.04	39.81	393,176	1.2649	1.56	1.2045	9.20
11	ESF 05+57.1 Cdy-1(1)	0.470	n.d.	n.d.	n.d.	n.d.	n.d.	n.d.	n.d.	n.d.	n.d.	n.d.	n.d.	1.0237	0.95	1.0374	7.86
12	ESF 05+57.1 Cdy-1(2)	0.062	160	b.d.l.	n.d.	1.48	247.5	0.43	358.6	9.92	28.73	38.89	654,552	1.0194	1.14	0.9956	1.67
13	ESF 05+57.1 Cdy-2(1)	0.799	42.2	9.95	2.4E-04	10.9	227.3	2.10	232.9	2.23	22.08	32.89	203,314	1.0162	1.22	1.0144	1.44
14	ESF 13+19 Cdy-2(1)	0.872	74.4	4.81	6.5E-05	2.16	30.1	0.74	30.1	0.75	16.04	37.42	14,898	1.0475	1.62	1.1555	7.60
15	ESF 13+19 Op-1(1)	0.418	123	3.05	2.5E-05	4.00	412.8	0.36	444.0	1.63	28.15	39.99	894,429	1.0899	1.23	1.0870	0.81
16	ESF 27+84 Op-1(1)	0.148	160	0.53	3.3E-06	0.63	1179	1.80	2232	18.6	78.13	38.41	4,590,870	1.0234	0.81	1.0392	1.80
17	ESF 27+84 Op-1(2)	0.046	130	8.21	6.3E-05	0.95	214.0	1.40	2240	218	78.89	34.24	4,818,200	1.0276	1.47	1.0559	5.86
18	ESF 27+84 Op-1(3)	0.066	153	2.89	1.9E-05	2.34	150.0	0.57	222.1	10.9	21.60	37.70	439,300	1.6189	0.96	0.9974	2.41
19	ESF 27+84 Op-2(1)	0.175	103	2.65	2.6E-05	0.68	525.7	0.84	1411	35.7	39.44	35.20	4,783,750	1.0276	1.47	1.0559	5.86
20	ESF 27+84 Op-2(2)	0.280	88.6	0.56	6.3E-06	1.17	481.8	0.89	1788	57.0	51.05	42.12	5,248,790	1.2877	1.02	1.3759	1.73
21	ESF 27+84 Op-3(1)	0.161	276	238.1	8.6E-04	0.72	374.8	1.10	6503	14.8	275.52	37.78	6,883,780	1.0036	0.95	n.d.	n.d.
22	ESF 27+84 Op-3a(1)	0.049	192	b.d.l.	n.d.	0.88	372.5	0.91	830.5	26.6	37.79	38.75	1,811,180	1.0309	1.75	1.0111	2.14
23	ESF 27+84 Op-4a(1)	0.007	122	b.d.l.	n.d.	1.01	44.0	0.80	51.1	13.7	16.14	37.02	109,001	1.4777	2.29	1.5662	4.41
24	ESF 27+84 Op-5a(1)	0.114	129	34.85	2.7E-04	1.30	322.0	1.20	506.1	12.5	27.20	38.18	1,194,820	1.0566	0.81	1.0880	1.04
25	ESF 27+84 Op-6a(1)	0.022	79.5	198.1	2.5E-03	6.36	27.4	0.47	26.7	0.74	15.67	38.18	19,160	1.1853	2.76	1.1580	7.01
26	ESF 28+80 Op-1(1)	0.316	127	b.d.l.	n.d.	14.7	108.6	0.25	110.1	0.44	19.77	38.94	178,630	1.0057	0.45	1.0075	0.46
27	ESF 28+80 Op-1(2)	0.274	98.9	0.54	5.5E-06	12.6	102.6	0.33	108.3	1.29	19.69	38.92	148,603	1.0243	0.59	1.0089	1.43
28	ESF 28+80 Op-1(3)	0.356	127	0.46	3.0E-06	18.8	109.9	0.23	114.1	0.85	20.01	39.16	161,374	1.0072	0.85	1.0070	1.42
29	ESF 28+80 Op-2(1)	0.453	82.1	2.05	2.5E-05	1.67	251.8	0.66	494.5	20.9	21.45	38.03	2,968,300	3.6667	0.32	3.5906	0.60
30	ESF 28+80 Op-2(2)	0.245	90.0	1.91	2.1E-05	1.32	221.8	0.75	598.0	37.8	23.04	39.13	3,154,360	3.3338	0.57	3.4200	1.50
31	ESF 29+11 Op-1(1)	0.156	44.1	5.99	1.4E-04	0.83	190.1	1.40	272.1	10.9	17.82	40.69	831,669	3.4335	1.42	3.5109	2.00
32	ESF 29+11 Op-2(1)	0.167	177	21.33	1.2E-04	1.93	456.9	0.31	535.1	3.64	25.18	39.46	1,170,930	1.2144	1.63	1.2620	2.89
33	ESF 32+31 Cdy-1(1)	0.861	17.3	1.32	7.6E-05	15.0	114.3	0.16	115.9	0.39	19.29	39.52	64,892	1.0213	1.77	1.0257	3.54
34	ESF 60+52.5 Op-1(1)	0.071	71.4	b.d.l.	n.d.	1.34	116.4	0.64	136.5	5.11	17.47	37.96	311,924	1.4685	0.72	1.6793	1.23
35	ESF 60+52.5 Op-1(2)	0.105	61.3	0.27	4.4E-06	0.61	297.4	0.91	543.7	19.0	21.76	38.27	1,329,590	1.7628	0.45	2.0037	0.68
36	ESF 64+95 Op-1(1)	0.959	90.1	1.90	2.1E-05	23.5	177.6	0.14	184.3	0.83	22.91	39.61	246,611	1.0076	0.47	1.0136	1.13
37	ESF 67+81 Op-1(1)	0.611	62.9	2.96	4.7E-05	6.94	348.0	3.30	362.6	3.56	30.49	37.52	371,335	1.0235	1.11	1.0436	1.15
38	ESF 72+25 Op-1(1)	0.078	131	10.78	8.2E-05	1.91	222.7	0.60	256.4	3.58	23.92	37.16	407,065	1.0034	1.16	1.0010	3.38
39	ESF 76+59.5 Op-1(1)	0.578	8.1	21.75	2.7E-03	14.2	55.9	0.28	56.15	0.42	16.81	39.65	21,514	1.0370	2.76	1.0126	2.05
40	ESF 76+59.5 Op-2(1)	0.024	63.3	52.88	8.3E-04	0.57	91.5	3.30	139.8	20.9	17.33	36.07	359,910	1.2885	1.77	0.9026	26.15
41	ESF 76+59.5 Op-2(2)	0.118	68.3	8.54	1.3E-04	0.50	331.3	1.10	776.4	30.6	32.23	39.16	2,649,140	1.3271	0.85	1.4458	1.13

n.d. - not determined

b.d.l.-below detection limit (amount of Th in an analysis is indistinguishable from analytical blank)

Sample names: Op-opal, Cdy-Chalcedony. Numbers in parentheses indicate replicate analyses.

a) Total common Pb content in analysis, including initial common Pb and procedure blank.

b) Measured ratios, corrected for fractionation only.

c) Isotopic ratios, corrected for fractionation, spike contribution, and procedure blank.

d) Activity ratios, calculated from measured isotopic ratios corrected for fractionation, spike contribution, and procedure blank.

APPENDIX – ADDITIONAL DESCRIPTIONS OF DATED SAMPLES

In all samples the locations of 2-phase FIAs are marked by black squares and those that were used for microthermometry are marked with yellow squares. Homogenization temperatures are adjacent to the 2-phase FIA locations. The locations of material sampled for dating are shown in red and dated material was opal unless specified as chalcedony. A dashed black line shows the contact between MGSC and earlier minerals.

ECRB 01+25 – Lithophysal cavity sample with bladed calcite overgrown by MGSC and associated brown opal. No 2-phase FIAs were observed in this sample. Calcite dissolution is indicated by the presence of irregular calcite blades, abundant porosity, and the presence of brown opal from the base of the sample to the outermost surface (with MGSC). Textures indicate that brown opal is associated with precipitation of MGSC. Brown opal filling a pore in the basal part of the crust has a U-Pb age of 0.77 ± 0.46 Ma. This sample indicates that brown opal can be relatively young.

ECRB 07+40.5 – Lithophysal cavity sample with older moderately fine-grained, darker calcite and bladed calcite overgrown by MGSC. Two-phase FIAs were not observed in this sample. Two opal samples were dated, one from within the MGSC and one from the outermost surface that is partially overgrown by younger MGSC. Opal from within the MGSC gave an age of 1.03 ± 0.01 Ma and opal from the outermost part of the crust gave an U-Pb age of 0.67 ± 0.01 Ma. These ages indicate that MGSC precipitated before and after 1.03 ± 0.01 Ma.

ECRB 14+49 – Lithophysal cavity sample with fine-grained calcite at the base overgrown by bladed calcite, which is in turn, overgrown by MGSC. No 2-phase FIAs were observed in this sample. An opal sample was collected along the boundary between bladed calcite and the MGSC and gave a U-Pb age of 1.22 ± 0.02 Ma, indicating that MGSC precipitated after this time.

ESF 04+44 – Fracture sample with layers of chalcedony overgrown by brown opal and MGSC. No 2-phase FIAs were identified in this sample. Brown layered opal has an age of 4.21 ± 0.03 Ma and MGSC precipitated after this time.

ESF 05+09.1 – Fracture sample containing chalcedony and quartz overgrown by MGSC and an outer layer of brown opal (red). No 2-phase FIAs are present in this sample. Brown opal from the outermost surface has an age of 0.91 ± 0.09 Ma and MGSC is older than this age. This sample also shows that brown opal can be young.

ESF 05+57.1 – Fracture with chalcedony-quartz and fluorite at the base of the crust overgrown by layers of chalcedony-brown opal with minor fluorite. Two-phase FIAs occur in basal quartz but not in outer minerals. Chalcedony in the outer part of the sample forms thin layers within opal layers and has an age of 4.49 ± 0.26 Ma indicating that the 2-phase FIAs in quartz are older than this age. Younger chalcedony precipitated in open space in the central region of the section and has an age of 2.85 ± 0.04 Ma.

ESF 29+11 – Lithophysal cavity sample containing fine-grained dark calcite at base overgrown by bladed calcite, which was overgrown by intergrown MGSC and opal. Two-phase FIAs occur in the basal calcite and basal bladed calcite but not in outer bladed calcite or MGSC. Opal from within the MGSC layer has an age of 1.19 ± 0.02 Ma and MGSC precipitated before and after this time. Opal from the outer most surfaces that is partially overgrown by MGSC has an age of 0.42 ± 0.08 Ma, indicating that the MGSC precipitated before and after this time.

ESF 32+31 – Lithophysal cavity sample containing basal calcite containing chalcedony after calcite, overgrown by bladed calcite and an outer layer of MGSC. Two-phase FIAs occur in basal calcite but their temporal relationship to the chalcedony layer is ambiguous owing to lateral variations in the crust. The chalcedony had an age of 7.94 ± 0.22 Ma and bladed calcite and MGSC are younger than this age.

ESF 60+52.5 – Fracture sample containing minor early calcite overgrown by MGSC. An opal layer within the center of the MGSC has ages of 0.69 ± 0.04 and 0.88 ± 0.08 Ma and MGSC formed before and after this time. No 2-phase FIAs occur in this sample.

ESF 64+95 – Lithophysal cavity sample with basal calcite containing 2-phase FIAs overgrown by chalcedony-brown opal-quartz after early calcite, by bladed calcite, and then by MGSC. No 2-phase FIAs are present in the bladed calcite or MGSC. Brown opal associated with quartz has an age of 4.18 ± 0.06 Ma and bladed calcite and MGSC are younger than this age.

ESF 67+81 – Fracture sample containing basal calcite overgrown by chalcedony-brown opal-calcite-quartz, overgrown by MGSC. No 2-phase FIAs occur in this sample. Brown opal below the quartz layer and MGSC has an age of 5.64 ± 0.24 Ma and MGSC precipitated after this time.

ESF 76+59.5 – Fracture sample with brown opal adjacent to wall rock. Brown opal is overgrown by clear bladed calcite, which is overgrown by brown opal and then by MGSC. No 2-phase FIAs were identified in this sample. Brown opal from the base of the section gave an age of 7.79 ± 0.67 Ma. Opal on the boundary between bladed calcite and MGSC has an age between 0.71 ± 0.48 Ma and 0.92 ± 0.03 Ma indicating that MGSC precipitated after this time.

